

University of Alberta

Development of Surface Plasmon Resonance Imaging Assays for Detection
of Bacterial Proteins and Whole Bacteria

by



Hongmei Shang

A thesis submitted to the Faculty of Graduate Studies and Research
in partial fulfillment of the requirements for the degree of
Doctor of Philosophy

Department of Chemistry

Edmonton, Alberta, Canada

Fall 2008



Library and
Archives Canada

Bibliothèque et
Archives Canada

Published Heritage
Branch

Direction du
Patrimoine de l'édition

395 Wellington Street
Ottawa ON K1A 0N4
Canada

395, rue Wellington
Ottawa ON K1A 0N4
Canada

Your file *Votre référence*
ISBN: 978-0-494-46421-2
Our file *Notre référence*
ISBN: 978-0-494-46421-2

NOTICE:

The author has granted a non-exclusive license allowing Library and Archives Canada to reproduce, publish, archive, preserve, conserve, communicate to the public by telecommunication or on the Internet, loan, distribute and sell theses worldwide, for commercial or non-commercial purposes, in microform, paper, electronic and/or any other formats.

The author retains copyright ownership and moral rights in this thesis. Neither the thesis nor substantial extracts from it may be printed or otherwise reproduced without the author's permission.

AVIS:

L'auteur a accordé une licence non exclusive permettant à la Bibliothèque et Archives Canada de reproduire, publier, archiver, sauvegarder, conserver, transmettre au public par télécommunication ou par l'Internet, prêter, distribuer et vendre des thèses partout dans le monde, à des fins commerciales ou autres, sur support microforme, papier, électronique et/ou autres formats.

L'auteur conserve la propriété du droit d'auteur et des droits moraux qui protègent cette thèse. Ni la thèse ni des extraits substantiels de celle-ci ne doivent être imprimés ou autrement reproduits sans son autorisation.

In compliance with the Canadian Privacy Act some supporting forms may have been removed from this thesis.

Conformément à la loi canadienne sur la protection de la vie privée, quelques formulaires secondaires ont été enlevés de cette thèse.

While these forms may be included in the document page count, their removal does not represent any loss of content from the thesis.

Bien que ces formulaires aient inclus dans la pagination, il n'y aura aucun contenu manquant.


Canada

Dedicated to my dearest parents and Ruokun

Abstract

Pathogen detection has a wide range of applications in many research fields, such as food health and safety. Food contamination with pathogens causes millions of foodborne illnesses every year. Bacterial pathogens including *Escherichia coli* and *Salmonella* are responsible for over 90% of foodborne illnesses. In recent years, a large number of detection techniques have been developed for identification of bacterial pathogens in food and water, which can be classified into two categories: conventional methods and biosensors. Compared to the conventional methods, biosensor technology has the potential to provide much faster detection with equal sensitivity and specificity. Surface plasmon resonance (SPR) is a label-free, optical biosensor that is often used to monitor biomolecular interactions on metal surfaces (e.g., Au, Ag). To date, several bacterial pathogens have been successfully captured by specific bacterial antibodies and detected with various SPR biosensors.

The main goal of our research work is to develop surface chemistry and methodology for analysis of bacterial protein interactions and for detection of whole bacteria as well. Here, we present a facile approach to immobilize bacterial proteins on gold surfaces, which allows SPR imaging to investigate protein–protein, protein–DNA and protein–sugar interactions. This method involved synthesis of a thiol-functionalized nitrilotriacetic acid (NTA) that was utilized to specifically anchor histidine-tagged bacterial proteins on the surface. The structure of NTA monolayers was characterized by infrared reflection absorption spectroscopy (IRRAS). The immobilized bacterial protein

served as a binding ligand to capture whole *E. coli* cells. The specificity of bacterial binding was evaluated by testing different strains and types of bacteria using SPR imaging. The limit of detection (LOD) was estimated to be approximately 1×10^7 cells/mL in our assays. The results demonstrate that bacterial proteins could be used for rapid and specific detection of bacterial pathogens. In addition, a representative bacterial protein released after *E. coli* lysis was identified on the same sensor chip where the bacterial cell was captured, which may offer a possible route to differentiate pathogenic from non-pathogenic bacteria.

Acknowledgements

I would like to express my heartfelt thanks to Prof. Mark T. McDermott for his scientific guidance and continuous support throughout my graduate studies. Over the past four years, my knowledge and experimental skills have greatly improved in order to accomplish the research projects he gave me.

I am very grateful to my collaborators, Prof. Joel Weiner and Mr. Glen Zhang (Department of Biochemistry, University of Alberta), for generously providing proteins and bacterial cultures. Special thanks go to Mr. Glen Zhang for his constructive suggestions and enthusiastic personality.

I thank every member of the McDermott group, including Dr. Aaron Skelhorne, Dr. Francis Nsiah, Bushra Sajed, Chris Grant, Dwayne Schewchuk, Rongbing Du, Wendy Friesen, Andrew Smith, Lars Laurentius, Ni Yang, Dr. Peng Wu, Dr. David Munoz-Paniagua, Rory Chisholm and Richard Adjei, for their technical assistance and friendship. I also acknowledge Ilona Baker, Arlene Figley, Lin Ferguson, Lynne Lechelt and Jeannette Loiselle for being so kind and helpful at all time.

Lastly, I wish to thank my wonderful parents for their endless love and care since I was born. Many thanks are given to my husband, Ruokun Zhou, for his understanding and patience throughout these years. Without them, I could not have reached the conclusion of my graduate studies.

Table of Contents

Chapter I: Introduction

| | |
|-----------------------------------|----|
| Pathogen Detection | 1 |
| Protein Immobilization | 7 |
| Surface Plasmon Resonance Imaging | 17 |
| Research Objectives | 27 |
| References | 28 |

Chapter II: Bioaffinity Immobilization of Proteins for Surface Plasmon Resonance

Imaging

| | |
|------------------------|----|
| Introduction | 36 |
| Experimental | 38 |
| Results and Discussion | 43 |
| Conclusions | 67 |
| References | 68 |

Chapter III: Surface Plasmon Resonance Imaging Studies of Bacterial Proteins

| | |
|------------------------|-----|
| Introduction | 75 |
| Experimental | 78 |
| Results and Discussion | 82 |
| Conclusions | 101 |
| References | 103 |

Chapter IV: Whole Bacterial Detection with Surface Plasmon Resonance Imaging

| | |
|------------------------|-----|
| Introduction | 108 |
| Experimental | 110 |
| Results and Discussion | 115 |
| Conclusions | 129 |
| References | 130 |

Chapter V: Protein Identification from Bacteria Captured and Lysed on a Single Chip

| | |
|------------------------|-----|
| Introduction | 134 |
| Experimental | 135 |
| Results and Discussion | 139 |
| Conclusions | 148 |
| References | 148 |

Chapter VI: Conclusions and Future Work

| | |
|-------------|-----|
| Conclusions | 150 |
| Future Work | 152 |
| References | 153 |

List of Tables

| | | |
|-------------------|--|-----|
| Table 2.01 | SPR signals for His ₆ -tagged CRP adsorption on mixed monolayers | 54 |
| Table 3.01 | SPR signals for His ₆ -tagged CRP adsorption in Figure 3.03 | 86 |
| Table 3.02 | SPR signals for the interaction between CRP and anti-CRP | 88 |
| Table 3.03 | SPR signals for CRP dimerization | 93 |
| Table 3.04 | SPR signals for His ₆ -tagged CRP immobilization, dimerization and binding to DNA | 98 |
| Table 3.05 | SPR signals for His ₆ -tagged MBP immobilization | 100 |
| Table 3.06 | SPR signals for the maltose–MBP binding | 102 |
| Table 4.01 | SPR signals for His ₆ -tagged Cma adsorption in Figure 4.02 | 118 |
| Table 4.02 | SPR signals for capture of <i>E. coli</i> in buffer | 120 |
| Table 4.03 | SPR signals for detection of <i>E. coli</i> from lettuce | 121 |
| Table 5.01 | SPR signals of Cma immobilization for bacterial capture | 143 |
| Table 5.02 | SPR signals of <i>E. coli</i> capture for bacterial lysis | 146 |
| Table 5.03 | SPR signals for CRP identification after bacterial lysis | 147 |

List of Figures

| | | |
|--------------------|---|----|
| Figure 1.01 | Sandwich ELISA | 3 |
| Figure 1.02 | FRET biosensor | 5 |
| Figure 1.03 | Different methods of protein immobilization | 9 |
| Figure 1.04 | Covalent attachment of proteins using NHS esters | 11 |
| Figure 1.05 | Affinity interaction between His ₆ -tag and NTA-Ni ²⁺ complex | 14 |
| Figure 1.06 | Antibody immobilization using protein A or protein G | 16 |
| Figure 1.07 | Kretschmann configuration | 20 |
| Figure 1.08 | SPR imaging setup | 21 |
| Figure 1.09 | Peptide immobilization scheme | 25 |
| Figure 2.01 | Synthesis of thiol-functionalized NTA | 45 |
| Figure 2.02 | IRRAS characterization of NTA monolayers | 47 |
| Figure 2.03 | IRRAS characterization of mixed monolayers | 49 |
| Figure 2.04 | Immobilization scheme of His ₆ -tagged protein on NTA monolayers | 51 |
| Figure 2.05 | SPR difference image of His ₆ -tagged CRP adsorption | 53 |
| Figure 2.06 | SPR sensorgrams of His ₆ -tagged Cma adsorption | 56 |
| Figure 2.07 | His ₆ -tagged Cma adsorption at various protein concentrations | 58 |
| Figure 2.08 | His ₆ -tagged Cma desorption using imidazole | 61 |
| Figure 2.09 | SPR sensorgram of surface regeneration with imidazole | 62 |
| Figure 2.10 | His ₆ -tagged Cma desorption using EDTA | 64 |
| Figure 2.11 | SPR sensorgram of surface regeneration with EDTA | 65 |
| Figure 2.12 | His ₆ -tagged Cma desorption using NiSO ₄ | 66 |

| | | |
|--------------------|--|-----|
| Figure 3.01 | Structure of the CRP–cAMP–DNA complex | 77 |
| Figure 3.02 | Structure of the MBP protein | 79 |
| Figure 3.03 | SPR difference image of His ₆ -tagged CRP immobilization | 85 |
| Figure 3.04 | SPR difference image of the CRP–anti-CRP interaction | 87 |
| Figure 3.05 | His ₆ -tagged CRP adsorption, dimerization and binding to DNA | 90 |
| Figure 3.06 | SPR difference image of CRP dimerization | 92 |
| Figure 3.07 | CRP dimerization at various protein concentrations | 94 |
| Figure 3.08 | Dependence of CRP dimerization on cAMP concentration | 96 |
| Figure 3.09 | SPR difference image of His ₆ -tagged MBP immobilization | 99 |
| Figure 4.01 | Scheme of bacterial capture using Cma | 111 |
| Figure 4.02 | SPR difference image of His ₆ -tagged Cma immobilization | 119 |
| Figure 4.03 | SPR difference image of bacterial capture | 117 |
| Figure 4.04 | Optical images of bacterial capture | 123 |
| Figure 4.05 | Bar graph for the binding of different <i>E. coli</i> strains | 125 |
| Figure 4.06 | Bar graph for the detection of different bacteria | 126 |
| Figure 4.07 | Bacterial capture at various concentrations | 128 |
| Figure 5.01 | Detection scheme of proteins released from captured bacterial lysis | 138 |
| Figure 5.02 | Layout of SPR chip used for protein detection after bacterial lysis | 140 |
| Figure 5.03 | SPR difference image of His ₆ -tagged Cma immobilization | 142 |
| Figure 5.04 | SPR difference image of <i>E. coli</i> capture | 145 |

List of Symbols

| | |
|----------------|--------------------------------------|
| λ | Wavelength |
| pI | Isoelectric point |
| k_{sp} | SP's propagation constant |
| ω | Angular frequency |
| c | Light speed in vacuum |
| ϵ_d | Dielectric constant of medium |
| ϵ_m | Dielectric constant of metal film |
| θ | Incident angle |
| θ_{SPR} | SPR angle |
| n | Refractive index |
| I | Reflectivity |
| I_p | Reflectivity of p -polarized light |
| I_s | Reflectivity of s -polarized light |
| ΔI | Difference in reflectivity |
| Δn | Difference in refractive index |
| $\Delta\%R$ | Change of percent reflectivity |
| K_{ads} | Adsorption coefficient |
| K_d | Dissociation constant |

List of Abbreviations

| | |
|----------------------|---|
| ATR | Attenuated total reflection |
| B-PER | Bacterial protein extraction reagent |
| BSA | Bovine serum albumin |
| CAP | Catabolite gene activator protein |
| CFU | Colony forming unit |
| Cma | Colicin M |
| CRP | Cyclic AMP receptor protein |
| DPDS | 2,2'-dipyridyl disulfide |
| DTT | Dithiothreitol |
| <i>E. coli</i> | <i>Escherichia coli</i> |
| EDC | 1-Ethyl-3-(3-dimethylaminopropyl)carbodiimide |
| EG3-OMe | (1-Mercaptoundec-11-yl)tri(ethylene glycol)methyl ether |
| ELISA | Enzyme-linked immunosorbent assay |
| FhuA | Ferric hydroxamate uptake protein component A |
| FRET | Fluorescence resonance energy transfer |
| GST | Glutathione <i>S</i> -transferase |
| His ₆ | Hexahistidine |
| IRRAS | Infrared reflection absorption spectroscopy |
| ISE | Ion-selective electrode |
| LC | Liquid crystal |
| <i>L. bulgaricus</i> | <i>Lactobacillus bulgaricus</i> |

| | |
|------|---|
| LOD | Limit of detection |
| MBP | Maltose-binding protein |
| MUA | 11-Mercaptoundenoic acid |
| MUAM | 11-Mercaptoundecylamine |
| MUO | 11-Mercapto-1-undecanol |
| NHS | <i>N</i> -hydroxysuccinimide |
| NTA | Nitrilotriacetic acid |
| PBP | Periplasmic binding protein |
| PBS | Phosphate-buffered saline |
| PCR | Polymerase chain reaction |
| PDMS | Poly(dimethylsiloxane) |
| PEG | Poly(ethylene glycol) |
| ROI | Region of interest |
| SAM | Self-assembled monolayer |
| SATP | <i>N</i> -Succinimidyl <i>S</i> -acetylthiopropionate |
| SP | Surface Plasmon |
| SPP | Surface Plasmon polariton |
| SPR | Surface plasmon resonance |
| tNTA | Thiol-functionalized NTA |

Chapter I

Introduction

1. Pathogen Detection

Foodborne diseases are caused by the consumption of contaminated food, and have become a global issue for public health in that they lead to millions of illnesses and deaths in the world every year. A number of pathogenic agents, such as bacteria and viruses, can give rise to foodborne illnesses if food handling, preparation or storage is improper. As a common pathogenic agent, bacteria are responsible for more than 90% of foodborne illnesses. *Escherichia coli*, *Salmonella*, *Campylobacter jejuni* and *Listeria monocytogenes* are bacterial foodborne pathogens that are most thoroughly studied by researchers.¹ To date, various detection techniques have been developed to identify bacterial pathogens in food and water.²⁻⁵ The following sections describe several methods that are currently used for detection of bacterial pathogens.

1.1. Conventional Methods

Traditional approaches for bacterial detection are reliable, selective and sensitive, which are divided into three categories: the culturing and plating method,⁶ polymerase chain reaction (PCR)⁷⁻⁹ and enzyme-linked immunosorbent assay (ELISA).^{10,11} The conventional culturing method is a standard technique for bacterial pathogen detection, but it is extremely time-consuming. A series of procedures are involved in the culturing and plating method, including pre-enrichment, selective enrichment, colony isolation and

biochemical testing, to produce detection results. Obviously, this method is inconvenient for detecting bacterial pathogens in food. PCR and ELISA can provide faster bacterial detection than the culturing method. PCR is a method based on isolation and amplification of a DNA sequence targeting bacterial genetic material.¹² The amplified DNA sequence is then detected and quantified by gel electrophoresis. In addition, PCR has been used in combination with other techniques, such as ELISA and fluorescence, to yield more robust results in bacterial detection.¹³⁻¹⁵ But PCR cannot distinguish viable from non-viable cells because DNA sequences exist in both dead and alive bacterial cells. ELISA is another powerful tool used for pathogen detection with high sensitivity and specificity.¹⁶ In this technique, the presence of an antibody or antigen is recognized by specific antigen-antibody interactions. Figure 1.01 shows a cartoon of “sandwich” ELISA. First, a primary antibody is immobilized on a solid surface. A solution containing a target antigen is flowed over the surface, and the antigen binds to the primary antibody. Then, an enzyme-labeled secondary antibody is applied and specifically bound to the captured antigen. Finally, a substrate is introduced over the surface, which is converted by the enzyme into a fluorescent response. Since PCR and ELISA often involve an enrichment step, they still require about one day to obtain results. Hence, there is a demand for developing new methods that could offer rapid detection of bacterial pathogens without any loss of sensitivity and specificity.

1.2. Biosensors

A biosensor refers to a detection device that converts a biological response into a physicochemical signal.¹⁷ Compared to the conventional methods for pathogen detection,

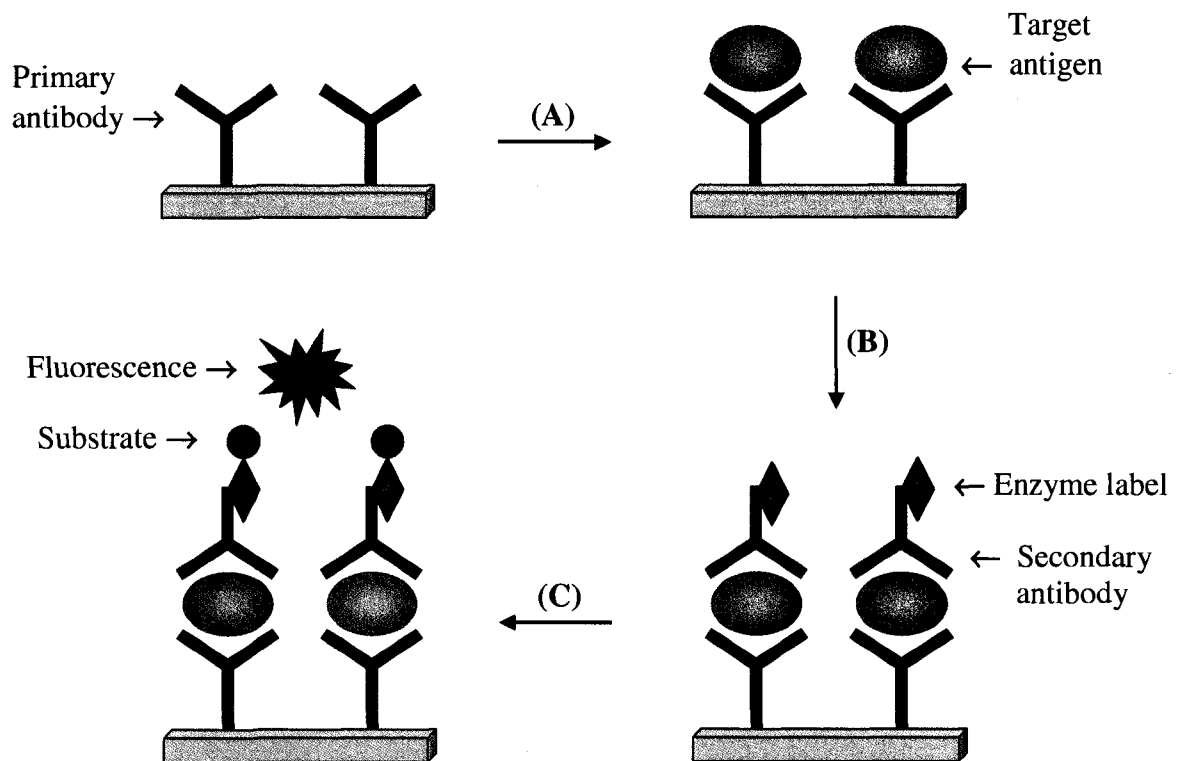


Figure 1.01. Diagram of “sandwich” ELISA. (A) Target antigen binds to immobilized primary antibody on a solid surface. (B) Enzyme-labeled secondary antibody interacts with the antigen. (C) Enzyme converts a substrate into a fluorescent response.

this technique has the potential to shorten the detection time, and also to provide high sensitivity and specificity. Most biosensors can be classified into optical biosensors and electrochemical biosensors based on their transduction methods. Optical biosensors are more popular in pathogen detection because they are more sensitive and selective than electrochemical biosensors. However, electrochemical biosensors have the advantages of low cost and easy operation for most users.¹

1.2.1. Optical Biosensors

One example of optical biosensors is a fluorescence resonance energy transfer (FRET) biosensor.^{18,19} This biosensor is used to detect a fluorescent signal arising from an energy transfer between two close fluorophores. Figure 1.02 illustrates the interaction between a donor fluorophore and an acceptor fluorophore in a FRET biosensor. First, an antibody is labeled with a donor fluorophore, and an antigen is coupled to an acceptor fluorophore. Then, an antigen solution is applied to the immobilized antibody on a surface. When the antibody binds to the antigen, the two fluorophores will be close to each other (i.e., 1–10 nm). As a result, the FRET process occurs via a transfer of energy from the excited donor fluorophore to the acceptor fluorophore. λ_0 and λ_1 are the excitation and emission wavelengths of the donor fluorophore, respectively. λ_2 is the emission wavelength of the acceptor fluorophore. The ratio of acceptor to donor emission intensity is measured as a diagnostic for the specificity of antigen–antibody interactions. Ko and Grant²⁰ developed a FRET-based method for detecting *Listeria monocytogenes* and *Salmonella*, and found that the detection limits for both bacteria were 2.0 $\mu\text{g/mL}$. In addition, surface plasmon resonance (SPR) is an optical biosensor that has been widely

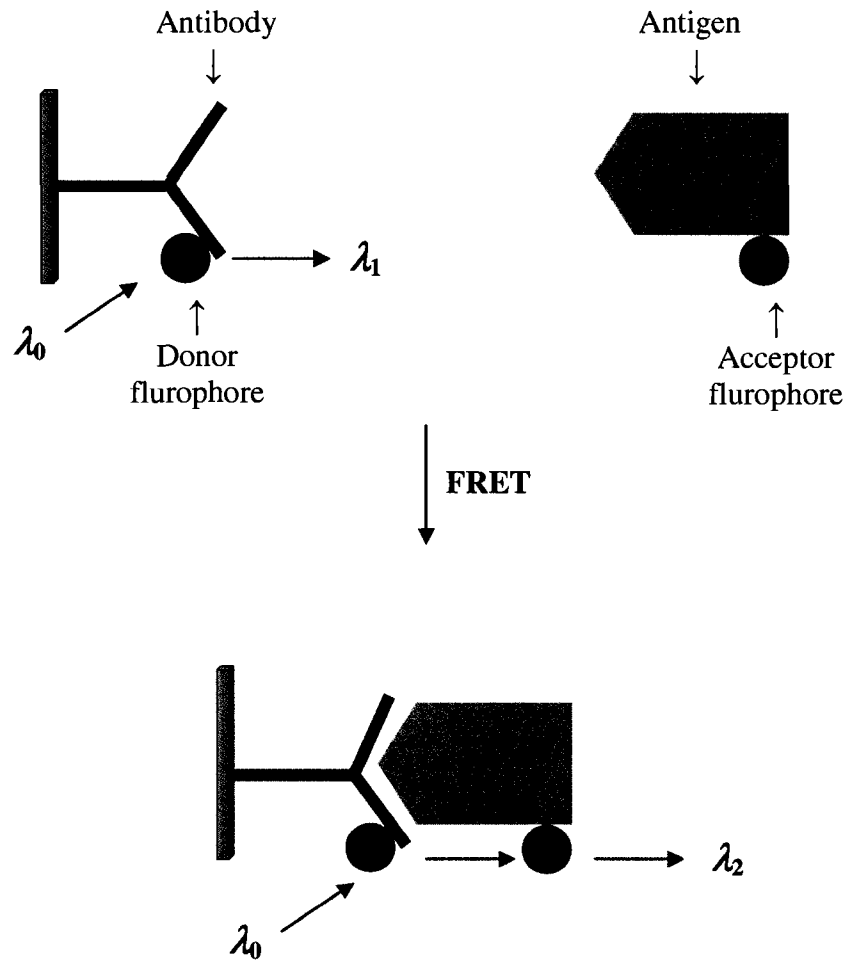


Figure 1.02. Cartoon of a FRET biosensor in which an antibody is labeled with a donor fluorophore and an antigen is conjugated with an acceptor fluorophore. FRET occurs when the antigen binds to the antibody.

used for bacterial pathogen detection.^{21–24} This biosensor can provide sensitive, label-free, and real-time measurements of biomolecular (e.g., peptide, proteins, DNA) interactions on a noble metal surface, which greatly contributes to successful applications in food health and safety.²⁵ SPR theory, instrumentation and applications will be discussed later in this chapter (see Section 3).

1.2.2. Electrochemical Biosensors

Another attractive branch of biosensors are electrochemical biosensors that rely on the detection of a current, potential or impedance change resulting from a bio-recognition process at a solid–liquid interface.²⁶ Compared to optical biosensors, they are simple and inexpensive, but less sensitive and selective. Amperometric biosensors monitor a current change at a constant potential. A redox enzyme is added to catalyze a reaction that produces or consumes electrons. The current change is proportional to the concentration of an electroactive analyte involved in the bio-recognition event. Che et al.²⁷ used an amperometric immunosensor coupled with the immunomagnetic separation method to rapidly detect *Campylobacter jejuni* in both pure culture and poultry samples. The detection of bacterial pathogens was completed within 2.5 h, and the detection limit was found to be 2.1×10^4 colony forming unit per milliliter (CFU/mL). A potentiometric sensor is another example of electrochemical biosensors used for pathogen detection. This sensor usually contains an ion-selective electrode (ISE) and an enzyme. ISE is used to detect a substance that is produced from or consumed by an enzyme-catalyzed reaction. This detection method is able to identify bacteria with high sensitivity in that the potential response has a logarithmic relationship with the concentration of analyte. Several

applications of potentiometric biosensors in pathogen detection have been reported in recent years.²⁸⁻³⁰

In the near future, biosensors are expected to increasingly contribute to pathogen detection because conventional methods are very slow, and therefore impractical for monitoring bacterial contamination in food. However, the performance of biosensors is still not reliable, which requires considerable developments. The sensitivity of biosensors needs to be improved to reach the same detection limit as established techniques. In addition, the combined use of microfluidic devices in biosensors will definitely be beneficial to pathogen detection due to the following advantages: (1) low sample volumes; (2) reduced reagent costs; (3) shorter analysis time; (4) multiple analysis in the same device.³¹⁻³³

2. Protein Immobilization

Immobilization of proteins on solid supports plays a crucial role in protein microarrays,³⁴⁻³⁶ and has a large number of applications in proteomics,³⁷⁻⁴⁰ drug discovery^{41,42} and medical diagnosis.^{43,44} Over the past years, enormous efforts have been made to immobilize proteins on different substrates including membranes, glass, microwells, and beads.⁴⁵⁻⁴⁹ However, protein immobilization is still a challenging task, which requires further technological improvement to obtain protein adsorption with high density. The conformation of proteins is very sensitive to the surrounding environment, and protein biological activity will be damaged due to structural deformation.^{50,51} Also, nonspecific protein adsorption needs to be minimized to increase the sensitivity. To date, most methods for protein immobilization rely on three mechanisms of interactions

between the protein and the surface: physical, covalent, and bioaffinity immobilization.⁵⁰ Figure 1.03 presents examples of protein immobilization by physical adsorption, covalent coupling, and bioaffinity immobilization. To immobilize different proteins on various surfaces, an appropriate method must be decided based on the chemical and physical properties of both proteins and surfaces.

2.1. Physical Adsorption

Physical adsorption allows proteins to be immobilized on solid surfaces via intermolecular forces. This method is widely used for protein immobilization in immunoassays due to the simplicity. But random orientation and weak attachment result from immobilizing proteins by physical adsorption.^{52,53} Thus, this method may lead to partial loss of protein activity and function due to random orientation and structural deformation.³⁹ Moreover, nonspecific binding of proteins is relatively high in physical adsorption, which may produce false results. One example of physical adsorption is to incubate a gold surface into a solution of an amine- or a carboxyl-terminated alkanethiol to create a self-assembled monolayer (SAM). Proteins are then immobilized on the SAM through the formation of ammonium–carboxylate ion pairs.⁵⁴ In addition, the Biacore SPR technology fabricates sensor chips that are mainly modified with a carboxymethylate dextran layer. This dextran hydrogel layer physically adsorbs proteins by the combination of electrostatic and hydrophobic interactions. A hydrophilic environment created by the hydrogel can maintain immobilized biomolecules in a non-denaturation state.⁵⁵ To date, a variety of derivatized dextran surfaces are commercially available to fit different immobilization chemistries.

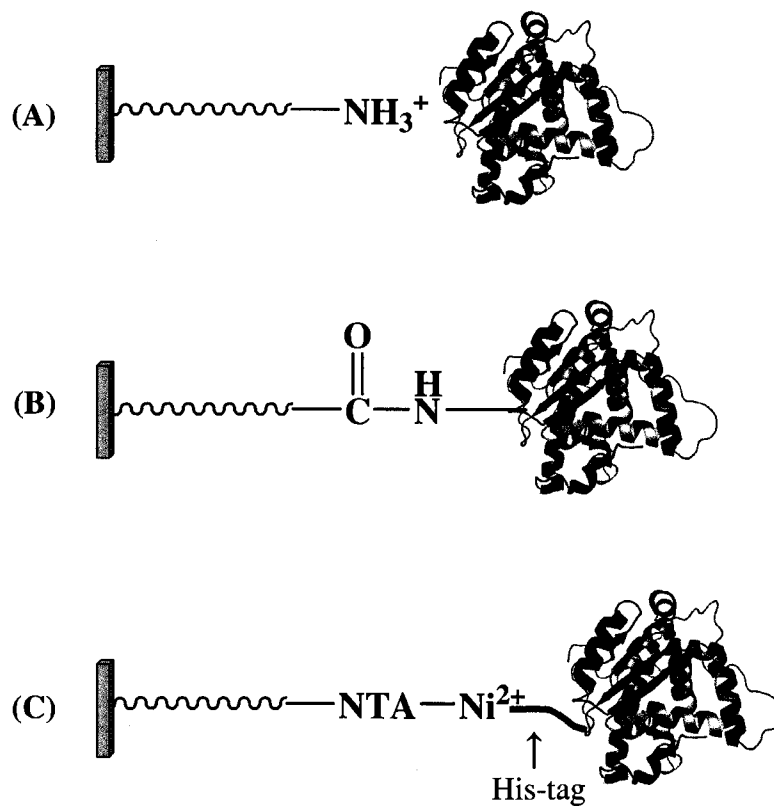


Figure 1.03. Examples of protein immobilization using three different methods: (A) physical adsorption, (B) covalent coupling, and (C) bioaffinity immobilization.

2.2. Covalent Coupling

Covalent coupling can provide strong attachment of proteins to a surface, and is achieved by the formation of covalent bonds between functional groups of proteins and reactive groups of molecules on the surface.^{56,57} The functional groups of proteins commonly employed for immobilization include amine ($-\text{NH}_2$), carboxyl ($-\text{COOH}$), thiol ($-\text{SH}$) and hydroxyl groups ($-\text{OH}$). On the other hand, the surface can be modified with a wide range of functionalities, such as aldehyde, *N*-hydroxysuccinimide (NHS) ester, maleimide, amine, carboxylic acid and epoxy, before protein immobilization. Because this immobilization method produces an irreversible binding, immobilized proteins cannot be removed by a buffer or detergent, which ensures reproducible results of protein interaction analysis. Depending on the protein residue exposed to the functionalized surface, covalent coupling can afford the immobilization of proteins in either random or well-defined orientation.⁵⁰ Sometimes protein modification, surface functionalization, or both are required in order to attain site-specific immobilization.

NHS esters are the most useful reactive groups attached to the surface, and can react with amine groups of a protein to form a stable amide bond.⁵⁸⁻⁶⁰ Figure 1.04 depicts a scheme for protein immobilization on a gold surface using NHS esters. First, the gold surface is exposed to a solution of 11-mercaptoundecanoic acid (MUA) to form a carboxyl-terminated SAM. The MUA SAM is subsequently activated by a mixture of 1-ethyl-3-(3-dimethylaminopropyl)carbodiimide (EDC) and NHS to yield an NHS ester. Finally, the NHS ester reacts with amine groups of a target protein to produce an amide bond linkage for immobilizing the protein on the gold surface. For different proteins, immobilization conditions need to be optimized to increase the efficiency of protein adsorption. Several

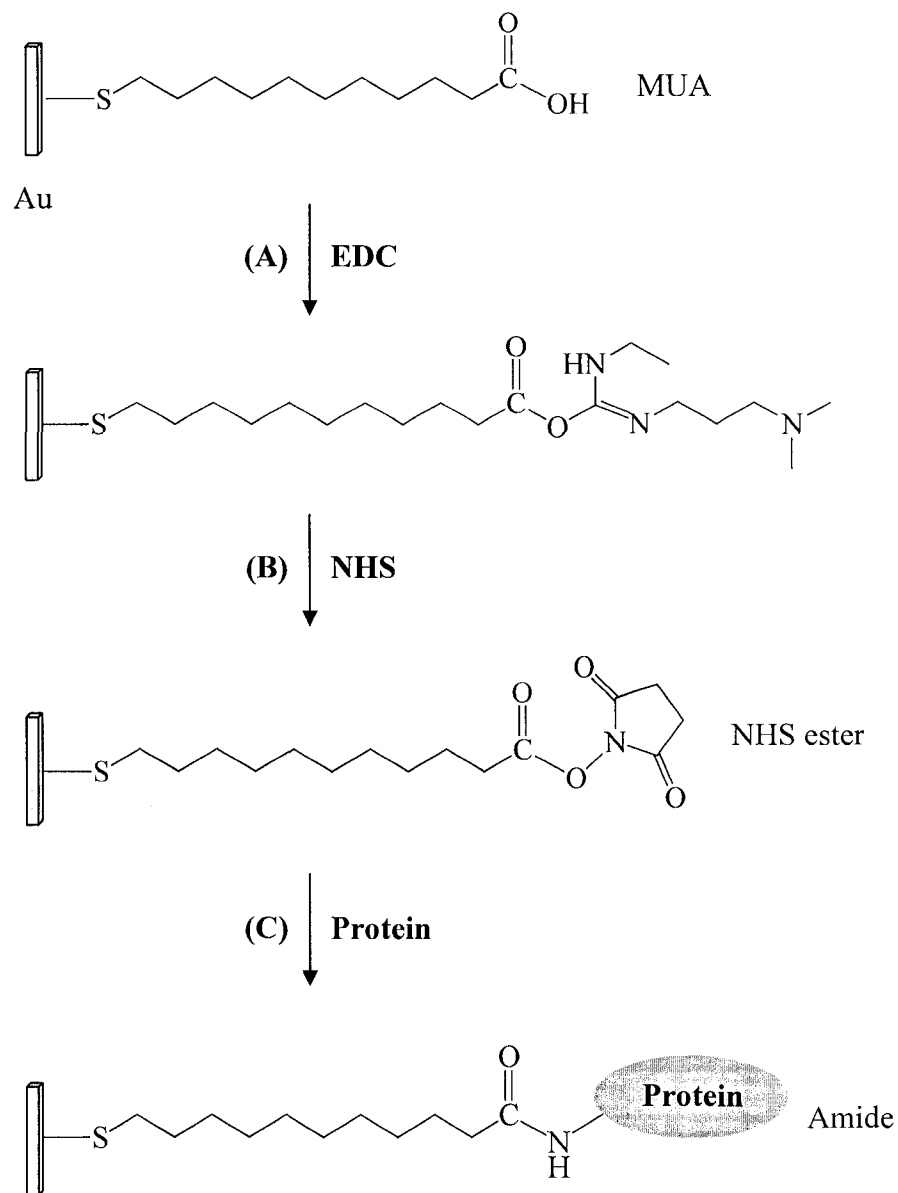


Figure 1.04. Surface modification procedure for covalent coupling of proteins on a gold surface using NHS esters: (A) MUA monolayer reacts with EDC to form an active intermediate; (B) NHS ester is produced by mixing the intermediate with NHS; (C) target protein is immobilized via the formation of an amide bond between the NHS ester and the amino group of protein.

parameters must be considered, such as pH, buffer and reaction time. Also, the chain length and the composition of carboxyl-terminated SAMs will affect the ability to react with NHS.⁶¹ Besides, maleimide is another common functional group for immobilizing proteins that contain thiols. The double bond of maleimide can undergo a reaction, called Michael addition, with the thiol group to generate a thioether bond.^{62,63} Since deprotonated thiols, rather than thiols, are the active species that react with maleimide, this addition reaction is rapid under basic conditions. However, at a higher pH value, there is a cross reaction between maleimide and amine groups of protein. Therefore, reactivity and selectivity must be well controlled by pH.

2.3. Bioaffinity Immobilization

In bioaffinity immobilization, proteins are immobilized via specific bioaffinity interactions. A number of affinity pairs are used for protein immobilization, including lectin–sugar, protein–DNA and avidin–biotin.^{64–66} Also, fusion proteins with affinity tags, such as histidine-tagged proteins, can bind to a desired matrix called Ni–nitrilotriacetic acid (NTA).^{67,68} The nature of bioaffinity interactions offers some advantages over other immobilization methods. An oriented immobilization can be obtained by bioaffinity immobilization, which is beneficial to maintaining protein activity and function.^{50,51} Moreover, the reversibility of bioaffinity interactions allows immobilized proteins to be dissociated from a surface, and the regenerated surface can be reused for multiple experiments. Avidin–biotin is the most common bioaffinity pair employed for protein immobilization. Avidin, a tetrameric protein, contains four identical subunits, and each subunit can specifically bind to biotin with the dissociation constant K_d of $\sim 10^{-15}$ M.

Biotin, also called vitamin H or B₇, consists of a bicyclic ring and a valeric side chain. The bicyclic ring interacts with avidin, and the side chain undergoes functionality in order to conjugate with target proteins. The small size of biotin ensures that the conformation and activity of protein are unaffected. The strong and specific affinity of avidin for biotin is often utilized to capture biotin-labeled proteins on an avidin-modified surface. Streptavidin is another tetrameric protein showing a strong affinity for biotin. Compared to avidin, it lacks carbohydrate modification (i.e., glycosylation), and has a near-neutral isoelectric point (pI \approx 5). Hence, streptavidin has the advantage of low nonspecific adsorption over avidin. So far, a variety of biotinylated proteins are commercially available, and the surface density of binding sites is usually controlled by biotin photochemistry or using mixed monolayers.

Fusion proteins with affinity tags also find their applications in protein immobilization. Fusion proteins are produced by genetic engineering, which is a biological technique used to combine two or more genes originally coded for different proteins. Initially, fusion proteins are prepared for protein identification and separation. Glutathione *S*-transferase (GST), FLAG peptide and hexahistidine (His₆) are common fusion tags employed for the purification of proteins by column chromatography. In the past few years, the His₆-tag has been applied to protein immobilization due to its specific chelating interaction with NTA in the presence of Ni²⁺ ions.^{67,69,70} As shown in Figure 1.05, one Ni²⁺ ion is octahedrally coordinated with two imidazole rings from the His₆-tag and four ligands donated by the NTA molecule. The widespread use of the His₆-tag in protein immobilization is attributed to the following advantages. First of all, the affinity interaction between His₆-tags and NTA molecules is independent of protein primary

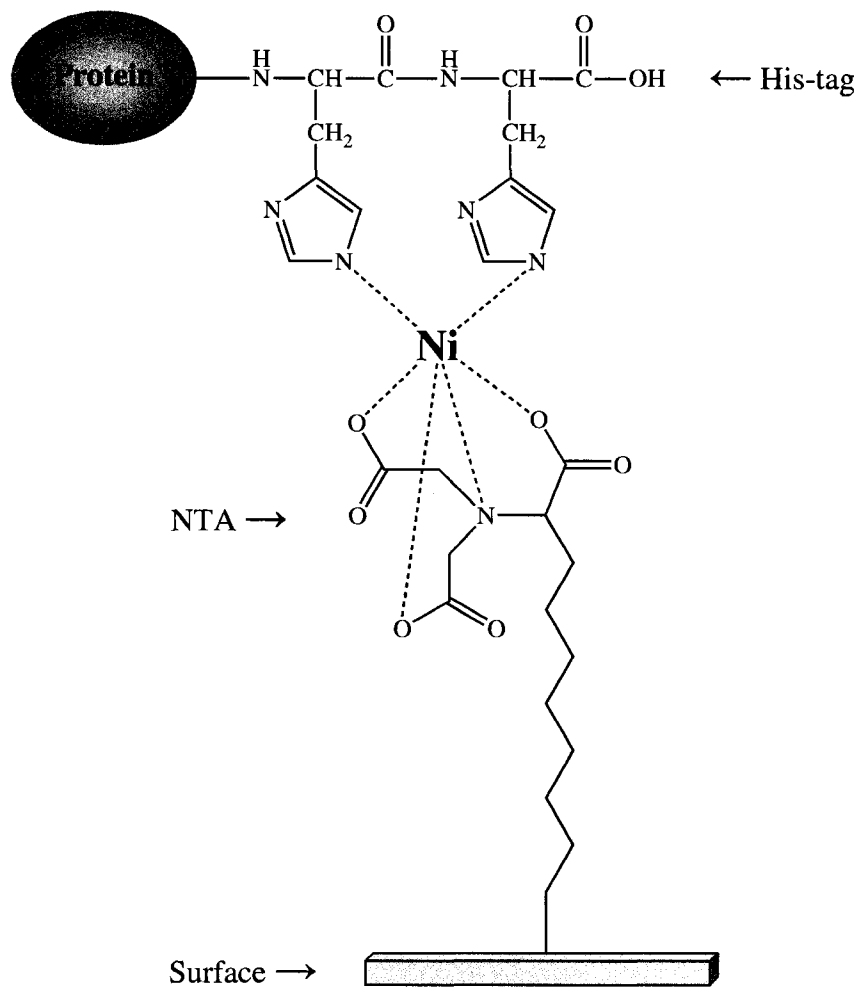


Figure 1.05. Schematic representation of the specific affinity interaction between His-tagged protein and NTA–Ni²⁺ on a solid surface. The Ni²⁺ ion is coordinated with six ligands: two from His-tag and four donated by NTA molecule.

structure, so proteins can be purified under denaturation conditions. Secondly, since the His₆-tag is quite small, its conjugation with proteins is very easy and cannot affect protein activity and function. Thirdly, a wide range of preparation kits are commercially available for expressing His₆-tagged proteins. Because the tag is added at either the C- or the N-terminus of target proteins, the resulting protein layer is oriented in the same way, which allows to improve the accessibility of protein active sites to other biomolecules. Moreover, this chelating interaction between His₆-tags and NTA–Ni²⁺ is non-covalent and reversible, so it is possible to remove immobilized His₆-tagged proteins from the surface by the addition of a regenerating agent, such as imidazole or EDTA.

Protein A and protein G has found their applications in immunoassays and affinity chromatography because of their ability to bind antibodies.^{71–73} Protein A is an immunoglobulin-binding protein expressed in the *Staphylococcus aureus* bacterium. This protein can tightly bind the Fc region of antibodies, and thus the Fab portion remains accessible for interacting with antigens. Protein G is another bacterial protein applied to proper orientation of antibodies. Compared to protein A, it exhibits affinity interactions for a wider range of antibodies. Fratamico et al.²¹ employed protein A and protein G to capture antibodies that in turn bound to the *E. coli* O157:H7 bacterium. Figure 1.06 depicts a diagram of bacterial antibody immobilization using protein A or protein G.⁷³ First, a carboxymethylate dextran layer reacted with EDC/NHS to afford an NHS ester on the sensor surface. Then, protein A or protein G was covalently immobilized by the coupling of the NHS ester with amine groups of the protein. A monoclonal or polyclonal antibody against *E. coli* O157:H7 was captured on the layer of protein A or protein G in well-defined orientation. The binding of the antibody to protein A or protein G and the

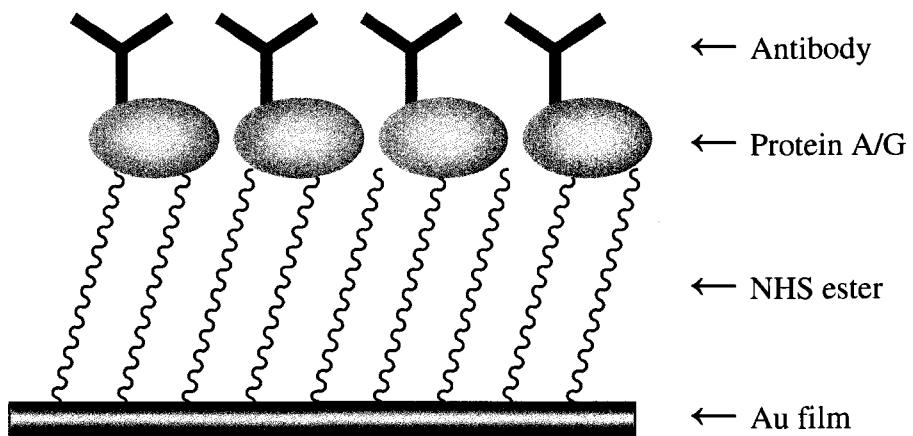


Figure 1.06. Scheme of *E. coli* antibody immobilization by protein A or protein G that is covalently attached to a gold surface using NHS esters.

antibody–bacterium interaction were characterized with SPR.

Protein immobilization is of the utmost importance for the development of biotechnology and biophysics. Optimal protein immobilization in protein microarrays allows high-throughput analysis of thousands of proteins and simultaneous screening of various biomolecular interactions. Site-specific immobilization of proteins on surfaces has the potential to retain protein biological activity, which can be achieved by covalent coupling and bioaffinity immobilization. In addition, the combination of nanolithography technique with protein immobilization provides a route to better understanding of macromolecular assembly processes.^{51,74}

3. Surface Plasmon Resonance Imaging

Surface plasmon resonance (SPR) is an optical technique that is often used to monitor material adsorption on a noble metal surface (e.g., Au, Ag). Since it can offer label-free, sensitive and real-time analysis of interactions between biological molecules, SPR has found a number of applications in biochemistry, bioanalytical chemistry and biomedicine.^{75–77} Recently, this method has been successfully applied to the investigation of various biomolecular interactions, such as antigen–antibody,^{78–80} protein–DNA,^{81,82} DNA hybridization,^{83,84} DNA–RNA,^{85,86} and protein–carbohydrate interactions.^{87,88} As a variation of SPR, SPR imaging allows simultaneous measurements of biomolecular interactions in an array format.⁸⁹ The following sections describe three respects of SPR imaging: principles, instrumentation and applications.

3.1. Principles

SPR imaging is a detection method based on the excitation of surface plasmons (SPs) by light. SPs, also known as surface plasmon polaritons (SPPs), are oscillations of free electrons that propagate parallel to a metal–dielectric interface. They exist as evanescent waves whose electromagnetic field intensity decays exponentially away from the interface into both the metal and the dielectric medium. The penetration depth (d_p) is used as a measure of how SPs can penetrate into the dielectric medium. In the SPR imaging setup, the d_p value ranges from 200 to 300 nm. The following equation provides the expression of SP's propagation constant k_{sp} at a metal–dielectric interface:⁹⁰

$$k_{sp} = \frac{\omega}{c} \sqrt{\frac{\epsilon_m \cdot \epsilon_d}{(\epsilon_m + \epsilon_d)}}$$

Where ω and c are the angular frequency and the speed of light in vacuum, respectively; (ω / c) represents the free space wavenumber; ϵ_m and ϵ_d are the dielectric constant of the metal film and the dielectric medium, respectively. It is clear from the equation that the excitation of SPs is associated with the properties of the metal and the dielectric medium. In order to produce SPs, the signs of ϵ_m and ϵ_d must be opposite, and the magnitude of ϵ_m must be greater than that of ϵ_d . These conditions are met in the visible and near-IR wavelength regions (ca. 630–1200 nm) for air–metal and water–metal interfaces.⁹¹ Au is the most common metal used in SPR imaging due to its unique optical and chemical characteristics.

Usually, p -polarized light is exploited to excite SPs in that the component of the optical wave vector is parallel to that of SPs. However, the length of the SP wave vector is much larger than that of optical waves. Thus, it is difficult to excite SPs on planar

metal surfaces by a simple reflection configuration. To better match the SP wave vector with the optical wave vector, a prism or grating coupler is normally applied to the coupling of the optical energy into the metal. Figure 1.07 illustrates the Kretschmann configuration that is typically used in SPR imaging to excite SPs by means of attenuated total reflection (ATR).⁹² In this setup, a beam of light is incident upon the backside of a thin metal film (ca. 50 nm). This metal film is coated on a glass substrate, and optically coupled with a glass prism. The incident angle (θ) is greater than the critical angle, which ensures that the optical wave is totally reflected. At SPR angle (θ_{SPR}), the optical wave vector matches the wave vector of SPs, resulting in an attenuated light reflection. The value of SPR angle depends on the refractive index (n) of the dielectric medium near the sensor surface, and will increase upon material adsorption. Therefore, SPR imaging is widely used to characterize biomolecular interactions on metal surfaces without the attachment of labels to analytes.

3.2. Instrumentation

A schematic diagram of SPR imaging manufactured by GWC Technologies (Madison, WI) is presented in Figure 1.08.²⁵ In this instrument, *p*-polarized light is generated by the combination of a white light source with a polarizer, and impinges on the backside of a SPR chip through a SF-10 glass prism. The SPR chip is prepared by the thermal evaporation of a 45 nm gold film deposited on SF-10 glass with a 1 nm adhesive chromium layer. The reflected light is passed through a narrow band-pass filter ($\lambda = 830$ nm), and subsequently detected by a CCD camera. A rotation stage is used to optimize the incident angle to improve the sensitivity of SPR measurements. In addition, a flow

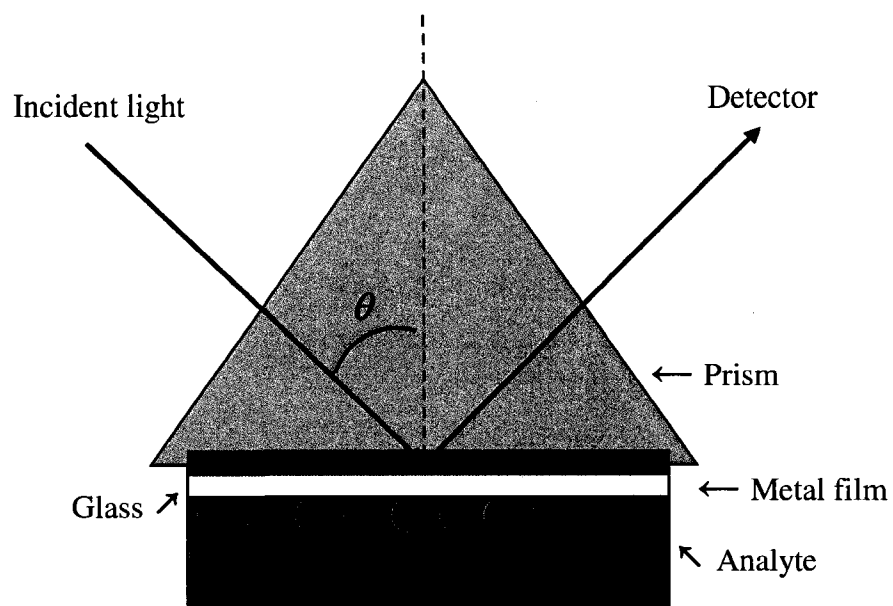


Figure 1.07. Diagram of the Kretschmann configuration that is commonly used in SPR imaging to excite surface plasmons (SPs) on a metal film.

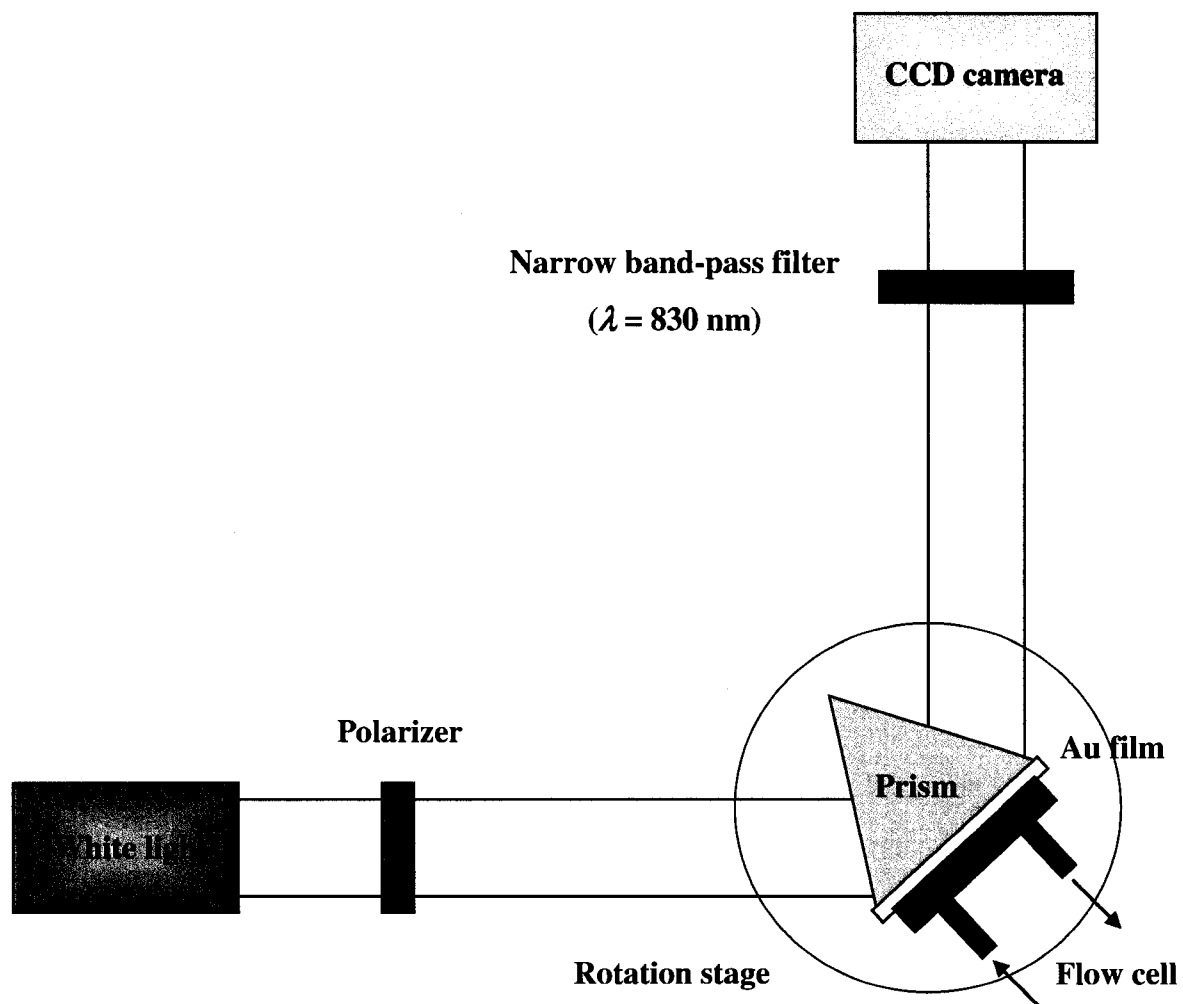


Figure 1.08. Setup of SPR imaging manufactured by GWC Technologies.

cell is attached to the chip surface for the delivery of a desired solution via a peristaltic pump, which allows to collect experimental data of kinetics studies in real time.

During SPR imaging experiments, the incident angle is optimized and maintained at a fixed light wavelength (λ). The reflected intensity (reflectivity, I_p) across the sensor surface is measured before and after material adsorption. The difference in reflectivity (ΔI) is obtained by subtracting the reflectivity before adsorption from the reflectivity after adsorption. The conversion of ΔI into a change of percent reflectivity ($\Delta\%R$) is expressed by the following equation:⁹³

$$\Delta\%R = \frac{0.85 \times \Delta I}{I_s} \times 100\%$$

where I_s refers to the reflectivity obtained when *s*-polarized light is incident on the SPR chip. Since the electric field of *s*-polarized light is parallel to the metal film, this type of light cannot excite SPs, and is totally reflected by the sensor surface. Here, *s*-polarized light is employed to afford a reference image in order to enhance the contrast of SPR images. In addition, difference images are generated by subtracting a reference image taken prior to a binding event from the image taken after the binding event. The use of difference images allows SPR imaging to quantify a number of biomolecular interactions on a surface in an array format.

SPR imaging also enables quantitative analysis of material adsorption and desorption on metal surfaces. However, one limitation is that the $\Delta\%R$ value must be linearly proportional to a change in refractive index (Δn), and thus to the number of molecules adsorbed on the surface. Nelson et al.⁹⁴ calibrated the $\Delta\%R$ value for a range

of Δn at the optimal incident angle 53.7° using Fresnel calculations. They found that $\Delta\%R$ was approximately linear with Δn when its value was less than 10%. Shumaker-Parry et al.⁹⁵ also studies the relationship between $\Delta\%R$ and Δn at a higher angle 54.6° . The results showed that there was a linear relationship for $\Delta\%R$ of less than 20%. Thus, any quantitative information cannot be obtained if the value of $\Delta\%R$ is more than 20%.

3.3. Applications

SPR imaging is primarily applied to two research areas: characterization of thin films and biosensing. As a detection method with high sensitivity, SPR imaging has been utilized for the investigation of adsorbed thin films on surfaces. Steiner et al.⁹⁶ employed SPR imaging to probe patterned organic monolayers on gold surfaces. The SAM of 11-mercaptopundecanoic acid (MUA) or 11-mercaptopundecylamine (MUAM) was patterned on the surface by microcontact printing. Reasonable SPR image contrast could be achieved for organic monolayers with a ~ 1.8 nm thickness. Moreover, the lateral resolution of $2\ \mu\text{m}$ was obtained using a SPR imaging system that was equipped with a HeNe laser source ($\lambda = 632.8$ nm) and a Kretschmann ATR prism coupler. This resolution allowed to monitor the process of SAM formation in real time. Evans et al.⁹⁷ controlled the anchoring of the nematic liquid crystal (LC) 4'-*n*-octyl-4-cyanobiphenyl at functionalized SAMs with SPR imaging. The SAM surface was photo-patterned with two alkanethiols containing different ω -terminated functional groups, $-\text{CF}_3$ and $-\text{OH}$. Their results indicated that SPR imaging was able to detect the adsorption of LC films within

~300 nm of the interface. In addition, the surface-melting phenomena of crystalline phases at the SAM interface were successfully observed by SPR imaging.

A key function of SPR imaging is to analyze biomolecular interactions on metal surfaces. In the recent years, SPR imaging has become a powerful tool for biosensing because it can provide sensitive, label-free and real-time monitoring of binding events. Corn and co-workers have extensively studied biomolecular interactions using SPR imaging. In 2001, they utilized SPR imaging and DNA arrays to quantitatively detect DNA–DNA and DNA–RNA interactions on gold surfaces.⁹⁴ To fabricate DNA arrays, the gold surface was first modified with a SAM of 11-mercaptoundecylamine (MUAM). Then, two DNA sequences terminated with thiol groups (–SH) were chemically immobilized on MUAM SAMs through a bifunctional linker sulfosuccinimidyl 4-(*N*-maleimidomethyl) cyclohexane-1-carboxylate (SSMCC). *N*-hydroxysuccinimidyl ester of methoxypoly (ethylene glycol) propionic acid (NHS-PEG) reacted with the MUAM SAM surrounding immobilized DNA sequences to create the background between DNA spots. The LOD of 10 nM was observed for the binding of DNA or RNA to the DNA array with SPR imaging. Moreover, SPR data was fitted with a Langmuir adsorption isotherm to yield an adsorption isotherm for DNA or RNA hybridization on the DNA array. The resulting adsorption coefficient K_{ads} was $1.8 \times 10^7 \text{ M}^{-1}$.

Wegner et al.⁹⁸ reported the characterization of peptide–antibody interactions on peptide arrays with SPR imaging. Figure 1.09 presents a scheme of surface chemistry reactions used for peptide immobilization. First, a gold surface was treated with a solution of MUAM to form an amine-terminated SAM. Then, *N*-Succinimidyl *S*-acetylthiopropionate (SATP) reacted with the SAM of MUAM to produce a protected

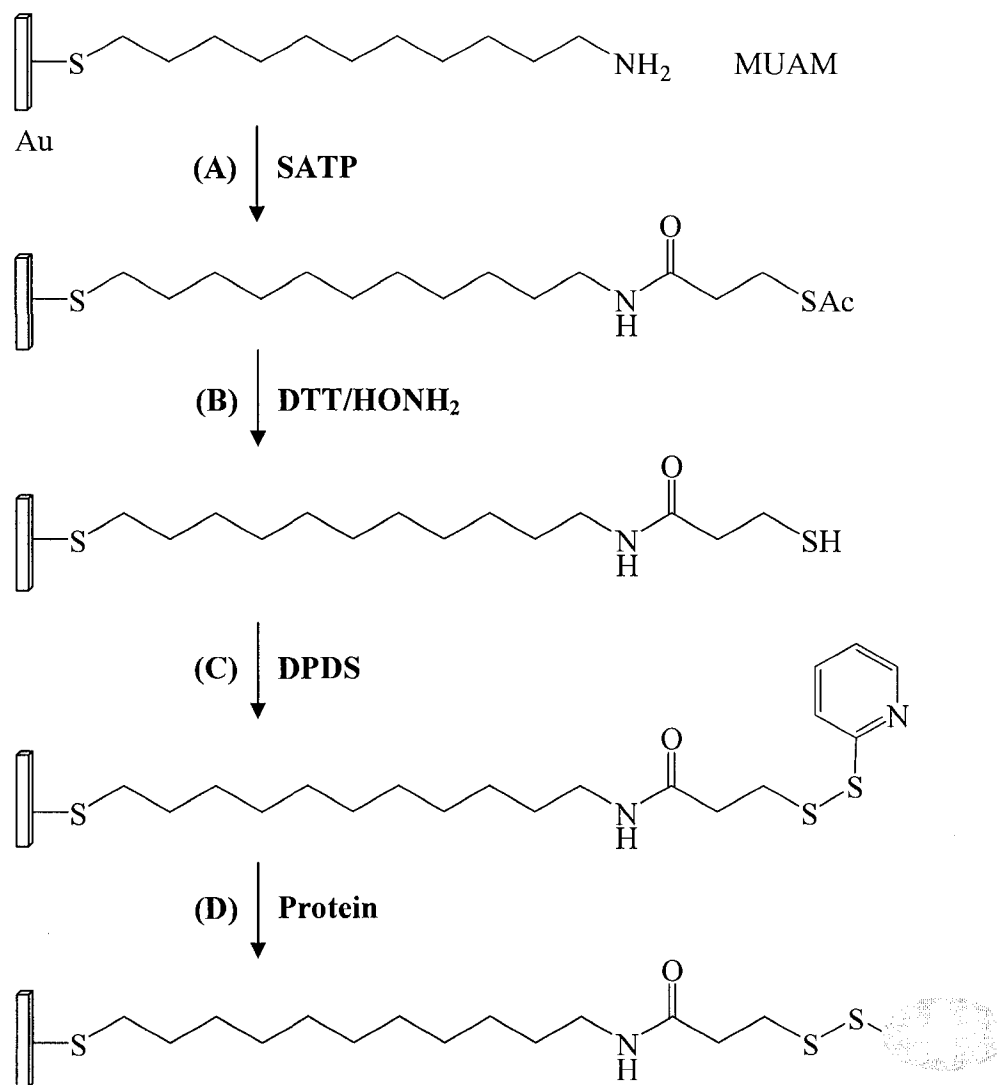


Figure 1.09. Scheme of surface chemistry reactions for peptide immobilization. (A) MUAM monolayers react with SATP to form protected thiol groups. (B) Mixture of DTT and HONH₂ was used for deprotection to yield free thiol groups. (C) Thiols were treated with DPDS to produce pyridyl groups. (D) Peptides labeled with cysteines were immobilized through a thiol-disulfide exchange reaction.

thiol surface, which was followed by deprotection with a hydroxylamine solution of dithiothreitol (DTT). The resulting surface contained free sulfhydryl groups, and was subsequently exposed to 2,2'-dipyridyl disulfide (DPDS) to generate a surface containing pyridyl groups. Lastly, peptides were labeled with cysteines, and covalently immobilized on the surface by a thiol–disulfide exchange reaction. Different peptides were patterned by poly(dimethylsiloxane) (PDMS) microfluidic channels. The surface density of peptide was varied by the formation of mixed monolayers of MUAM and an alkanethiol terminated with either $-\text{NH}_2$ or $-\text{OH}$ group. The fabricated peptide array exhibited the ability to discriminate peptides different by a single amino acid substitution. Also, quantitative measurements were performed with SPR imaging, yielding K_{ads} of $1.5 \times 10^8 \text{ M}^{-1}$.

In addition, Smith et al.⁸⁷ developed carbohydrate arrays on gold surfaces that were used to probe carbohydrate–protein interactions using SPR imaging. An immobilization method involving the formation of a disulfide bond was exploited to anchor thiol-terminated carbohydrates onto the gold surface. The interaction of concanavalin A (ConA) or jacalin with the carbohydrate array was quantitated by SPR imaging. The adsorption coefficients K_{ads} for ConA binding to a mannose layer and jacalin binding to a galactose were determined to be $5.6 \pm 1.7 \times 10^6 \text{ M}^{-1}$ and $2.2 \pm 0.8 \times 10^7 \text{ M}^{-1}$, respectively. The solution equilibrium dissociation constants K_{d} for ConA–mannose and jacalin–galactose interactions were found to be $200 \pm 50 \text{ }\mu\text{M}$ and $16 \pm 5 \text{ }\mu\text{M}$, respectively.

3.4. Summary

SPR imaging is an attractive technique used for the detection of biomolecular interactions on metal surfaces. To become a common tool for bioanalysis and biosensing, the sensitivity must be enhanced to widen the scope of SPR imaging applications. Goodrich et al.⁹⁹ developed an enzymatic amplification method to increase the detection limit of ssDNA adsorbing on the RNA microarrays. The enzyme RNase H was exploited to react with the RNA–DNA heteroduplex and to release DNA back into the solution. The released DNA bound to another RNA molecule on the surface to form a new RNA–DNA heteroduplex that was again destroyed by RNase H. Thus, all RNA molecules were removed from the surface, resulting in a decrease in percent reflectivity. This enzymatic amplification method improved the sensitivity for DNA detection from 1 nM to 1 fM. Besides, the sensitivity could be improved by the labeling of gold nanoparticles,¹⁰⁰ coupling with bioconjugates,^{101,102} or the use of sandwich assays.¹⁰³ The combination of SPR imaging with other analytical or optical techniques, such as mass spectrometry (MS),¹⁰⁴ fluorescence¹⁰⁵ or Raman scattering,¹⁰⁶ also provides a possible alternative to achieve the enhancement of sensitivity in SPR imaging.

4. Research Objectives

In this thesis, SPR imaging assays were developed for analysis of bacterial proteins and for the detection of bacterial pathogens. To monitor interactions of bacterial proteins with other biomolecules, bioaffinity immobilization method was used to anchor target proteins on gold surfaces through a specific affinity interaction between His-tags and NTA–Ni²⁺ matrix. Surface modification using a SAM of alkanethiol terminated with NTA groups was characterized with infrared reflection absorption spectroscopy (IRRAS).

SPR imaging measurements were performed to demonstrate that bacterial proteins were efficiently attached on the NTA-modified surface. Some regenerating agents allowed to reuse the NTA surface by protein desorption. Immobilized bacterial proteins can specifically bind to other biomolecules including proteins, DNA and carbohydrates. In addition, *E. coli* was captured by the bacterial protein Colicin M (Cma), and the protein–bacterium interaction was successfully detected with SPR imaging. The sensitivity and specificity of bacterial pathogen detection was examined by measuring the binding of a mutant strain of *E. coli* and the *Lactobacillus bulgaricus* bacterium. Finally, captured bacteria on the surface underwent lysis and released the bacterial protein cyclic AMP receptor protein (CRP) that was recognized by the anti-CRP antibody and detected with SPR imaging.

5. References

- (1) Lazcka, O.; Del Campo, F. J.; Muñoz, F. X. *Biosens. Bioelectron.* **2007**, *22*, 1205–1217.
- (2) Blasco, R.; Murphy, M. J.; Sanders, M. F.; Squirrell, D. J. *J. Appl. Microbiol.* **1998**, *84*, 661–666.
- (3) Wong, Y. Y.; Ng, S. P.; Ng, M. H.; Yao, S. Z.; Fung, Y. S. *Biosens. Bioelectron.* **2002**, *17*, 676–684.
- (4) Higgins, J. A.; Nasarabadi, S.; Karns, J. S.; Shelton, D. R.; Cooper, M.; Gbakima, A.; Koopman, R. P. *Biosens. Bioelectron.* **2003**, *18*, 1115–1123.
- (5) Radke, S. M.; Alocilja, E. C. *Biosens. Bioelectron.* **2005**, *20*, 1662–1667.
- (6) Leoni, E.; Legnani, P. P. *J. Appl. Microbiol.* **2001**, *90*, 27–33.

- (7) Lazaro, D. R.; Hernandez, M.; Esteve, R.; Hoorfar, J.; Pla, M. *J. Microbiol. Methods* **2003**, *54*, 381–390.
- (8) Touron, A.; Berther, T.; Pawlak, B.; Petit, F. *Res. Microbiol.* **2005**, *156*, 541–553.
- (9) Jofré, A.; Martin, B.; Garriga, M.; Pla, M.; Rodriguez-Lázaro, D.; Aymerich, T. *Food Microbiol.* **2005**, *22*, 109–115.
- (10) Andresen, L. O.; Klausen, J.; Barfod, K.; Sorensen, K. *Vet. Microbiol.* **2002**, *89*, 61–67.
- (11) Brooks, B. W.; Devenish, J.; Lutze-Wallace, C. L.; Milnes, D.; Robertson, R. H.; Berlie-Surujballi, G. *Vet. Microbiol.* **2004**, *103*, 77–84.
- (12) Engvall, E.; Perlman, P. *Immunochemistry* **1971**, *8*, 871–874.
- (13) Deisingh, A. K.; Thompson, M.; *J. Appl. Microbiol.* **2004**, *96*, 419–429.
- (14) Perelle, S.; Dilasser, F.; Malorny, B.; Grout, J.; Hoorfar, J.; Fach, P. *Mol. Cell. Probes* **2004**, *18*, 409–420.
- (15) Lehtola, M. J.; Loades, C. J.; Keevil, C. W. *J. Microbiol. Methods* **2005**, *62*, 211–219.
- (16) Bartlett, J. M. S.; Stirling, D. *Methods Mol. Biol.* **2003**, *226*, 3–6.
- (17) <http://www.lsbu.ac.uk/biology/enztech/biosensors.html>.
- (18) Wu, P.; Brand, L. *Anal. Biochem.* **1994**, *218*, 1–13.
- (19) Grant, S. A.; Xu, J.; Bergeron, E. J.; Mroz, J. *Biosens. Bioelectron.* **2001**, *16*, 231–237.
- (20) Ko, S.; Grant, S. A. *Sens. Actuators B* **2003**, *96*, 372–378.
- (21) Fratamico, P. M.; Strobaugh, T. P.; Medina, M. B.; Gehring, A. G. *Biotechnol. Tech.* **1998**, *12*, 571–576.

- (22) Koubova, V.; Brynda, E.; Karasova, L.; Skvor, J.; Homola, J.; Dostalek, J.; Tobiska, P.; Rosicky, J. S. *Sens. Actuators B* **2001**, *74*, 100–105.
- (23) Taylor, A. D.; Yu, Q.; Chen, S.; Homola, J.; Jiang, S. *Sens. Actuators B* **2005**, *107*, 202–208.
- (24) Oh, B.-K.; Lee, W.; Chun, B. S.; Bae, Y. M.; Lee, W. H.; Choi, J.-W. *Biosens. Bioelectron.* **2005**, *20*, 1847–1850.
- (25) Brockman, J. M.; Nelson, B. P.; Corn, R. M. *Annu. Rev. Phys. Chem.* **2000**, *51*, 41–63.
- (26) Ivnitski, D.; Abdel-Hamid, I.; Atanasov, P.; Wilkins, E.; Stricker, S. *Electroanalysis* **2000**, *12*, 317–325.
- (27) Che, Y.; Li, Y.; Slavik, M. *Biosens. Bioelectron.* **2001**, *16*, 791–797.
- (28) Libby, J. M.; Wada, H. G. *J. Clin. Microbiol.* **1989**, *27*, 1456–1459.
- (29) Gehring, A. G.; Patterson, D. L.; Tu, S. I. *Anal. Biochem.* **1998**, *258*, 293–298.
- (30) Schoning, M. J.; Poghossian, A. *Analyst* **2002**, *127*, 1137–1151.
- (31) Gomez, R.; Bashir, R.; Bhunia, A. K. *Sens. Actuators B* **2002**, *86*, 198–208.
- (32) Lagally, E. T.; Scherer, J. R.; Blazej, R. G.; Toriello, N. M.; Diep, B. A.; Ramchandani, M.; Sensabaugh, G. F.; Riley, L. W.; Mathies, R. A. *Anal. Chem.* **2004**, *76*, 3162–3170.
- (33) Zaytseva, N. V.; Goral, V. N.; Montagna, R. A.; Baeumner, A. J. *Lab on a Chip* **2005**, *5*, 805–811.
- (34) Zhu, H.; Synder, M. *Curr. Opin. Chem. Biol.* **2001**, *5*, 40–45.
- (35) Wilson, D. S.; Nock, S. *Angew. Chem., Int. Ed.* **2003**, *42*, 494–500.
- (36) Tomizaki, K.; Usui, K.; Mihara, H. *ChemBioChem* **2005**, *6*, 782–799.

- (37) Seong, S.; Choi, C. *Proteomics* **2003**, *3*, 2176–2189.
- (38) Zhu, H.; Bilgin, M.; Bangham, R.; Hall, D.; Casamayor, A.; Berton, P.; Lan, N.; Jansen, R.; Bidlingmaier, S.; Houfek, T.; Mitchell, T.; Miller, P.; Dean, R. A.; Gerstein, M.; Snyder, M. *Science* **2001**, *293*, 2101–2105.
- (39) Phizicky, E.; Philippe, I. H.; Bastiaens, P. I.; Zhu, H.; Snyder, M.; Fields, S. *Nature* **2003**, *422*, 208–215.
- (40) Schweitzer, B.; Predki, P.; Snyder, M. *Proteomics* **2003**, *3*, 2190–2199.
- (41) Lueking, A.; Cahill, D. J.; Müllner, S. *Drug Discovery Today* **2005**, *10*, 789–794.
- (42) Liotta, L. A.; Espina, V.; Mehta, A. I.; Calvert, V.; Rosenblatt, K.; Geho, D.; Munson, P. J.; Young, L.; Wulfkühle, J.; Petricoin, E. M. *Cancer Cell* **2003**, *3*, 317–325.
- (43) Habb, B. B. *Curr. Opin. Biotechnol.* **2006**, *17*, 415–421.
- (44) Robinson, W. H. *Curr. Opin. Chem. Biol.* **2006**, *10*, 67–72.
- (45) Dubitsky, A.; DeCollibus, D.; Ortolano, G. A. *J. Biochem. Biophys. Methods* **2002**, *51*, 47–56.
- (46) MacBeath, G.; Schreiber, S. L. *Science* **2000**, *289*, 1760–1763.
- (47) Angenendt, P.; Glökler, J.; Konthur, Z.; Lehrach, H.; Cahill, D. J. *Anal. Chem.* **2003**, *75*, 4368–4372.
- (48) Zhu, H.; Klemic, J. F.; Chang, S.; Bertone, P.; Casamayor, A.; Klemic, K. G.; Smith, D.; Gerstein, M.; Reed, M. A.; Snyder, M. *Nat. Genet.* **2000**, *26*, 283–289.
- (49) Varnum, S. M.; Warner, M. G.; Dockendoff, B.; Anheier Jr, N. C.; Lou, J.; Marks, J. D.; Smith, L. A.; Feldhaus, M. J.; Grate, J. W.; Bruckner–Lea, C. J. *Anal. Chim. Acta* **2006**, *570*, 137–143.

- (50) Rusmini, F.; Zhong, Z.; Feijen, J. *Biomacromolecules* **2007**, *8*, 1775–1789.
- (51) Camarero, J. A. *Biopolymers* **2008**, *90*, 450–458.
- (52) Arenkov, P.; Kukhtin, A.; Gemmell, A.; Voloshchuk, S.; Chupeeva, V.; Mirzabekov, A. *Anal. Biochem.* **2000**, *278*, 123–131.
- (53) Lee, K. B.; Park, S. J.; Mirkin, C. A.; Smith, J. C.; Mrksich, M. *Science* **2002**, *295*, 1702–1705.
- (54) Frey, B. L.; Jordan, C. E.; Kornguth, S.; Corn, R. M. *Anal. Chem.* **1995**, *67*, 4452–4457.
- (55) <http://www.protein.iastate.edu/seminars/BIACore/TechnologyNotes/Technology-Brochure.pdf>
- (56) Chan, W. C.; Nie, S. *Science* **1998**, *281*, 2016–2018.
- (57) Liu, G. Y.; Amro, N. A. *Proc. Natl. Acad. Sci. U.S.A.* **2002**, *99*, 5165–5170.
- (58) Johnsson, B.; Löfås, S.; Lindquist, G. *Anal. Biochem.* **1991**, *198*, 268–277.
- (59) Yan, M.; Cai, S. X.; Wybourne, M. N.; Keana, J. F. W. *J. Am. Chem. Soc.* **1993**, *115*, 814–816.
- (60) Jiang, K.; Schadler, L.S.; Siegel, R. W.; Zhang, X.; Zhang, H. *J. Mater. Chem.* **2004**, *14*, 37–39.
- (61) Patel, N.; Davies, M. C.; Hartshorne, M.; Heaton, R. J.; Roberts, C. J.; Tendler, S. J. B.; Williams, P. M. *Langmuir* **1997**, *13*, 6485–6490.
- (62) Wacker, R.; Schröder, H.; Niemeyer, C. M. *Anal. Biochem.* **2004**, *330*, 281–287.
- (63) Jongsmä, M. A.; Litjens, R. H. G. M. *Proteomics* **2006**, *6*, 2650–2655.
- (64) Niemeyer, C. M.; Boldt, L.; Ceyhan, B.; Blohm, D. *Anal. Biochem.* **1999**, *268*, 54–63.

- (65) Lesaicherre, M L.; Lue, R. Y.; Chen, G. Y.; Zhu, Q.; Yao, S. Q. *J. Am. Chem. Soc.* **2002**, *124*, 8768–8769.
- (66) Lue, R. Y.; Chen, G. Y.; Hu, Y.; Zhu, Q.; Yao, S. Q. *J. Am. Chem. Soc.* **2004**, 1055–1062.
- (67) Sigal, G. B.; Bamdad, C.; Barberis, A.; Strominger, J.; Whitesides, G. M. **1996**, *68*, 490–497.
- (68) Thomson, N. H.; Smith, B. L.; Almqvist, N.; Schmitt, L.; Kashlev, M.; Kool, E. T.; Hansma, P. K. *Biophys. J.* **1999**, *76*, 1024–1033.
- (69) Kroger, D.; Liley, M.; Schiweck, W.; Skerra, A.; Vogel, H. *Biosens. Bioelectron.* **1999**, *14*, 155–161.
- (70) Wegner, G. J.; Lee, H. J.; Marriott, G.; Corn, R. M. *Anal. Chem.* **2003**, *75*, 4740–4746.
- (71) Lu, B.; Smyth, M. R.; O’Kennedy, R. *Analyst* **1996**, *121*, 29R–32R.
- (72) Turková, J. *J. Chromatogr. B* **1999**, *722*, 11–13.
- (73) Oh, B.-K.; Lee, W.; Chun, B. S.; Bae, Y. M.; Lee, W. H.; Choi, J.-W. *Colloids and Surfaces A: Physicochem. Eng. Aspects* **2005**, 257–258, 369–374.
- (74) Lee, S. W.; Oh, B.-K.; Sanedrin, R. G.; Salaita, K.; Fujigaya, T.; Mirkin, C. A. *Adv. Mater.* **2006**, *18*, 1133–1136.
- (75) Yu, X.; Cheng, Q. *Proteomics* **2006**, *6*, 5493–5503.
- (76) Ramanavičius, A.; Herberg, F. W.; Hutschenreiter, S.; Zimmermann, B.; Lapėnaite, I.; Kaušaitė, A.; Finkelšteinas, A.; Ramanavičienė, A. *Acta Medica Lituanica* **2005**, *12*, 1–9.
- (77) Lee, H. J., Yan, Y.; Marriott, G.; Corn, R. M. *J. Physiol.* **2005**, *563.1*, 61–71.

- (78) Rahn, J. R.; Hallock, R. B. *Langmuir* **1995**, *11*, 650–654.
- (79) Jung, L. S.; Shumaker-Parry, J. S.; Campbell, C. T.; Yee, S. S.; Gelb, M. H. *J. Am. Chem. Soc.* **2000**, *122*, 4177–4184.
- (80) Kanda, V.; Kariuki, J. K.; Harrison, D. J.; McDermott, M. T. *Anal. Chem.* **2004**, *76*, 7257–7262.
- (81) Bondeson, K.; Frostell–Karlsson, A.; Fagerstam, L.; Magnusson, G. *Anal. Chem.* **1993**, *214*, 245–251.
- (82) Brockman, J. M.; Frutos, A. G.; Corn, R. M. *J. Am. Chem. Soc.* **1999**, *121*, 8044–8051.
- (83) Peterlinz, K. A.; Georgiadis, R. M.; Herne, T. M.; Tarlov, M. J. *J. Am. Chem. Soc.* **1997**, *119*, 3401–3402.
- (84) He, L.; Musick, M. D.; Nicewarner, S. R.; Salinas, F. G.; Benkovic, S. J.; Natan, M. J.; Keating, C. D. *J. Am. Chem. Soc.* **2000**, *122*, 9071–9077.
- (85) Goodrich, T. T.; Lee, H. J.; Corn, R. M. *J. Am. Chem. Soc.* **2004**, *126*, 4086–4087.
- (86) Goodrich, T. T.; Lee, H. J.; Corn, R. M. *Anal. Chem.* **2004**, *76*, 6173–6178.
- (87) Smith, E. A.; Thomas, W. D.; Kiessling, L. L.; Corn, R. M. *J. Am. Chem. Soc.* **2003**, *125*, 6140–6148.
- (88) Kanda, V.; Kitov, P.; Bundle, D. R.; McDermott, M. T. *Anal. Chem.* **2005**, *77*, 7497–7504.
- (89) Smith, E. A.; Corn, R. M. *Appl. Spectrosc.* **2003**, *57*, 320A–332A.
- (90) Raether, H. *Springer Tracts in Modern Physics* **1988**, *111*, 1–133.
- (91) Johnson, P. B.; Christy, R. W. *Phys. Rev. B* **1972**, *6*, 4370–4379.
- (92) Kretschmann, E.; Raether, H.; *Naturforsch., Z. A: Phys. Sci.* **1968**, *23*, 2135–2136.

- (93) Kanda, V. In *Analytical Methods for the Investigation of Adsorbed Protein Films at Chemically Modified Surfaces*; University of Alberta, Ed.; Edmonton, AB, **2004**, pp60–88.
- (94) Nelson, B. P.; Grimsrud, T. G.; Liles, M. R.; Goodman, R. M.; Corn, R. M. *Anal. Chem.* **2001**, *73*, 1–7.
- (95) Shumaker-parry, J. S.; Campbell, C. T. *Anal. Chem.* **2004**, *76*, 907–917.
- (96) Steiner, G.; Sablinskas, V.; Hübner, A.; Kuhne, C.; Salzer, R. *J. Mol. Structure* **1999**, *509*, 265–273.
- (97) Evans, S. D.; Allinson, H.; Boden, N.; Flynn, T. M.; Henderson, J. R. *J. Phys. Chem. B* **1997**, *101*, 2143–2148.
- (98) Wegner, G. J.; Lee, H. J.; Corn, R. M. *Anal. Chem.* **2002**, *74*, 5161–5168.
- (99) Goodrich, T. T.; Lee, H. J.; Corn, R. M. *Anal. Chem.* **2004**, *76*, 6173–6178.
- (100) Nikitin, P. I.; Beloglazov, A. A.; Kochergin, V. E.; Valeiko, M. V.; Ksenevich, T. I. *Sens. Actuators B* **1999**, *54*, 43–50.
- (101) Li, Y.; Wark, A. W.; Lee, H. J.; Corn, R. M. *Anal. Chem.* **2006**, *78*, 3158–3164.
- (101) Okumura, A.; Sato, Y.; Kyo, M.; Kawaguchi, H. *Anal. Biochem.* **2005**, *339*, 328–337.
- (102) Wink, S.; van Zuiken, S. J.; Bult, A.; van Bennekom, W. P. *Anal. Chem.* **1998**, *70*, 827–832.
- (103) Nedelkov, D.; Nelson, R. W. *Methods Mol. Biol.* **2006**, *328*, 131–139.
- (104) Vareiro, M. M. L. M.; Liu, J.; Knoll, W.; Zak, K.; Williams, D.; Jenkins, A. T. A. *Anal. Chem.* **2005**, *77*, 2426–2431.
- (105) Corn, R. M.; Philpott, M. R. *J. Chem. Phys.* **1984**, *80*, 5245–5249.

Chapter II

Bioaffinity Immobilization of Proteins for Surface Plasmon Resonance Imaging

1. Introduction

Protein immobilization on a solid surface is one of the crucial issues in a number of research areas, such as protein microarrays¹⁻³ and biosensors.⁴⁻⁶ To enhance interactions of immobilized proteins with ligands in solution, the orientation of proteins on the surface needs to be well controlled.^{7,8} As mentioned in Chapter I, bioaffinity immobilization has the potential to offer oriented attachment of proteins on the surface, which allows to improve the accessibility of protein active sites.⁹⁻¹⁴ A variety of strategies have recently been developed for bioaffinity immobilization of proteins based on chemical or biological interactions, including avidin–biotin,¹⁵⁻¹⁹ histidine–nickel,²⁰⁻²⁵ antigen–antibody,²⁶⁻²⁹ and protein–protein (e.g., protein A or protein G) interactions.³⁰⁻³⁴ Since these interactions are selective and non-covalent, target proteins are site-specifically bound on the surface and can be easily removed from the surface. Thus, the regenerated surface could be reused for subsequent experiments.

In recent years, self-assembled monolayers (SAMs) have been widely utilized to modify solid surfaces for immobilization of biomolecules.³⁵⁻³⁷ For a gold substrate, the spontaneous adsorption of alkanethiols can result in a highly ordered and densely packed

layer on the gold surface.³⁸ Moreover, the use of ω -functionalized alkanethiols provides a variety of active surface groups that can interact with functional groups of proteins. Since poly(ethylene glycol) (PEG) groups have shown the ability to resist protein binding, they are often incorporated into alkanethiols to minimize nonspecific protein adsorption.^{39–41} In addition, mixed SAMs have been developed to avoid nonspecific protein adsorption and steric hindrance between proteins and ligands. Sigal et al.²¹ prepared mixed SAMs by immersing gold into a mixture of two different alkanethiols. One alkanethiol was terminated with a nitrilotriacetic acid (NTA) group, and the other was terminated with a PEG group. Histidine-tagged proteins were specifically bound to the mixed SAM through the affinity interaction between histidine and NTA–Ni²⁺ complex. Protein adsorption and interaction with antibodies were characterized with surface plasmon resonance (SPR). Their results showed that immobilized proteins exhibited a greater ability to bind antibodies than covalent attachment.

SPR is an optical detection technique that is commonly employed to monitor the adsorption and interactions of biomolecules on metal surfaces (e.g., Au, Ag).^{42–46} The widespread application of SPR biosensors is attributed to the following advantages: (1) no labeling step is required to detect biomolecular binding on the surface; (2) the kinetics of biomolecular interactions can be measured in real time; (3) high sensitivity allows to identify biomolecules in a relatively low concentration.⁴⁴ SPR imaging is one format of SPR, which detects a change of reflectivity after adsorption at fixed angle and

wavelength. This method combines the advantages of traditional SPR with high-throughput capabilities, and therefore offers important information about biomolecular interactions in an array format.⁴⁷ To date, a variety of biomolecular interactions have been investigated with SPR imaging, including protein–protein,^{48,49} protein–DNA,^{50,51} DNA hybridization,^{52,53} DNA–RNA,^{53,54} peptide–protein⁵⁵ and protein–carbohydrate interactions.^{56,57}

In this chapter, we present a simple method for bioaffinity immobilization of His₆-tagged proteins on a gold surface modified with NTA–Ni²⁺ species. The formation of NTA monolayers on the gold surface was characterized by infrared reflection absorption spectroscopy (IRRAS). SPR imaging studies were performed to quantify immobilization of His₆-tagged protein on various mixed monolayers. Moreover, the kinetics of protein adsorption and desorption was investigated in real time. In addition, the regeneration of SPR chips can be achieved by treatment with several regenerating agents.

2. Experimental

2.1. Materials

1,9-Nonanedithiol, 11-mercapto-1-undecanol (MUO) and bovine serum albumin (BSA) were purchased from Sigma–Aldrich (St. Louis, MO). *N*-[5-(3'-Maleimido-

propylamido)-1-carboxypentyl]iminodiacetic acid, disodium salt (maleimido-C₃-NTA) was obtained from Dojindo Laboratories (Kumamoto, Japan). Tridecafluoro-1,1,2,2-tetrahydrooctyl-1-dimethylchlorosilane was purchased from United Chemical Technologies (Bristol, PA). (1-Mercaptoundec-11-yl)tri(ethylene glycol) methyl ether (EG3-OMe) was obtained from ProChimia (Gdansk, Poland). *E. coli* cyclic AMP receptor protein (CRP, 22.5 kDa) and colicin M (Cma, 27.0 kDa) were fused with His₆-tags by Glen Zhang in the laboratory of Professor Joel Weiner (Biochemistry Department, University of Alberta). Tris buffers were used to prepare His₆-tagged CRP and His₆-tagged Cma. For His₆-tagged CRP, the buffer contained 50 mM Tris-HCl (pH 7.8) and 100 mM KCl. For His₆-tagged Cma, the buffer was composed of 25 mM Tris-HCl (pH 7.4), 150 mM NaCl and 0.1% Triton X-100. 0.1% BSA was diluted in phosphate-buffered saline (PBS, pH 7.4), consisting of 8.1 mM Na₂HPO₄, 1.5 mM KH₂PO₄, 137 mM NaCl and 2.7 mM KCl.

2.2. Fabrication of Gold Substrates

To be used for IRRAS studies, microscope slides (Propper Manufacturing Co., Long Island City, NY) were soaked into freshly made piranha solution (3:1 H₂SO₄-H₂O₂) for 1 h, thoroughly washed with 18 MΩ Nanopure water (Barnstead International, Dubuque, IA) and dried by argon gas. 5 nm Cr and 200 nm Au were sequentially coated

on the slides with the thermal evaporation (Torr International Inc., New Windsor, NY). To prepare SPR chips, SF-10 glass slides (Schott Glass, Toronto, ON) were immersed into piranha solution for at least 30 min, then rinsed by 18 M Ω water and dried with argon gas. The clean glass were deposited with tridecafluoro-1,1,2,2-tetrahydrooctyl-1-dimethylchlorosilane under reduced pressure for 12 h. The purpose of this step is to create a hydrophobic background on the glass, which can facilitate spotting of aqueous solutions. After insertion into a home-built shadow mask, 1 nm Cr and 45 nm Au were coated onto the glass chips using the thermal evaporation. The resulting SPR chips contained nine separate gold spots surrounded by the hydrophobic background. Consequently, different aqueous solutions of analytes can be confined to an individual gold spot without any cross contamination.

2.3. Generation of NTA Monolayers

To form NTA monolayers on a gold surface, a compound thiol-functionalized NTA (tNTA) was produced by the reaction of maleimide-C₃-NTA (10 mg, 20 μ mol) with 1,9-nonanedithiol (8 μ L, 40 μ mol) in 1 mL DMSO. Triethylamine (Et₃N) was added dropwise into the reaction mixture until pH was \sim 8. After the reaction was carried out at room temperature for 12 h, the solvent DMSO was removed by rotary evaporation under reduced pressure, and a Sepak-C18 cartridge (Waters Corp., Milford, MA) was used to

purify the product tNTA (8.8 mg, 64%). ^1H NMR and mass spectra were collected to confirm the identification of tNTA. A gold slide coated with 5 nm Cr and 200 nm Au was cleaned by piranha solution for 30 min, rinsed with 18 M Ω water and dried under a stream of argon gas. The gold surface was then exposed to an aqueous solution of 1 mM purified tNTA at room temperature for 3–4 h to create NTA monolayers.

2.4. Infrared Reflection Absorption Spectroscopy (IRRAS)

IRRAS spectra were recorded using a VERTEX 70 FT-IR spectrometer (Bruker Optics Inc., Billerica, MA) equipped with a mercury-cadmium-telluride (HgCdTe) detector. The SeagullTM (Harrick Scientific Products, Pleasantville, NY) was employed as a variable angle reflection accessory to adjust *p*-polarized light incident at 80° on a substrate surface. A bare gold surface was chosen for the reference. Before scanning the spectra, substrate surfaces were purged with an atmosphere of nitrogen for 15 min in order to minimize the interference of water or carbon dioxide from air. IRRAS spectra were collected by 1000 scan times at a resolution of 4 cm⁻¹, an aperture setting of 6 mm and a beam splitter of KBr. The software OPUSTM version 5.5 was utilized to analyze the IRRAS spectra.

2.5. SPR Imaging

SPR imaging measurements were performed using an SPR imager (GWC Technologies, Madison, WI). This instrument employed an incoherent white light and a polarizer to generate *p*-polarized light, which was coupled into the backside of the gold film through an SF-10 prism. The incident angle was manipulated by the rotation stage where a sample assembly (i.e., prism/thin gold film) was placed. A liquid flow cell was attached to the sample assembly for the introduction of any desired solution to a SPR chip. The reflected light was selected by a narrow band-pass filter ($\lambda = 830$ nm), and then detected with a CCD camera. The software Digital Optics V++ 4.0 was used to collect and analyze SPR images that were the results of averaging 100 frames.

2.6. Immobilization of His₆-Tagged Proteins

To attach His₆-tagged proteins on a gold surface, a SPR chip was first cleaned by oxidization with an UV–Ozone cleaner (Jelight Company Inc., Irvine, CA) for 5 min to remove any organic residue from the gold surface. The chip was then rinsed with 18 M Ω water and dried under a stream of argon gas. An aqueous solution of tNTA (2 μ L, 1 mM) was directly delivered onto some of gold spots using a micropipette, and the rest on the chip were treated with a solution of 11-mercapto-1-undecanol (MUO) (2 μ L, 1 mM). The gold chip with solutions was stored in a humid container at room temperature overnight to create NTA and MUO monolayers on the surface. Since the MUO monolayer has been

proved to resist nonspecific protein adsorption,⁵⁸ it was used as a negative control for protein immobilization. Following the preparation of NTA monolayers, 100 mM NaOH was added on the NTA monolayer to deprotonate carboxylic acids ($-\text{COOH}$) of NTA groups, and then 50 mM NiSO_4 was introduced to the surface for coordination with deprotonated NTA groups to afford an NTA- Ni^{2+} -terminated surface. Once the gold chip was rinsed with 18 M Ω water and mounted into the SPR imager, Tris buffer was injected onto the surface for 5 min followed by the addition of a His₆-tagged protein solution for 10 min. After protein adsorption, the surface was immediately washed by Tris buffer for 5 min to remove nonspecifically bound protein.

3. Results and Discussion

3.1. Formation and Characterization of NTA Monolayers

In recent years, several methods have been developed for the formation of NTA monolayers on gold surfaces, which can be used to immobilize histidine-tagged proteins for SPR measurements.²¹⁻²³ Sigal et al.²¹ synthesized an NTA-terminated thiol that was reacted with gold to create NTA monolayers. The SPR studies showed that efficient immobilization of active histidine-tagged proteins was achieved on the gold surface. However, the synthetic procedure used to produce NTA groups conjugated with alkanethiols was laborious and complicated. Wegner et al.²² employed a series of surface

reactions to prepare NTA monolayers on the gold surface. These monolayers were utilized to anchor histidine-tagged proteins in an array format for monitoring antigen–antibody and protein–DNA interactions with SPR imaging. While this method offered functional NTA monolayers, the use of surface reactions made it difficult to control the surface density of NTA groups. The IRRAS results showed a rather low coverage of NTA groups on the surface.

In this chapter, we present a facile method that only involves one-step synthesis of thiol-functionalized NTA (tNTA) from commercially available starting materials. The reaction scheme used for tNTA preparation is shown in Figure 2.01. The reagent maleimido- C_3 -NTA is mixed with 1,9-nonanedithiol in a molar ratio of 1:2. Each molecule of 1,9-nonanedithiol can undergo the Michael addition reaction with one or two maleimide- C_3 -NTA to give a mono-reacted (i.e., tNTA) or di-reacted product. Since 1,9-nonanedithiol is excessive in the reaction mixture, the mono-reacted product is expected to be dominant after the reaction is completed. Thus, when a gold substrate is treated with the reaction mixture, only the mono-reacted product and the remaining 1,9-nonanedithiol can adsorb to the surface.

We initially formed NTA monolayers by simply exposing a gold surface to the reaction mixture described in Figure 2.01 for 3–4 h. The resulting monolayers were then characterized by IRRAS with a representative spectrum I in Figure 2.02 A. The band frequencies and possible assignments are summarized as follows: the bands at 1778 and

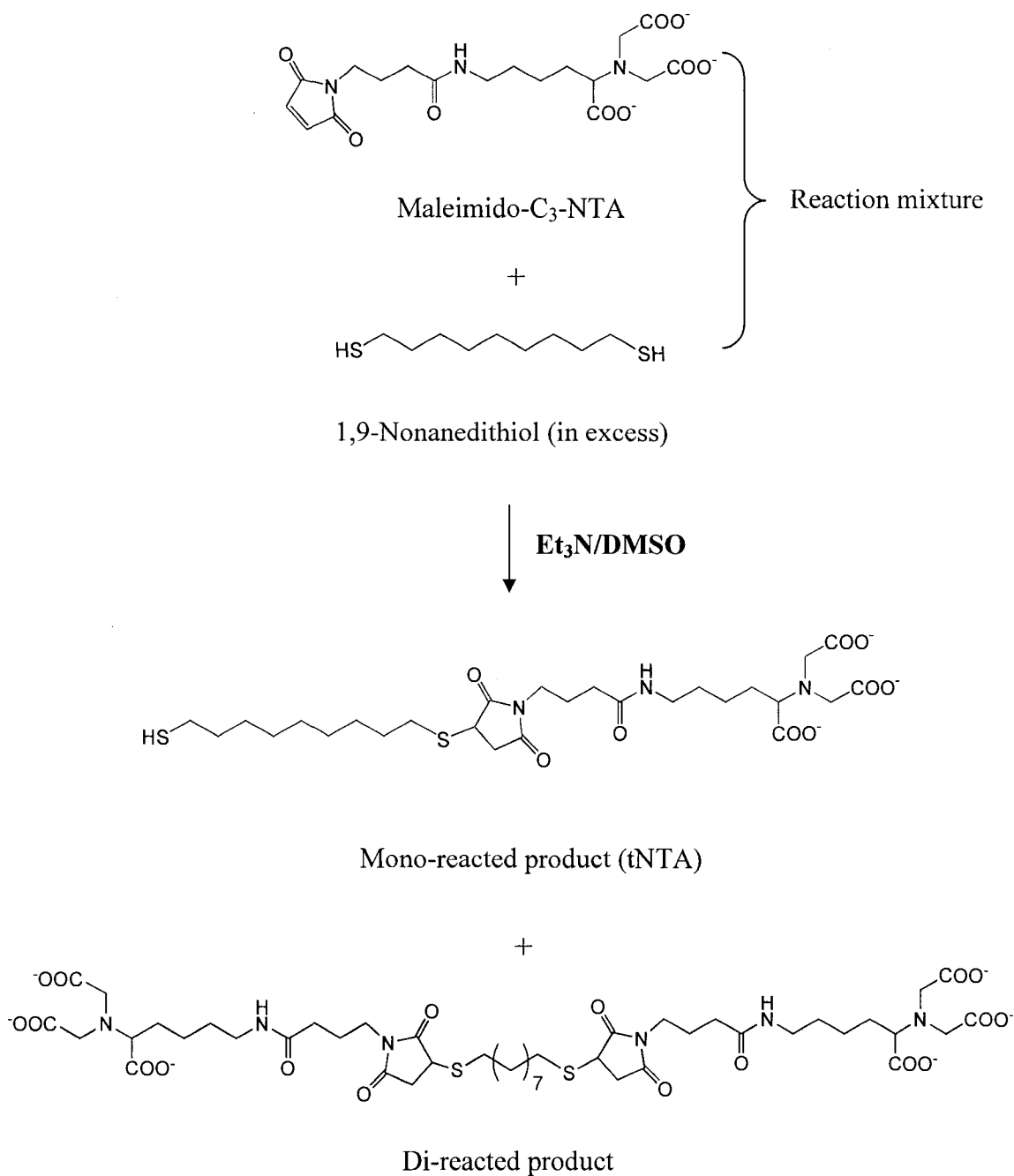


Figure 2.01. Synthesis of thiol-functionalized NTA (tNTA). Maleimido-C₃-NTA was reacted with 1,9-nonanedithiol in DMSO and the molar ratio was 1:2. Two possible compounds were produced in the reaction, which included the mono-reacted product and di-reacted product.

1710 cm^{-1} are attributed to the symmetric and asymmetric C=O stretch of the maleimide ring, respectively; the band at 1648 cm^{-1} arises from the C=O stretch of the amide bond linkage; the bands at 1400 and 1164 cm^{-1} are assigned to the C–N–C stretch of the maleimide ring and the C–N stretch of the NTA group, respectively. It is evident from Figure 2.02 A that monolayers of NTA groups were easily formed by incubating the gold surface into the reaction mixture of 1,9-nonanedithiol and maleimide- C_3 -NTA. However, the remaining 1,9-nonanedithiol was also a possible component of the resulting monolayers.

To obtain a pure monolayer of NTA groups, we isolated the product tNTA from the reaction mixture by passage through a Sepak-C18 cartridge. Monolayers were then created from an aqueous solution of purified tNTA, and identified with IRRAS spectrum II in Figure 2.02 A. Compared to spectrum I taken from monolayers formed in the reaction mixture, spectrum II contains all the bands characteristic of NTA groups, revealing the formation of NTA monolayer on the gold surface. Moreover, the band intensities in spectrum II are greater than spectrum I, which implies that a higher coverage of NTA groups was achieved on the gold surface. The increase in surface density of NTA groups can be attributed to the removal of excessive 1,9-nonanedithiol from the reaction mixture.

In addition, Figure 2.02 B illustrates the C–H stretching region in the IRRAS spectrum of NTA monolayers produced from the purified tNTA solution. The band at

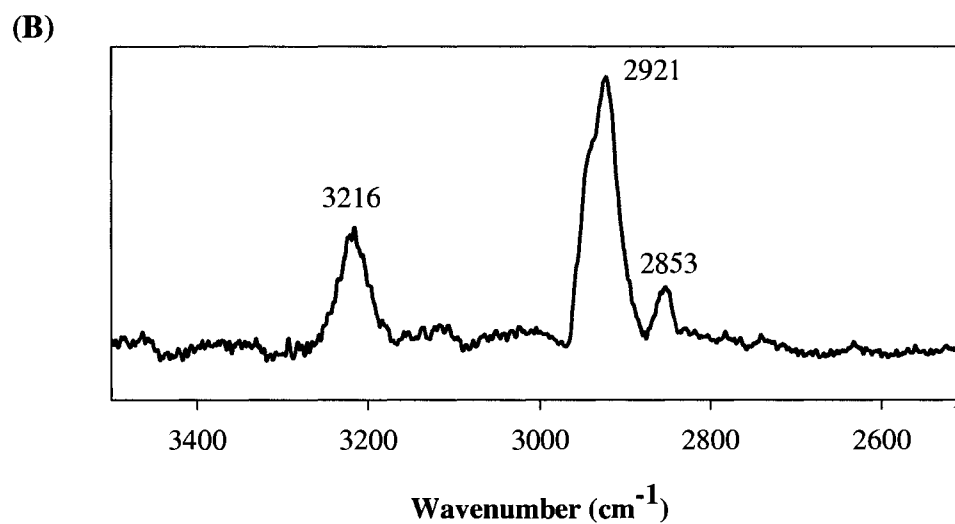
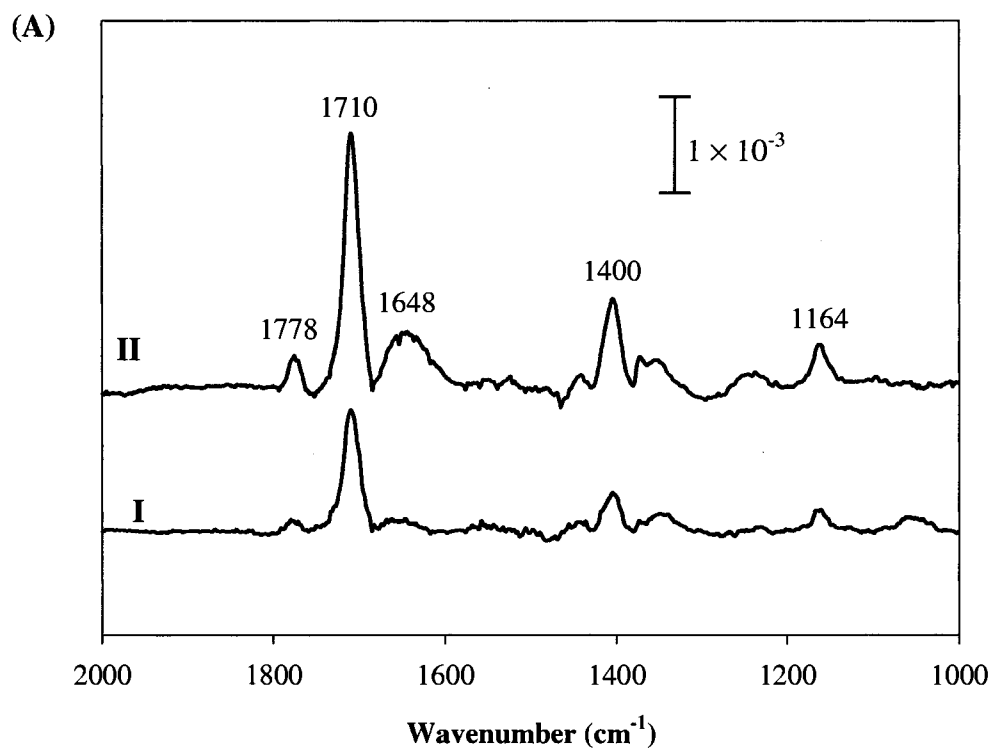


Figure 2.02. IRRAS spectra of NTA monolayers on gold surfaces. (A) Spectrum I was recorded from the reaction mixture and spectrum II taken after tNTA purification. (B) IRRAS spectrum showed the C–H stretching region of NTA monolayers formed from purified tNTA.

3216 cm^{-1} is probably from the N–H stretch of the amide bond linkage. The bands at 2921 and 1853 cm^{-1} correspond to the asymmetric and symmetric C–H stretch of the long alkanethiol chain ($n = 9$), respectively, suggesting that monolayers of NTA groups were fairly ordered and densely packed on the gold surface.⁵⁹ SPR imaging studies of His₆-tagged protein adsorption and interactions were performed on this relatively ideal interface.

3.2. Preparation and Characterization of Mixed Monolayers

We have also optimized the coverage of NTA groups on gold surfaces via the formation of mixed monolayers of tNTA and 11-mercapto-1-undecanol (MUO). MUO is a hydroxyl-terminated molecule that has the ability to resist nonspecific protein adsorption. His₆-tagged proteins strongly bind to NTA monolayers through the affinity interaction between His₆-tags and NTA groups in the presence of Ni²⁺ ions on the surface. Therefore, the surface density of immobilized His₆-tagged proteins can be controlled by varying the mole ratio of tNTA and MUO in solution.

Three mixtures of tNTA and MUO were prepared in the mole ratio of 20/80, 50/50 and 80/20. Gold surfaces were reacted with these mixtures to create mixed monolayers that were characterized by IRRAS. Figure 2.03 A shows IRRAS spectra taken from the pure NTA monolayer and three mixed monolayers. It was observed that all the spectra

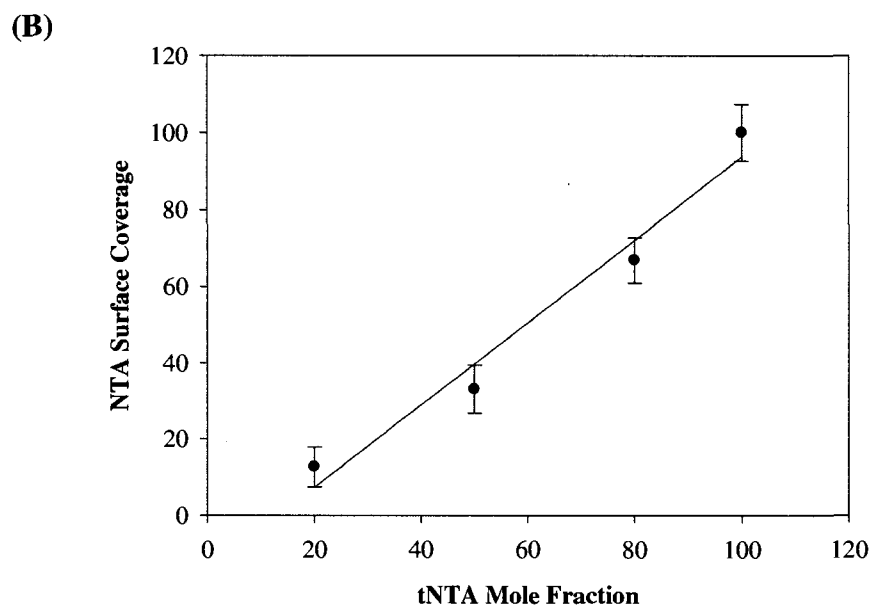
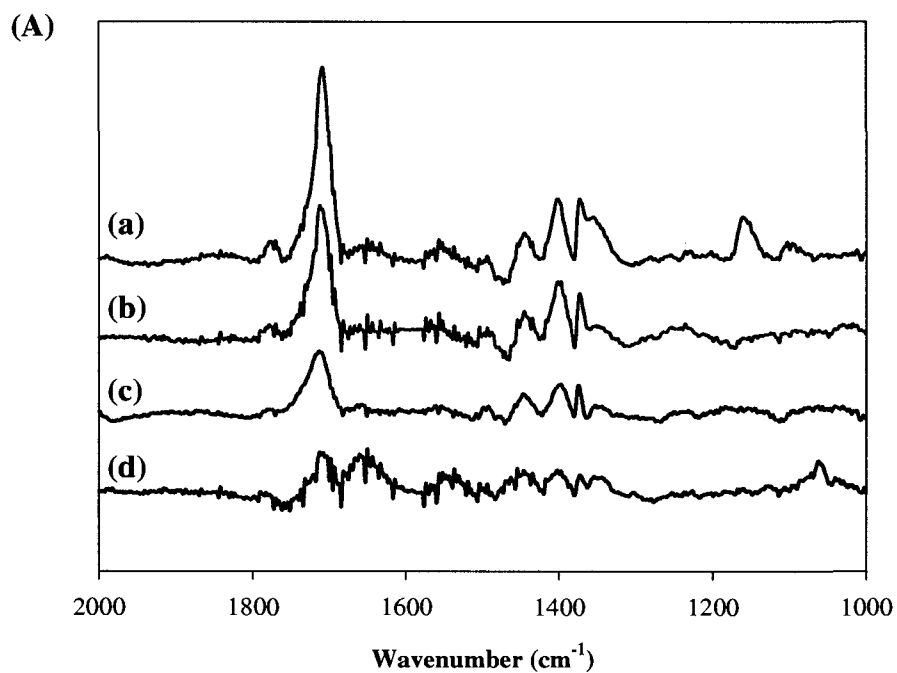


Figure 2.03. (A) IRRAS spectra of NTA monolayers formed from the following solutions: (a) pure tNTA; (b) 80/20 tNTA/MUO; (c) 50/50 tNTA/MUO and (d) 20/80 tNTA/MUO. (B) Plot of surface coverage of NTA groups as a function of tNTA mole fraction in tNTA/MUO mixture. The solid line is the fit using a linear least squares program with $R^2 = 0.97$.

contained similar bands that were diagnostic for NTA groups. The intensity of the bands increased when the mole fraction of tNTA was increased in the mixture of tNTA and MUO. And the pure tNTA solution gave a NTA monolayer with the highest IRRAS absorption. To quantify the surface density of NTA groups with the mole fraction of tNTA in solution, it was assumed that pure tNTA provided a complete monolayer of NTA groups on a gold film. The band intensity at 1710 cm^{-1} was used as a diagnostic for the density of NTA groups on the surface. The band intensity of 20/80, 50/50 and 80/20 tNTA/MUO was normalized relative to that of pure tNTA, and the resulting data were plotted as a function of the tNTA mole fraction in solution (Figure 2.03B). It is evident from the figure that NTA surface coverage was greater when the mole fraction of tNTA was increased in solution.

3.3. Bioaffinity immobilization of His₆-Tagged Proteins

The orientation of immobilized proteins on surfaces must be well controlled in order to maintain protein biological activity. Figure 2.04 depicts the surface modification scheme used to immobilize His₆-tagged proteins on gold surfaces. First, a gold surface was incubated in an aqueous solution of purified tNTA to form NTA monolayers. Secondly, a solution containing Ni²⁺ ions was introduced to the NTA-modified surface, and the Ni²⁺ ion was strongly coordinated with the NTA group to produce an NTA–Ni²⁺-

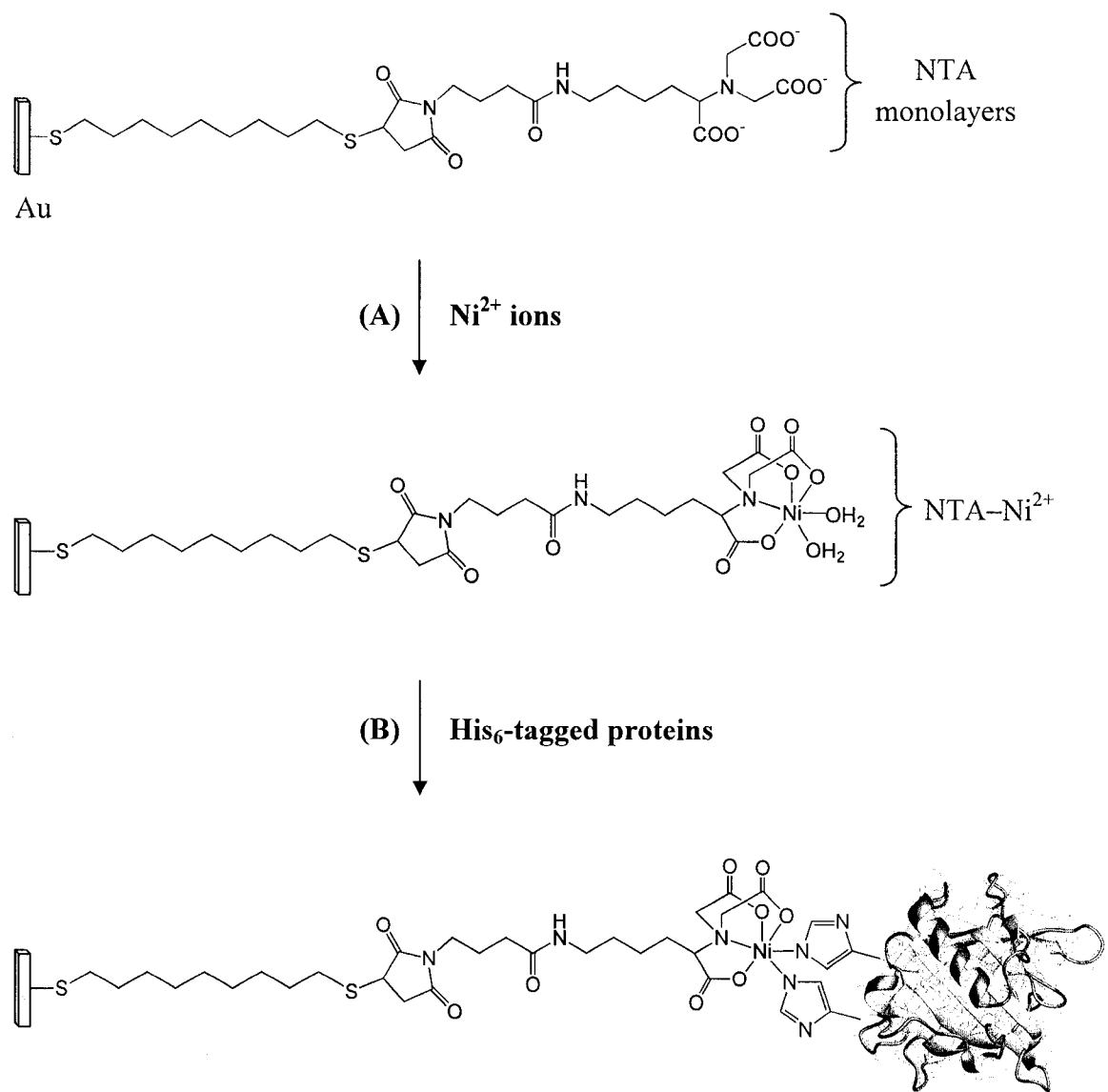


Figure 2.04. Scheme of His₆-tagged protein immobilization on the gold surface with NTA monolayers. (A) NTA monolayers were coordinated with Ni²⁺ ions to form an NTA-Ni²⁺ complex. (B) His₆-tagged proteins were specifically immobilized on the surface via the affinity interaction between NTA-Ni²⁺ and His₆-tag.

terminated monolayer. Thirdly, a protein fused with a His₆-tag was anchored to the monolayer of NTA–Ni²⁺ through bioaffinity interaction between histidines and NTA–Ni²⁺ complexes. Since the His₆-tag was genetically engineered to the C- or N-terminus of the protein, the specific interaction of the His₆ tag with NTA–Ni²⁺ species allows His₆-tagged proteins to be immobilized in well-defined orientation.

SPR imaging was used to characterize bioaffinity immobilization of His₆-tagged proteins on NTA monolayers. In this work, *E. coli* cyclic AMP receptor protein (CRP) was used as a model protein, which was labeled with a His₆-tag at the N-terminus. Figure 2.05 shows a SPR difference image, providing SPR signals for His₆-tagged CRP adsorption on the gold surface. This difference image was obtained by subtracting the image taken before protein adsorption from the image taken after the addition of a 2 μM His₆-tagged CRP solution. It is clear from Figure 2.05 that a significant SPR response was observed on pure NTA monolayers and mixed monolayers. In contrast, the signal on either MUO or EG3-OMe^{60,61} monolayers was very low due to little nonspecific protein binding. The SPR results suggest that the affinity interaction between His₆-tags and NTA–Ni²⁺ groups was very specific, and confirm that NTA groups must be present on the surface for bioaffinity immobilization of His₆-tagged proteins.

To quantify His₆-tagged protein adsorption in Figure 2.05, Table 2.1 lists SPR signals observed on various monolayers. The software V++ 4.0 was used to calculate SPR signals and the corresponding standard deviations. First, a region of interest (ROI)

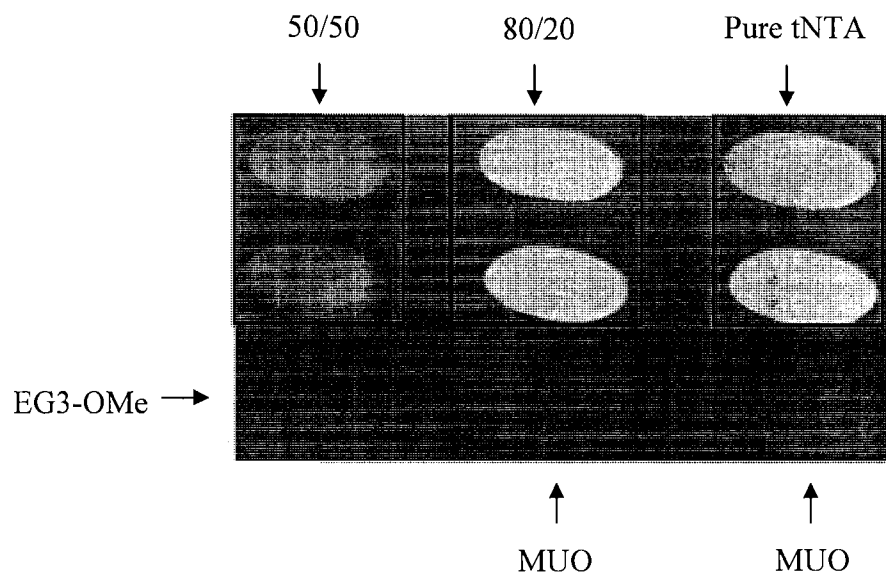


Figure 2.05. SPR difference image of 2 μM His₆-tagged CRP immobilization on the gold surface containing monolayers prepared from 50/50 tNTA/MUO, 80/20 tNTA/MUO, pure tNTA, EG3-OMe and MUO. Monolayers of EG3-OMe and MUO served as negative controls to avoid nonspecific protein adsorption.

| Monolayers | SPR signal ($\Delta\%R$) |
|-------------------|--|
| Pure tNTA | 22.7 (1.2) |
| 80/20 tNTA/MUO | 25.3 (1.2) |
| 50/50 tNTA/MUO | 11.6 (1.8) |
| EG3-OMe | 1.2 (0.2) |
| MUO | 1.1 (0.7) |

Table 2.1. SPR signals ($\Delta\%R$) for 2 μM His₆-tagged CRP adsorption on the gold surface with various monolayers shown in Figure 2.05. Numbers in parentheses are standard deviations of the indicated values.

was selected on each spot. The signal and standard deviation were the results of averaging all the pixels in the ROI. If two or more spots contained the same monolayer, the SPR signal was the average of the signals on the individual spots. As shown in Table 1, the mixed monolayer of 80/20 tNTA/MUO offered the highest SPR signal for protein adsorption. Compared to the negative controls MUO and EG3-OMe, much greater signals were observed on both pure tNTA and 50/50 tNTA/MUO monolayers. While IRRAS results indicate that pure tNTA solution yielded more NTA monolayers on the surface, less immobilization of proteins was actually obtained in comparison with 80/20 tNTA/MUO. One possible explanation is that on the complete NTA monolayer, some NTA groups can interact with adjacent NTA groups, resulting in a lower number of active NTA groups for immobilization of His₆-tagged proteins. In contrast, the mixed monolayer of 80/20 tNTA/MUO provided an optimal binding of His₆-tagged proteins due to more NTA groups accessible for protein immobilization. The mixed monolayer of 50/50 tNTA/MUO immobilized less His₆-tagged protein to the surface because it had a lower surface coverage of NTA groups than pure tNTA.

Nonspecific adsorption of His₆-tagged protein on NTA monolayers was also examined using SPR imaging. In this study, a solution of His₆-tagged colicin M (Cma, 2 μM) was introduced to NTA monolayers in the absence of Ni²⁺ ions, and the SPR signal was collected after protein adsorption was attributed to nonspecific protein binding. Figure 2.06 shows an overlay of two SPR sensorgrams, providing a comparison of His₆-

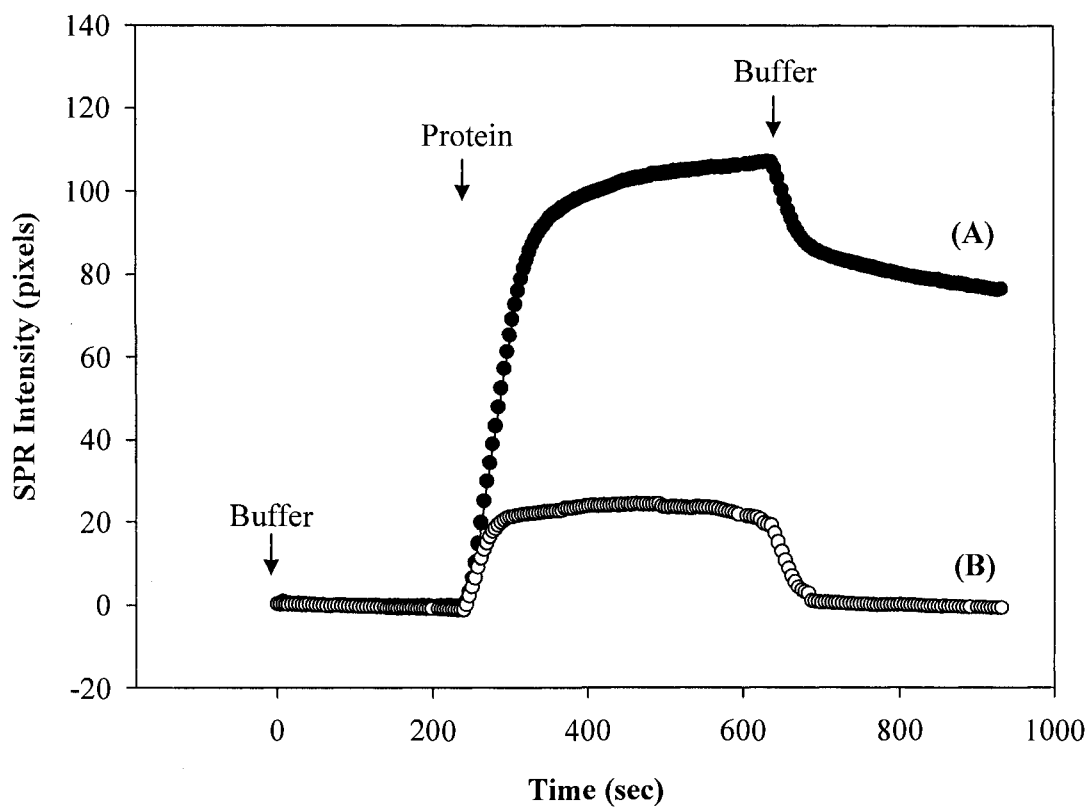


Figure 2.06. SPR sensorgrams of His₆-tagged Cma adsorption to NTA monolayers: (A) in the presence of Ni²⁺ ions; (B) in the absence of Ni²⁺ ions. The gold surface was sequentially treated with Tris buffer, 2 μM His₆-tagged Cma and Tris buffer.

tagged Cma adsorption to NTA monolayers with and without Ni^{2+} ions present on the surface. In Sensorgram A, a high SPR signal resulted from His₆-tagged protein immobilization was observed on an NTA- Ni^{2+} -modified surface. In contrast, Sensorgram B illustrates a minimal SPR signal obtained for protein adsorption on an NTA monolayer in the absence of Ni^{2+} ions. These results demonstrate that bioaffinity immobilization of His₆-tagged proteins on NTA monolayers requires the presence of Ni^{2+} ions on the surface.

To further characterize and control protein immobilization, the binding of His₆-tagged proteins on NTA monolayers was measured at various concentrations of protein solution. Prior to the immobilization of His₆-tagged proteins, NTA monolayers were sequentially treated with 100 mM NaOH and 50 mM NiSO_4 to produce an NTA- Ni^{2+} complex on gold surfaces. 0.1% BSA solution was used to block the surface for prevention of nonspecific protein adsorption.⁶² The SPR chip was exposed to a series of His₆-tagged Cma solutions from low to high concentrations. Each solution was allowed to sit on the surface for 10 min. Tris buffer was used to wash the surface for 5 min before and after protein immobilization. Figure 2.07 plots the SPR signal versus the concentration of His₆-tagged Cma solution. It is evident from the figure that the amount of adsorbed protein increased sharply at a low protein concentration and gradually reached a plateau at a high concentration, where the NTA-modified surface may be saturated with protein molecules. Since some of the $\Delta\%R$ values are more than 20%, they

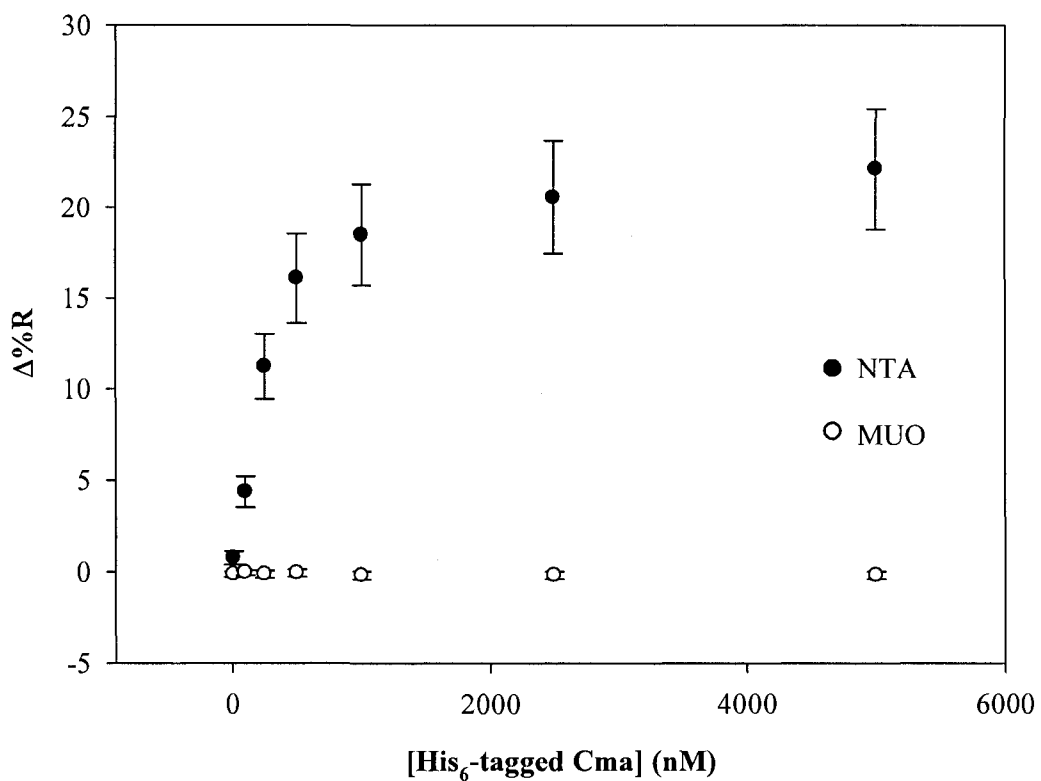


Figure 2.07. Plot of $\Delta\%R$ of protein adsorption versus His₆-tagged Cma concentration in solution. The error bars represent the average standard deviation of SPR signals over six-spot measurements. MUO monolayers were negative controls to prevent nonspecific protein binding.

are not linear with the number of proteins immobilized on the surface (see Chapter I). So we chose not to fit the data in Figure 2.07 with a binding curve model (e.g., Langmuir). However, the coverage of protein immobilized on NTA monolayers can still be controlled by varying the concentration of His₆-tagged protein in solution, which may affect the interaction of the adsorbed protein with other biomolecules. In addition, Figure 2.07 shows that the SPR response on MUO monolayers was very low at all the concentrations of protein solution, which demonstrates that MUO monolayers can successfully resist protein adsorption.

3.4. Desorption of His₆-Tagged Proteins and Regeneration of NTA Monolayers

The purpose of developing an immobilization method is to investigate the interaction of bound protein with other biomolecules in solution. Therefore, the His₆-tagged protein adsorbed on NTA monolayers must be relatively stable for a period of time. Our studies indicate that ~ 90% of His₆-tagged Cma remained on the NTA monolayer after Tris buffer was flowed over the surface for 1 h. Although the desorption of His₆-tagged proteins from the NTA monolayers is very slow, the use of some reagents, including imidazole, EDTA and Ni²⁺ ions, can easily dissociate His₆-tagged proteins from the surface in a very short time. As a result of protein desorption, the NTA-modified surface can be regenerated and reused for multiple experiments.

Imidazole is a reagent that has been commonly used to remove His₆-tagged proteins from an NTA-modified surface.^{21,63} Imidazole is a similar ligand to histidine, and a high concentration of imidazole can displace His₆-tagged proteins by coordinating with Ni²⁺ ions on the surface. Figure 2.08 shows a plot of the percentage of dissociated His₆-tagged CRP versus imidazole concentration. It is observed that the amount of His₆-tagged protein desorbed from the surface increased quickly with increasing imidazole concentration from 10 to 50 mM, and then gradually reached a plateau at 200 mM imidazole. These results prove that imidazole can efficiently dissociate His₆-tagged proteins from the NTA monolayer, and ~ 91% of the immobilized His₆-tagged protein was dissociated from the surface at 200 mM imidazole. When imidazole concentration was increased to 500 mM, no more His₆-tagged protein was desorbed from the surface. This observation suggests that the remaining protein on the surface may bind to more than one Ni²⁺ ion and can resist the imidazole competition.

Protein desorption with imidazole results in the regeneration of NTA monolayers so that other His₆-tagged proteins can be immobilized on the regenerated surface. As a chelating agent, one His₆-tag can replace two imidazole molecules to coordinate with a NTA–Ni²⁺ complex on the surface. A total increase in the number of molecules involved in this displacement reaction leads to an increase in entropy. Figure 2.09 illustrates three cycles of His₆-tagged CRP immobilization followed by protein dissociation with imidazole. The amount of immobilized His₆-tagged protein was observed to increase by

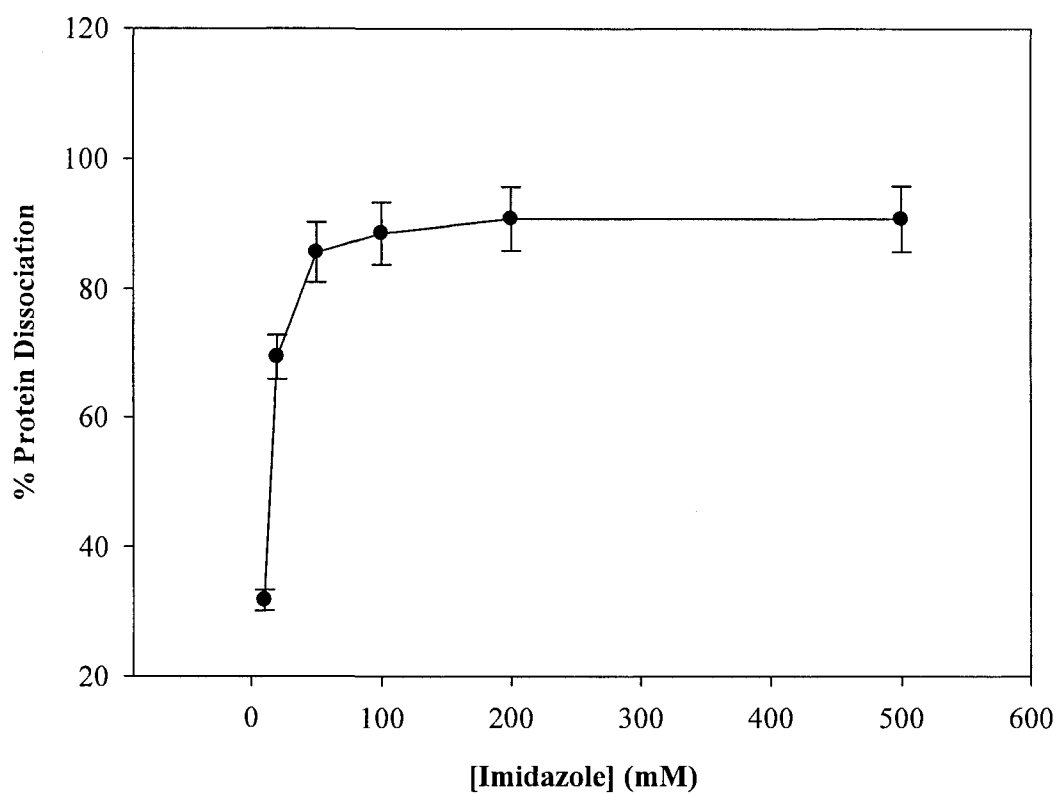


Figure 2.08. Plot of His₆-tagged Cma dissociated from NTA monolayers versus imidazole concentration. The error bars are the average standard deviation of SPR signals on three-spot measurements.

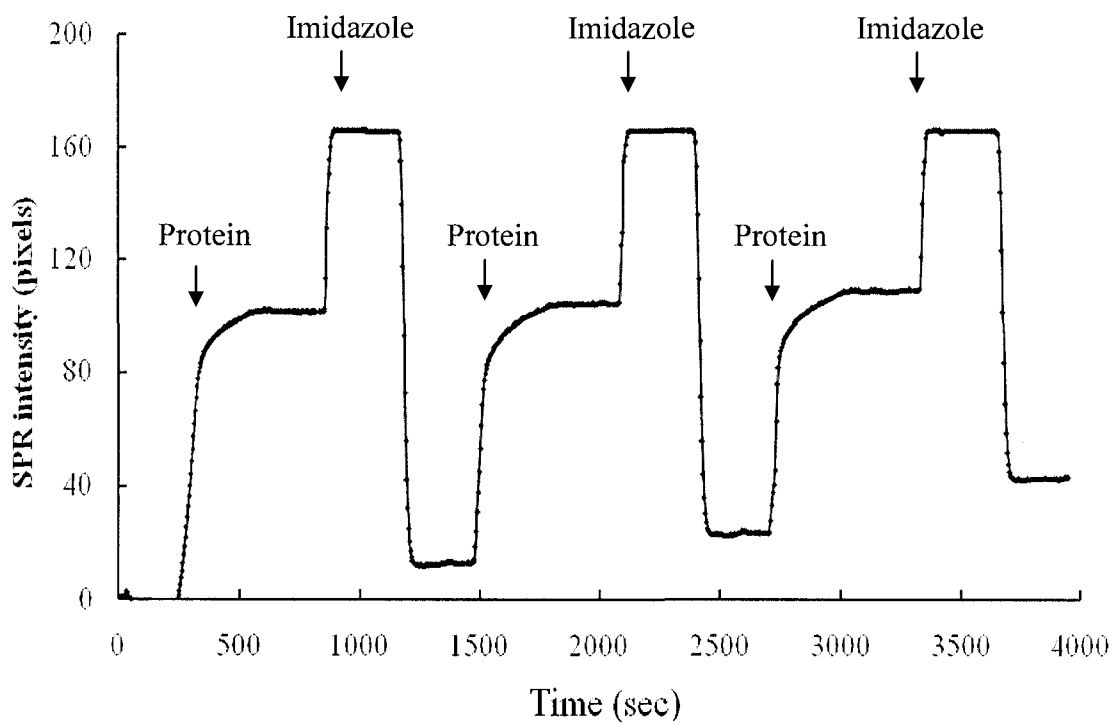


Figure 2.09. SPR sensorgram on the attachment of 2 μM His₆-tagged CRP to NTA monolayers followed by protein desorption from the surface by treatment with 200 mM imidazole. The surface was flushed with Tris buffer after each solution introduction.

~ 5%, which resulted from the remaining protein on the surface in the previous cycle.

EDTA can also be used to desorb His₆-tagged proteins from an NTA-modified surface because it binds to Ni²⁺ ions via four carboxylate and two amine groups.^{23,63} The removal of Ni²⁺ ions from NTA monolayers using EDTA can cause the dissociation of His₆-tagged proteins. A plot for the percentage of dissociated His₆-tagged CRP as a function of EDTA concentration is shown in Figure 2.10. It is clear from the plot that the amount of His₆-tagged CRP desorbed from the surface increased with EDTA concentration. At 800 mM EDTA, ~ 89% of His₆-tagged protein was dissociated from the surface. To reuse the NTA-modified surface for protein immobilization in subsequent experiments, a solution containing Ni²⁺ ions must be flowed over the surface to form an NTA–Ni²⁺ complex before loading other His₆-tagged protein solutions. As depicted in Figure 2.11, the immobilization of His₆-tagged CRP was repeated two more times by treatment with 500 mM EDTA and 50 mM NiSO₄. The SPR signal of protein adsorption gradually increased due to irreversibly bound protein on the surface after exposure to EDTA in each cycle.

Our studies also indicate that His₆-tagged protein adsorbed on NTA monolayers can be desorbed from the surface by a solution containing Ni²⁺ ions. Figure 2.12 presents a plot of the percentage of desorbed His₆-tagged protein versus NiSO₄ concentration. It is observed from the figure that ~ 97% of His₆-tagged protein was removed from the surface after treatment with 500 mM NiSO₄. Since the NiSO₄ solution contained much

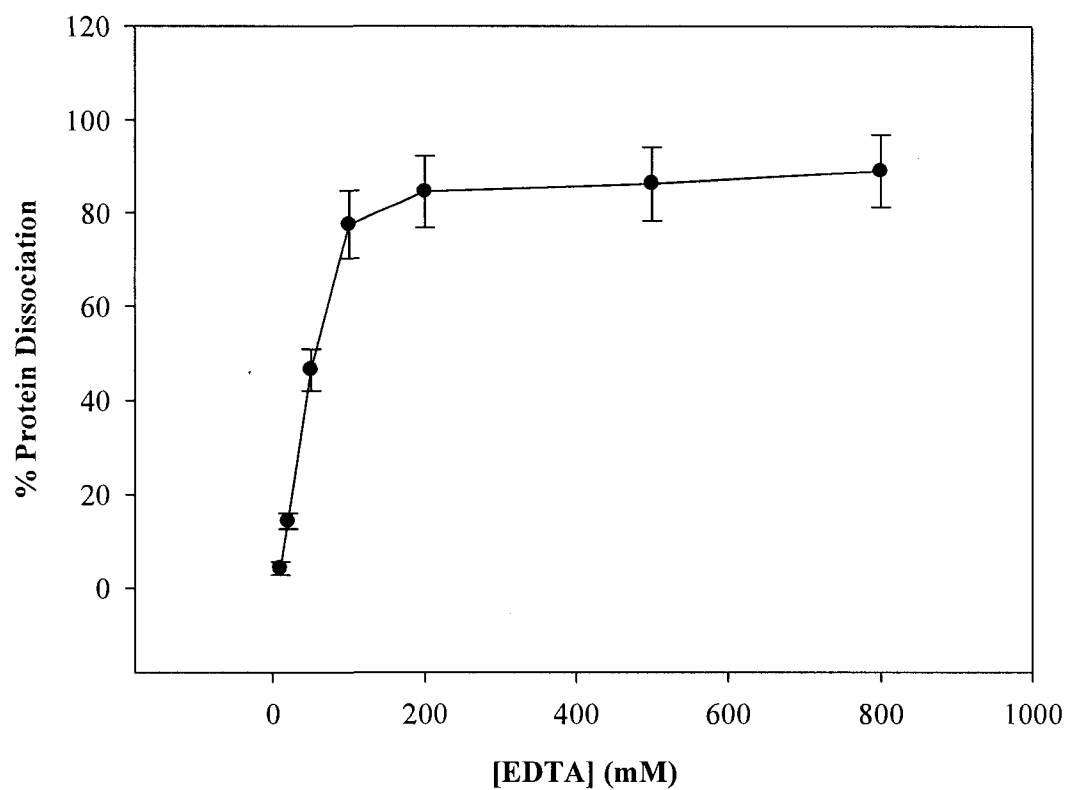


Figure 2.10. Plot of His₆-tagged Cma dissociation from NTA monolayers as a function of EDTA concentration. The error bars are the average standard deviation of SPR signals over three-spot measurements.

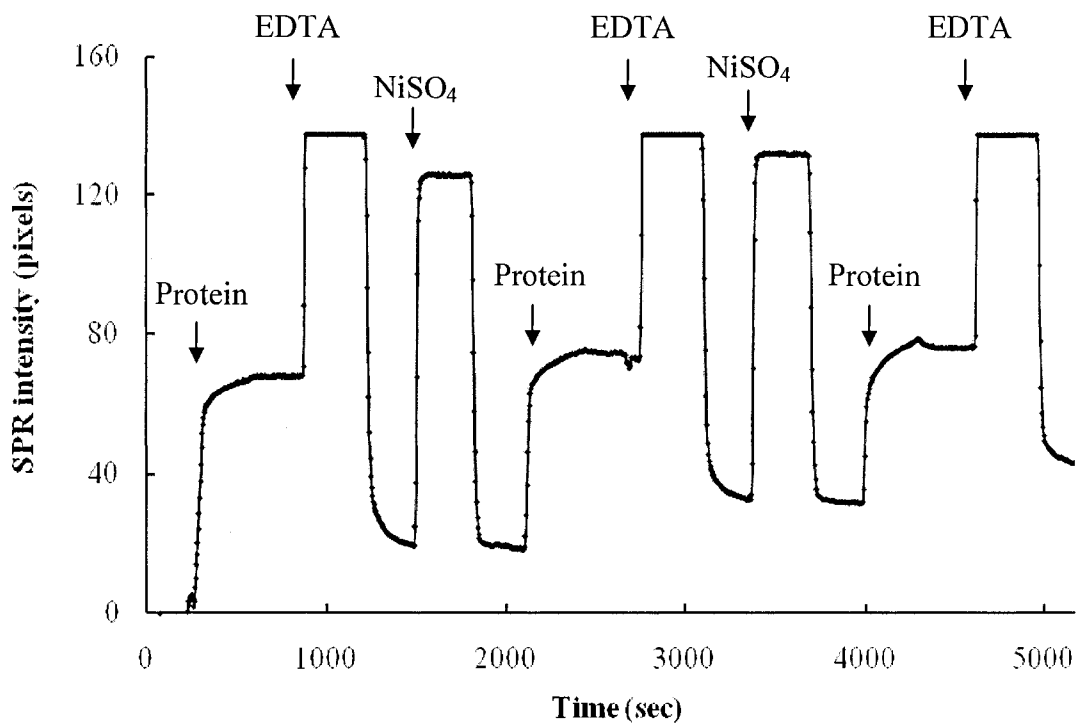


Figure 2.11. SPR sensorgram on binding of 2 μM His₆-tagged CRP to NTA monolayers followed by protein desorption with 500 mM EDTA. Prior to reloading another protein solution, 50 mM NiSO₄ was injected over the surface. The surface was washed with Tris buffer after each injection of solutions.

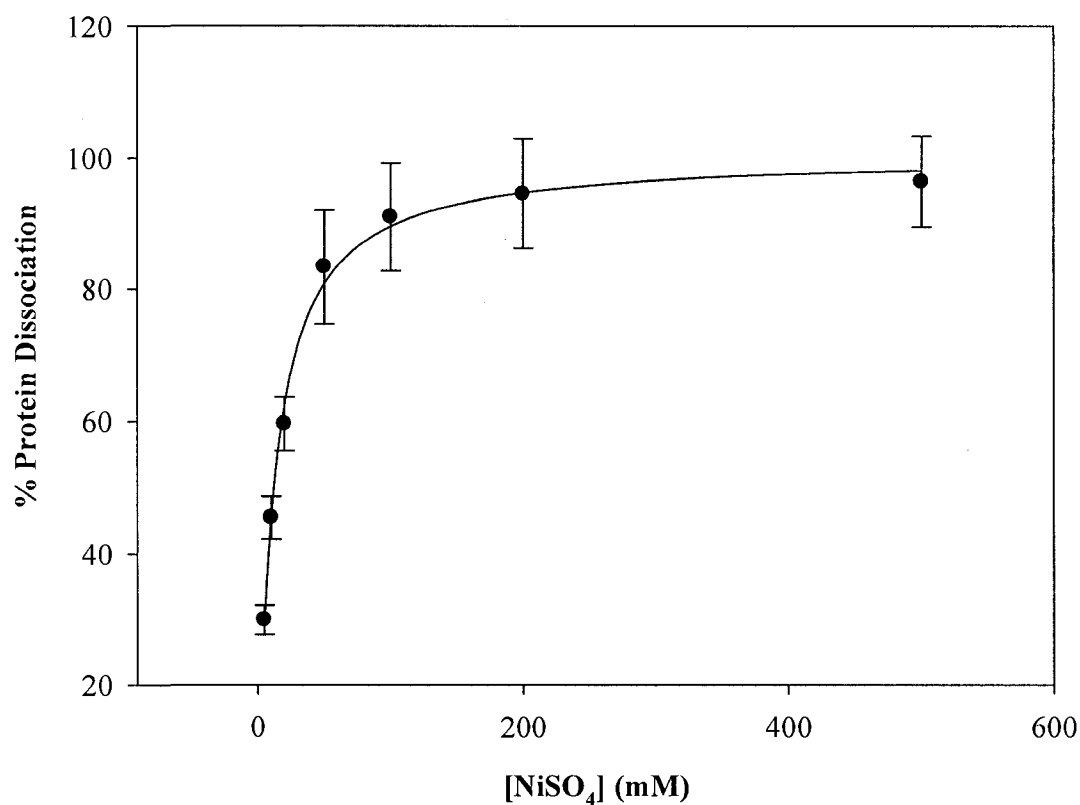


Figure 2.12. Dissociation of His₆-tagged Cma from NTA monolayers as a function of NiSO₄ concentration. The error bars show the standard deviation of SPR responses of three-spot measurements. The solid line through the data points is the Langmuir isotherm fit with $R^2 = 0.99$.

greater Ni^{2+} ions than on the surface, the immobilized His₆-tagged protein preferentially interacted with Ni^{2+} ions in solution, and protein desorption occurred as a result. In summary, the dissociation of His₆-tagged protein from NTA monolayers can be achieved using imidazole, EDTA or NiSO₄. NiSO₄ offers the best way for protein desorption because it can regenerate an NTA-modified surface with less remaining protein than imidazole or EDTA. Imidazole is more convenient for the reuse of NTA surfaces compared to EDTA that involves the addition of Ni^{2+} ions before the immobilization of other His₆-tagged proteins.

4. Conclusions

A simple method was developed to efficiently immobilize His₆-tagged proteins on gold surfaces with NTA monolayers. A thiol-functionalized NTA (tNTA) was synthesized by the reaction of maleimido-C₃-NTA with 1,9-noanedithiol, and purified by a Sepak-C18 cartridge. The surface density of NTA monolayers was varied via the formation of mixed monolayers of tNTA and MUO. Also, the amount of His₆-tagged proteins adsorbed on surfaces depended on the density of the NTA monolayer, and the mixed monolayer formed from 80/20 tNTA/MUO produced an optimal SPR signal for immobilization of His₆-tagged proteins.

We used SPR imaging to study the attachment of His₆-tagged proteins to the NTA-

modified surface. The results obtained are summarized as follows: (1) the interaction between NTA monolayers and His₆-tagged proteins was highly specific, which required the presence of Ni²⁺ ions on the surface; (2) monolayers of both EG3-OMe and MUO resisted nonspecific adsorption of His₆-tagged proteins, and thus they were used as negative controls for protein immobilization; (3) most of the immobilized His₆-tagged protein can be desorbed from an NTA-modified surface after exposure to a solution of imidazole, EDTA or NiSO₄; (4) The regenerated NTA surface can be reused to anchor other His₆-tagged proteins in further experiments. Since His₆-tagged proteins were immobilized in a well-defined orientation in our method, the investigation of interactions between adsorbed proteins and ligands in solution should be very accessible.

5. References

- (1) MacBeath, G.; Schreiber, S. L. *Science* **2000**, *289*, 1760–1763.
- (2) Zhu, H.; Bilgin, M.; Bangham, R.; Hall, D.; Casamayor, A.; Bertone, P.; Lan, N.; Jansen, R.; Bidlingmaier, S.; Houfek, T.; Mitchell, T.; Miller, P.; Dean, R. A.; Gerstein, M.; Snyder, M. *Science* **2001**, *293*, 2101–2105.
- (3) Wilson, D. S.; Nock, S. *Angew. Chem., Int. Ed.* **2003**, *42*, 494–500.
- (4) Scouten, W. H.; Luong, J. H. T.; Brown, R. S. *Trends Biotechnol.* **1995**, *13*, 178–185.

- (5) Aoyagi, S.; Oiw, Y.; Kudo, M. *Appl. Surf. Sci.* **2004**, *231–232*, 432–436.
- (6) Neves-Peterson, M.; Snabe, T.; Klitgaard, S.; Duroux, M.; Peterson, S. B. *Protein Sci.* **2006**, *15*, 343–351.
- (7) Lösche, M. *Curr. Opin. Solid State Mater. Sci.* **1997**, *2*, 546–556.
- (8) Zhu, H.; Synder, M. *Curr. Opin. Chem. Biol.* **2003**, *7*, 55–63.
- (9) Camarero, J. A. *Biopolymers* **2008**, *90*, 450–458.
- (10) Rusmini, F.; Zhong, Z.; Feijen, J. *Biomacromolecules* **2007**, *8*, 1775–1789.
- (11) Thomson, N. H.; Smith, B. L.; Almqvist, N.; Schmitt, L.; Kashlev, M.; Kool, E. T.; Hansma, P. K. *Biophys. J.* **1999**, *76*, 1024–1033.
- (12) Lesaicherre, M. L.; Lue, R. Y.; Chen, G. Y.; Zhu, Q.; Yao, S. Q. *J. Am. Chem. Soc.* **2002**, *124*, 8768–8769.
- (13) Zhang, K.; Diehl, M. R.; Tirrell, D. A. *J. Am. Chem. Soc.* **2005**, *127*, 10136–10137.
- (14) Luk, Y. Y.; Tingey, M. L.; Dickson, K. A.; Raines, R. T.; Abbott, N. L. *J. Am. Chem. Soc.* **2004**, *126*, 9024–9032.
- (15) Neumann, L.; Wohland, T.; Whelan, R. J.; Zare, R. N.; Kobilka, B. K. *ChemBioChem* **2002**, *3*, 993–998.
- (16) Herron, J. N.; Müller, W.; Paudler, M.; Riegler, H.; Ringsdorf, H.; Suci, P. A. *Langmuir* **1992**, *8*, 1413–1416.
- (17) Spinke, J.; Liley, M.; Guder, H.-J.; Angermaier, L.; Knoll, W. *Langmuir* **1993**, *9*, 1821–1825.

- (18) Pritchard, D. J.; Morgan, H.; Cooper, J. M. *Angew. Chem. Int. Ed.* **1995**, *34*, 91–93.
- (19) Kim, K.; Yang, H.; Jon, S.; Kim, E.; Kwak, J. *J. Am. Chem. Soc.* **2004**, *126*, 15368–15369.
- (20) Schmitt, L.; Dietrich, C.; Tampè, R. *J. Am. Chem. Soc.* **1994**, *116*, 8485–8491.
- (21) Sigal, G. B.; Bamdad, C.; Barberis, A.; Strominger, J.; Whitesides, G. M. *Anal. Chem.* **1996**, *68*, 490–497.
- (22) Wegner, G. J.; Lee, H. J.; Marriott, G.; Corn, R. M. *Anal. Chem.* **2003**, *75*, 4740–4746.
- (23) Lee, J. K.; Kim, Y. G.; Chi, Y. S.; Yun, W. S.; Choi, I. S. *J. Phys. Chem. B* **2004**, *108*, 7665–7673.
- (24) Schmid, E. L.; Keller, T. A.; Dienes, Z.; Vogel, H. *Anal. Chem.* **1997**, *69*, 1979–1985.
- (25) Du Roure, O.; Debiemme-Chouvy, C.; Malthête, J.; Silberzan, P. *Langmuir* **2003**, *19*, 4138–4143.
- (26) Browning-Kelley, M. E.; Wadu-Mesthrige, K.; Hari, V.; Liu, G. Y. *Langmuir* **1997**, *13*, 343–350.
- (27) Frecerix, F.; Bonroy, K.; Laureyn, W.; Reekmans, G.; Campitelli, A.; Dejaen, W.; Maes, G. *Langmuir* **2003**, *19*, 4351–4357.
- (28) Zhou, D.; Wang, X.; Birch, L.; Rayment, T.; Abell, C. *Langmuir* **2003**, *19*, 10557–10562.

- (29) Delamarce, E.; Sundarababu, G.; Biebuyck, H.; Michel, B.; Gerber, C.; Sigrist, H.; Ringsdorf, W. H.; Xanthopoulos, N.; Mathieu, H. J. *Langmuir* **1996**, *12*, 1997–2006.
- (30) Wang, Z.; Jin, G. *J. Biochem. Biophys. Methods* **2003**, *57*, 203–211.
- (31) Johnson, C. P.; Jensen, I. E.; Prakasam, A.; Vijayendran, R.; Leckband, D. *Bioconjugate Chem.* **2003**, *14*, 974–978.
- (32) Lee, W.; Lee, D.-B.; Oh, B.-K.; Lee, W. H.; Choi, J.-W. *Enzyme Microb. Technol.* **2004**, *35*, 678–682.
- (33) Schmid, A. H.; Stanca, S. E.; Thakur, M. S.; Thampia, K. R.; Suri, R. *Sens. Actuators, B* **2006**, *113*, 297–303.
- (34) Tanaka, G.; Funabashi, H.; Mie, M.; Kobatake, E. *Anal. Biochem.* **2006**, *350*, 298–303.
- (35) Häussling, L.; Ringsdorf, H.; Schmitt, F. J.; Knoll, W. *Langmuir* **1991**, *7*, 1837–1840.
- (36) Duschl, C.; Sévin-Landais, A. F.; Vogel, H. *Biophys. J.* **1996**, *70*, 1985–1995.
- (37) Vaughan, R. D.; O’Sullivan, C. K.; Guilbault, G. G. *Enzyme Microb. Technol.* **2001**, *29*, 635–638.
- (38) Nuzzo, R. G.; Allara, D. L. *J. Am. Chem. Soc.* **1983**, *105*, 4481–4483.
- (39) Pale-Grosdemange, C.; Simon, E. S.; Prime, K. L.; Whitesides, G. M. *J. Am. Chem. Soc.* **1991**, *113*, 12–20.

- (40) Prime, K. L.; Whitesides, G. M. *J. Am. Chem. Soc.* **1993**, *115*, 10714–10721.
- (41) Sekar, M. M. A.; Hampton, P. D.; Buranda, T.; Lopez, G. P. *J. Am. Chem. Soc.* **1999**, *121*, 5135–5141.
- (42) Silin, V.; Plant, A. *Trends Biotechnol.* **1997**, *15*, 353–359.
- (43) Knoll, W. *Annu. Rev. Phys. Chem.* **1998**, *49*, 569–638.
- (44) Brockman, J. M.; Nelson, B. P.; Corn, R. M. *Annu. Rev. Phys. Chem.* **2000**, *51*, 41–63.
- (45) Gokce, I.; Raggett, E. M.; Hong, Q.; Virden, R.; Cooper, A.; Lakey, J. H. *J. Mol. Biol.* **2000**, *304*, 621–632.
- (46) Nelson, B. P.; Grimsrud, T. E.; Liles, M. R.; Goodman, R. M.; Corn, R. M. *Anal. Chem.* **2001**, *73*, 1–7.
- (47) Boozer, C.; Kim, G.; Cong, S.; Guan, H.; Londergan, T. *Curr. Opin. Biotechnol.* **2006**, *17*, 400–405.
- (48) Kanda, V.; Kariuki, J. K.; Harrison, D. J.; McDermott, M. T. *Anal. Chem.* **2004**, *76*, 7256–7262.
- (49) Usui, Aoki, K.; Shimada, K.; Nagano, M.; Koga, H. *Proteomics* **2005**, *5*, 2396–2401.
- (50) Wegner, G. J.; Lee, H. J.; Marriott, G.; Corn, R. M. *Anal. Chem.* **2003**, *75*, 4740–4746.
- (51) Frutos, A. G.; Brockman, J. M.; Corn, R. M. *Langmuir* **2000**, *16*, 2192–2197.

- (52) Li, M.; Lee, H. J.; Condon, A. E.; Corn, R. M. *Langmuir* **2002**, *18*, 805–812.
- (53) Nelson, B. P.; Grimsrud, T. E.; Liles, M. R.; Goodman, R. M.; Corn, R. M. *Anal. Chem.* **2001**, *73*, 1–7.
- (54) Nelson, B. P.; Liles, M. R.; Frederick, K.; Corn, R. M.; Goodman, R. M. *Environ. Microbiol.* **2002**, *4*, 735–743.
- (55) Wegner, G. J.; Lee, H. J.; Corn, R. M. *Anal. Chem.* **2002**, *74*, 5161–5168.
- (56) Smith, E. A.; Thomas, W. D.; Kiessling, L. L.; Corn, R. M. *J. Am. Chem. Soc.* **2003**, *125*, 6140–6148.
- (57) Kanda, V.; Kitov, P.; Bundle, D. R.; McDermott, M. T. *Anal. Chem.* **2005**, *77*, 7497–7504.
- (58) Martins, M. C. L.; Fonseca, C.; Barbosa, M. A.; Ratner, B. D. *Biomaterials* **2003**, *24*, 3697–3706.
- (59) Porter, M. D.; Bright, T. B.; Allara, D. L.; Chidsey, C. E. D. *J. Am. Chem. Soc.* **1987**, *109*, 3559–3568.
- (60) Pale-Grosdemange, C.; Simon, E. S.; Prime, K. L.; Whitesides, G. M. *J. Am. Chem. Soc.* **1991**, *113*, 12–20.
- (61) Chapman, R. G.; Ostuni, E.; Yan, L.; Whitesides, G. M. *Langmuir* **2000**, *16*, 6927–6936.
- (62) Christofides, N. D. In *The Immunoassay Handbook*, 2nd ed.; Wild, D., Ed.; Nature Publishing Group: New York, 2001; pp 61–77.

(63) Schmitt, L.; Dietrich, C.; Tampè, R. *J. Am. Chem. Soc.* **1994**, *116*, 8485–8491.

Chapter III

Surface Plasmon Resonance Imaging Studies of Bacterial Proteins

1. Introduction

Protein arrays are defined as solid-phase binding assays on which a number of proteins or protein ligands are immobilized in an array manner.^{1,2} In recent years, they have become a powerful tool in a variety of applications, such as proteomics³⁻⁸ and drug discovery.⁹⁻¹¹ Protein arrays can be used to determine the presence and amount of proteins in biological samples,¹²⁻¹⁴ to identify protein-protein and protein-DNA interactions,^{3,15} and to discover new disease markers.¹⁶⁻¹⁸ The most popular format of protein array is the antibody array, where antibodies are deposited on a solid surface (e.g., glass, silicon) for antigen characterization and profiling.¹⁹⁻²¹ The widespread application of protein arrays is attributed to their intrinsic advantages.^{22,23} First, protein arrays are highly throughput, which allows numerous proteins to be detected simultaneously. Secondly, only a small amount of protein and reagent is required in protein arrays. Thirdly, a variety of surface modifications can be made in protein arrays to suit their diverse applications. Fluorescence²⁴⁻²⁶ and surface plasmon resonance (SPR)²⁷⁻²⁹ are the most common detection techniques used in protein arrays. In this chapter, protein immobilization method was employed to fabricate bacterial protein arrays, where the

protein interaction with other biomolecules was probed using SPR imaging. The bacterial proteins we tested include cyclic AMP (cAMP) receptor protein and maltose binding protein.

Cyclic AMP (cAMP) receptor protein (CRP), also called catabolite gene activator protein (CAP), is a DNA-binding protein in bacteria (e.g., *E. coli*). This protein functions as a global regulator to control the expression of many different genes.³⁰⁻³³ Most genes regulated by CRP code for enzymes that are involved in the metabolism of sugars, including galactose, maltose and lactose. Once cAMP is bound to CRP, a conformational change occurs and the protein will exhibit a higher affinity for specific DNA sequences. If the intracellular level of cAMP increases, CRP will form a dimer that consists of two chemically identical polypeptide chains. The cAMP-CRP complex binds to a conserved DNA sequence, which can stimulate transcription initiation from various promoters.^{34,35} Figure 3.01 shows a tube and arrow representation for the structure of the CRP-cAMP-DNA complex. The N-terminal terminus is responsible for protein dimerization and cAMP binding, and the C-terminus contains a DNA-binding motif.³⁶⁻³⁹

Maltose-binding protein (MBP) is one of periplasmic binding proteins (PBPs)⁴⁰ that resides in the periplasm, a space between the inner and outer membranes of Gram-negative bacteria. PBPs are distinct from the proteins in the cytoplasm and play an important role in cellular processes. They function as receptors to identify and transport essential nutrients, including sugars, amino acids, inorganic ions and vitamins, into the



Figure 3.01. Tube and arrow representation for the CRP–cAMP–DNA complex. The N-terminal domains are colored red and green, and the C-terminal DNA binding domains are colored yellow and blue. The cAMP activator is bound at the center of CRP dimer.

cell in the translation process through signal sequences.^{41,42} As part of the maltose/maltodextrin transport system in *E. coli*, MBP has been used in biosensors to detect maltose.⁴³⁻⁴⁵ This protein tightly binds to maltose, and then conveys it to the inner membrane in which a membrane transporter MalFGK₂ is involved. The transporter is composed of two integral membrane proteins, i.e., MalF and MalG, and two ATP-hydrolyzing subunits MalK. The interaction of MalFGK₂ with the maltose-bound MBP can activate the ATPase activity of the MalK subunit. As a result, ATP is hydrolyzed to produce ADP and phosphate. In the meantime, maltose is released by MBP and passes through MalFGK₂ into the cytoplasm.⁴⁶ X-ray crystallography studies show that MBP contains two domains with similar secondary structures, and the maltose-binding site is located at the interface of the two domains (Figure 3.02).⁴⁷⁻⁵⁰

2. Experimental

2.1. Materials

The synthetic procedure of thiol-functionalized NTA (tNTA) was described in Chapter II. 11-Mercapto-1-undecanol (MUO), bovine serum albumin (BSA) and adenosine 3',5'-cyclic monophosphate (cAMP) were obtained from Sigma-Aldrich (St. Louis, MO). 11-Mercaptoundecylamine (MUAM) and tridecafluoro-1,1,2,2-tetrahydro-octyl-1-dimethylchlorosilane were purchased from Dojindo Laboratories

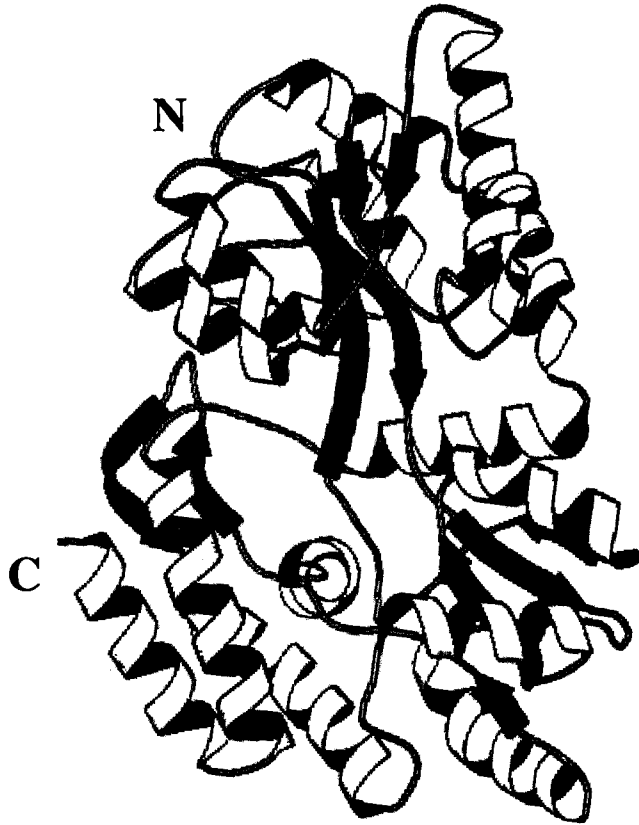


Figure 3.02. Band and arrow representation for maltose-binding protein (MBP) that contains two similar domains. The binding site of maltose is located at a deep groove between the domains. Source: Shilton, B.H.; Shuman, H.A.; Mowbray, S.L. *J. Mol. Biol.* **1996**, *264*, 364–376.

(Kumamoto, Japan) and United Chemical Technologies (Bristol, PA), respectively. *N*-Hydroxysuccinimidyl ester of 11-mercaptoundecanoic acid (thiol-NHS) and (1-mercaptoundec-11-yl)tri(ethylene glycol) methyl ether (EG3-OMe) were obtained from ProChimia (Gdansk, Poland). DNA oligonucleotides, lacPI (5'-ATT AAT GTG AGT TAG CTC ACT CAT TA-3') and lacPI2 (5'-TAA TGA GTG AGC TAA CTC ACA TTA AT-3') were purchased from Integrated DNA Technologies (Coralville, IA). His₆-tagged proteins, including CRP (22.5 kDa) and MBP (40.6 kDa), anti-CRP antibody and maltose were obtained from the laboratory of Professor Joel Weiner (Biochemistry Department, University of Alberta). His₆-tagged CRP, anti-CRP antibody and DNA oligonucleotides were diluted in 50 mM Tris·HCl (pH 7.8) and 100 mM KCl. His₆-tagged MBP and maltose were diluted in 10 mM Tris·HCl (pH 7.4) and 135 mM NaCl. 10 mM phosphate-buffered saline (PBS, pH 7.4) was used to prepare 0.1% BSA solution.

2.2. SPR Chip Preparation

SF-10 glass slides (Schott Glass, Toronto, ON) were pre-cleaned using fresh piranha solution (3:1 H₂SO₄-H₂O₂) for 30 min. 18 MΩ Nanopure water (Barnstead International, Dubuque, IA) was used to rinse the surfaces several times before they were totally dried under a stream of argon. The slides were then exposed to the vapor of tridecafluoro-1,1,2,2-tetrahydrooctyl-1-dimethylchlorosilane under reduced pressure for

12 h to create a hydrophobic background on the glass. Metal films of Cr (1 nm) and Au (45 nm) were sequentially coated on the glass through a home-built shadow mask using the thermal evaporation (Torr International Inc., New Windsor, NY). The fabricated SPR chips were stored in a desiccator under vacuum at room temperature. Prior to modification of SPR chips, gold surfaces were first cleaned by an UV–Ozone cleaner (Jelight Company Inc., Irvine, CA) for 5 min, then rinsed with 18 M Ω water and dried under a stream of argon.

2.3. Protein Immobilization

Self-assembled monolayers (SAMs) of alkanethiols were used to modify gold surfaces to immobilize target proteins for monitoring protein interactions with other biomolecules. First, different gold spots in a SPR chip were simultaneously incubated in a set of solutions of 1 mM tNTA, 1 mM MUAM and 1 mM thiol-NHS for 12 h to form different monolayers. After the gold surface was rinsed with 18 M Ω water and dried under a stream of argon gas, 100 mM NaOH and 50 mM NiSO₄ were sequentially reacted with NTA monolayers to produce an NTA–Ni²⁺ group on the surface. Finally, a solution of 2 μ M His₆-tagged CRP was introduced to the monolayers of NTA, MUAM and thiol-NHS and adsorbed for 10–15 min. Tris buffer was flowed through the entire surface for 5 min to minimize nonspecific protein adsorption.

2.4. Fabrication of Protein Arrays

To test the specificity of CRP dimerization in the presence of cAMP, protein arrays were designed and fabricated on a SPR chip. Initially, different gold spots were exposed to solutions of 1 mM tNTA, 1 mM MUAM and 1 mM MUO to create various monolayers. Next, the NTA monolayer was reacted with 100 mM NaOH for 5 min followed by 50 mM NiSO₄ for 15 min to yield the NTA–Ni²⁺ complex. Solutions of 2 μM His₆-tagged CRP, 2 μM His₆-tagged MBP and 2 μM His₆-tagged Cma were separately delivered on different spots modified with NTA–Ni²⁺ monolayers using a micropipette. At the same time, 0.1% BSA in PBS was introduced on the MUAM monolayer. All the protein solutions were adsorbed on the surface for 3–4 h at room temperature. The protein chip was then rinsed with Tris buffer carefully before the formation of protein dimer was characterized with SPR imaging. In addition, MUO monolayers can resist nonspecific protein binding and thus provides a negative control in the experiment.⁴⁷

2.5. SPR Imaging Apparatus

A SPR imager (GWC Technologies, Madison, WI) was employed to explore protein binding to other biomolecules. In this instrument, *p*-polarized light was produced from an incoherent white light with a polarizer, and then shone on the back of a gold

surface at a fixed angle. A sample assembly composed of a SF-10 prism and a SPR chip was located on a rotation stage by which the incident angle of light was adjusted. A solution was introduced to the entire chip surface through a flow cell using peristaltic flow. The reflected light passed through a narrow band-pass filter ($\lambda = 830$ nm), and immediately detected with a CCD camera. All SPR images were acquired by averaging 100 frames and analyzed with the software package Digital Optics V++ 4.0.

3. Results and Discussion

3.1. Antigen–Antibody Interaction

Three different methods were used to immobilize CRP on gold surfaces, which were: (1) physical adsorption to an amine-functionalized surface (MUAM); (2) covalent binding to an NHS-modified surface; (3) bioaffinity immobilization of His₆-tagged CRP to an NTA–Ni²⁺ surface. The efficacy of each immobilization method was examined by measuring the amount of anti-CRP binding to the immobilized CRP with SPR imaging. The covalent attachment method we employed involved the formation of amide bond linkages between NHS groups on the surface and free amines of the protein. Thus, both this method and physical adsorption produced a randomly oriented protein layer. In this experiment, three types of monolayers were formed on the surface by incubating different gold spots in a set of solutions containing tNTA, MUAM and thiol-NHS. These

monolayers anchored 2 μM His₆-tagged CRP on the gold surface via the various interactions described above. Figure 3.03 shows the SPR difference image of CRP adsorption on the three monolayers. It is clear from the figure that a larger amount of His₆-tagged CRP was immobilized on the NTA monolayers than MUAM and thiol-NHS surfaces. To better compare CRP adsorption on the various monolayers, SPR signals ($\Delta\%R$) were obtained from the difference image (Figure 3.03) using the software V++ 4.0, and summarized in Table 3.01. A much higher signal is observed on the NTA surface, which indicates that bioaffinity immobilization via a His₆-tag can offer a higher surface density of CRP. Also, the thiol-NHS monolayer anchored more CRP compared to the MUAM monolayer.

After CRP was immobilized on the surface, a diluted solution of anti-CRP antibody was introduced to the chip and allowed to sit for 10 min. Figure 3.04 provides the SPR difference image resulting from the antigen–antibody interaction. The $\Delta\%R$ values observed on the various monolayers are shown in Table 3.02. As we expected, the highest signal of anti-CRP binding was achieved on the NTA monolayer. This result is probably due to the following two reasons: (1) more His₆-tagged CRP was immobilized on the NTA monolayer, which allowed more antibodies to be bound on the surface; (2) the well-defined orientation of immobilized CRP on the NTA monolayer was useful in maintaining protein biological activity and consequently the antigen–antibody interaction was enhanced. In contrast, the monolayers of MUAM and thiol-NHS adsorbed CRP in

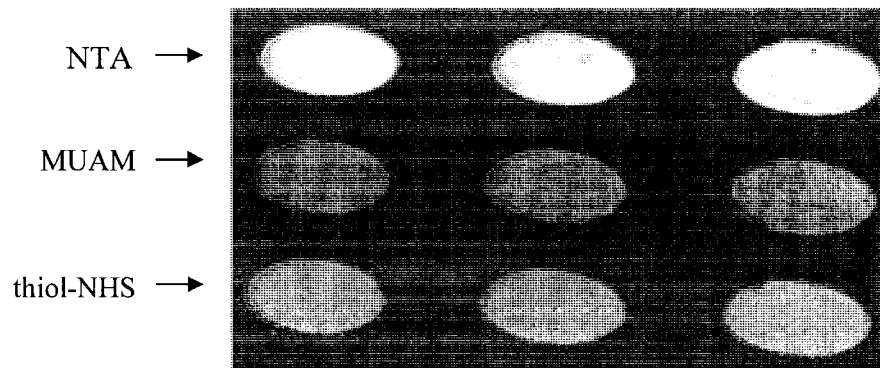


Figure 3.03. SPR difference image of 2 μM His₆-tagged CRP immobilization on the gold chip modified with monolayers of NTA, MUAM and thiol-NHS.

| Monolayers | SPR signal ($\Delta\%R$) |
|-------------------|--|
| NTA | 51.8 (0.7) |
| MUAM | 18.9 (1.7) |
| Thiol-NHS | 25.3 (1.5) |

Table 3.01. SPR signals for 2 μM His₆-tagged CRP adsorption on the various monolayers depicted in Figure 3.03. Numbers in parentheses are standard deviations of the indicated values.

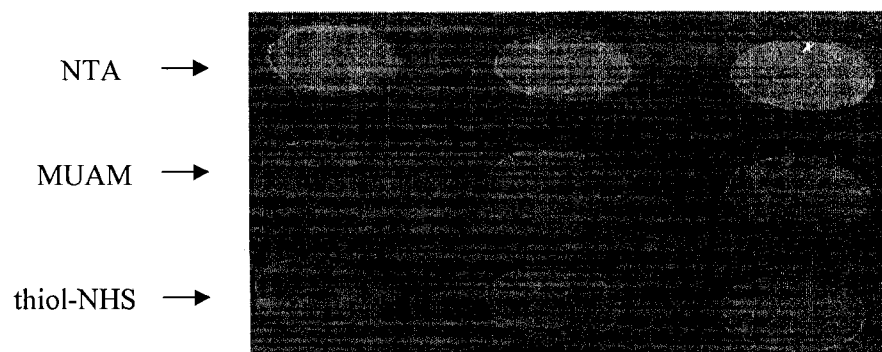


Figure 3.04. SPR difference image of the interaction between CRP and anti-CRP on the gold chip containing NTA, MUAM and thiol-NHS monolayers.

| Monolayers | SPR signal ($\Delta\%R$) |
|-------------------|--|
| NTA | 8.8 (0.5) |
| MUAM | 2.7 (0.6) |
| Thiol-NHS | 3.1 (0.4) |

Table 3.02. SPR signals for the CRP–anti-CRP binding on the various monolayers shown in Figure 3.04. Numbers in parentheses stand for standard deviations of the indicated values.

different orientations. This random orientation may lead to partial loss of protein activity and sterically block active sites of proteins. As a result, the interaction between CRP and anti-CRP was reduced on MUAM and thiol-NHS monolayers. So our method of His₆-tagged protein immobilization can produce a higher percentage of adsorbed proteins that are able to interact with other biomolecules in solution.

3.2. CRP Dimerization

In *E. coli* bacteria, CRP regulates the transcription of several genes that are responsive to the change of cAMP concentration inside the cell.³⁰⁻³³ CRP can interpret the message encoded in cAMP and transmit it to specific DNA sequences. Thus, in the presence of cAMP, CRP will form a dimer and bind specific DNA sequences.³⁵ Figure 3.05 illustrates a scheme for the screening of CRP immobilization, dimerization and binding to DNA with SPR imaging. First, His₆-tagged CRP is attached to a gold surface through the affinity interaction between the His-tag and NTA-Ni²⁺ complex. Secondly, the immobilized His₆-tagged CRP binds to His₆-tagged CRP in solution to form a dimer in the activation of cAMP. Thirdly, a specific DNA sequence is recognized and captured by the CRP-cAMP complex.

To probe the specificity of CRP dimerization, a protein array was fabricated on a SPR chip, which contained His₆-tagged CRP, His₆-tagged MBP, His₆-tagged Cma and

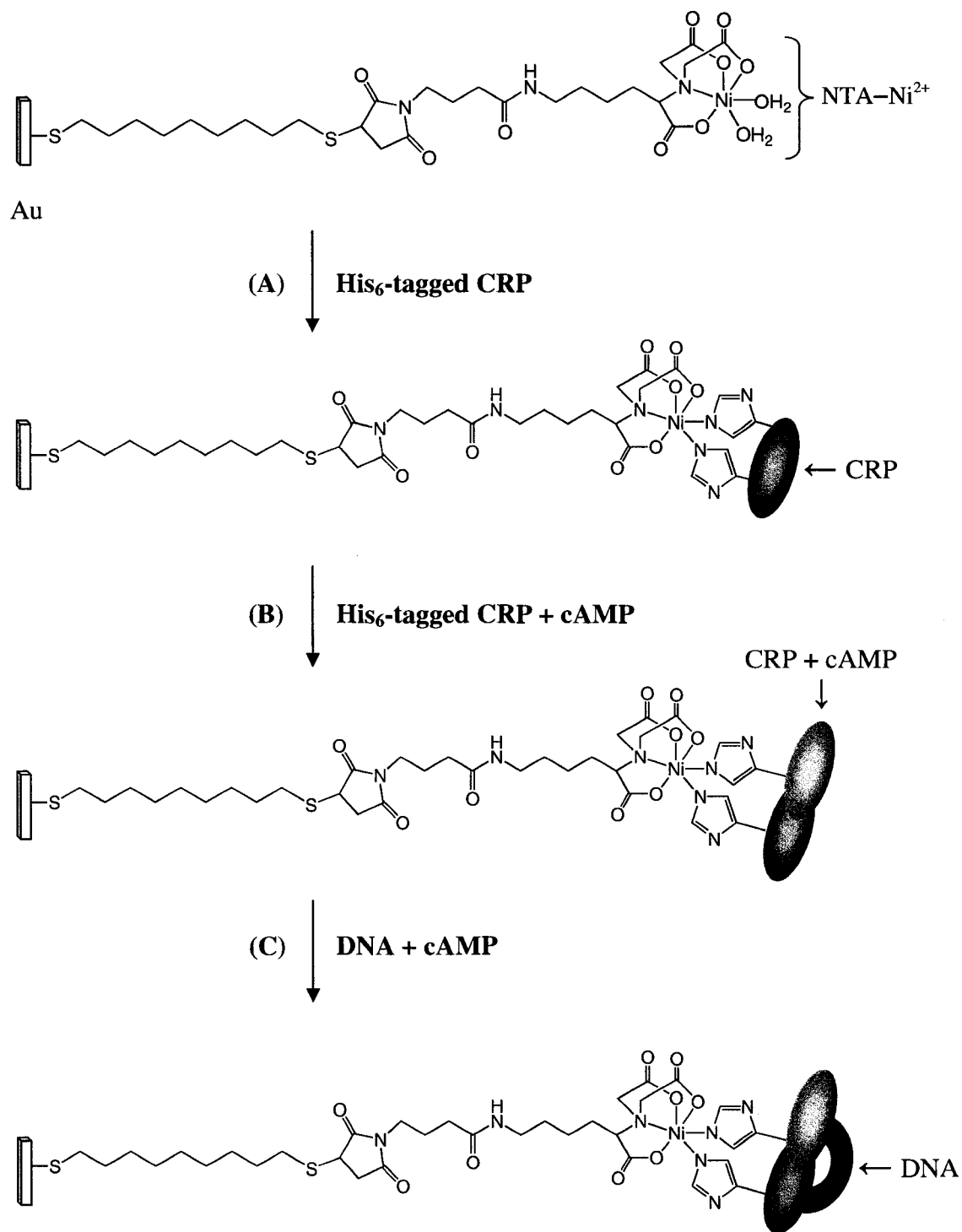


Figure 3.05. (A) Immobilization of His₆-tagged CRP on NTA-Ni²⁺ monolayers. (B) His₆-tagged CRP Dimerization in the presence of cAMP. (C) Specific binding of DNA to the His₆-tagged CRP dimer in the activation of cAMP.

BSA. All His₆-tagged proteins were specifically immobilized on the gold surface bearing NTA-Ni²⁺ species. Physisorbed BSA⁵¹ and MUO monolayers⁵² were used as negative control spots. A mixture of 2 μM His₆-tagged CRP and 1 mM cAMP was flowed over the chip surface for 10 min, and then the surface was rinsed with Tris buffer for 5 min. Figure 3.06 shows the SPR difference image that was obtained by subtraction before and after the addition of the mixture. A high SPR signal is observed on the CRP spots with a measurable signal at the Cma spots. Little signal is found on the MBP, MUO and BSA spots. Table 3.03 compares the Δ%R values on each protein layer. The largest signal obtained at the CRP spots was presumably due to the formation of CRP dimers. The small amount of CRP binding to the MBP and Cma layers probably arose from unreacted NTA-Ni²⁺ on those layers, resulting in bioaffinity immobilization of His₆-tagged CRP. In addition, BSA and MUO acted as good negative controls without CRP attached.

To further quantify CRP dimerization on NTA monolayers, we measured SPR signals of protein dimerization at different concentrations of CRP solution using the SPR imaging. A clean SPR chip with NTA monolayers was incubated in a solution of 2 μM His₆-tagged CRP for 10 min. A series of mixtures of CRP and 1 mM cAMP were then flowed over the surface from low to high concentrations for 5 min. The resulting SPR signal (Δ%R) is plotted as a function of CRP concentration in Figure 3.07. It is clear that more CRP dimers were formed when the concentration of His₆-tagged CRP in solution was increased. While the relationship between Δ%R and CRP concentration resembles

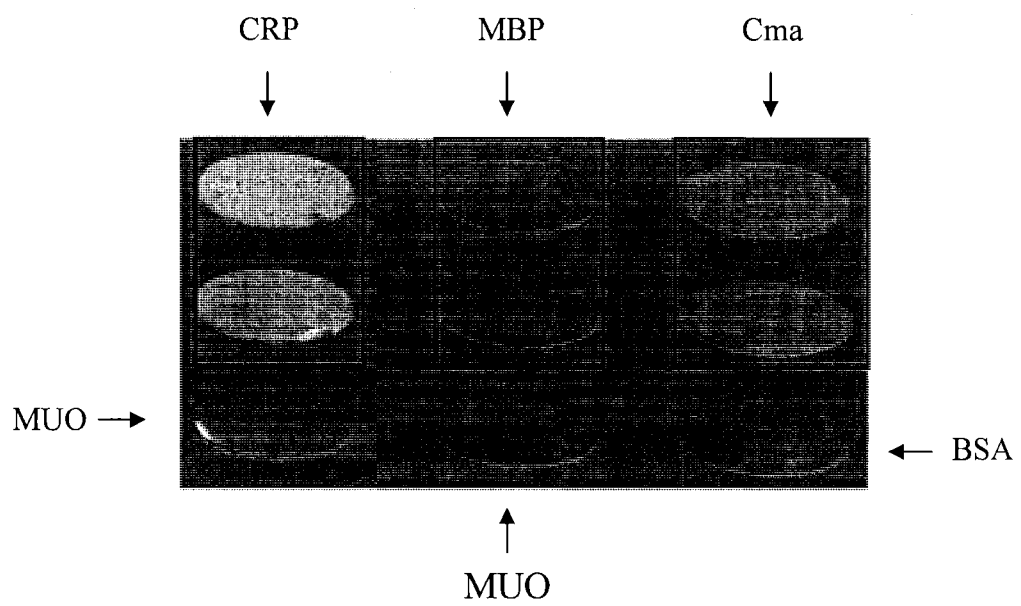


Figure 3.06. SPR difference image of the formation of CRP dimer in the presence of cAMP. The SPR chip contains various bacterial protein layers and negative control spots (i.e., MUO and BSA).

| Monolayers | SPR signal ($\Delta\%R$) |
|------------------------------|--|
| His ₆ -tagged CRP | 23.6 (3.1) |
| His ₆ -tagged MBP | 1.8 (0.1) |
| His ₆ -tagged Cma | 8.9 (0.5) |
| BSA | 0.2 (0) |
| MUO | 0.16 (0) |

Table 3.03. SPR signals for CRP dimerization on the protein array illustrates in Figure 3.06. Numbers in parentheses represent standard deviations of the indicated values.

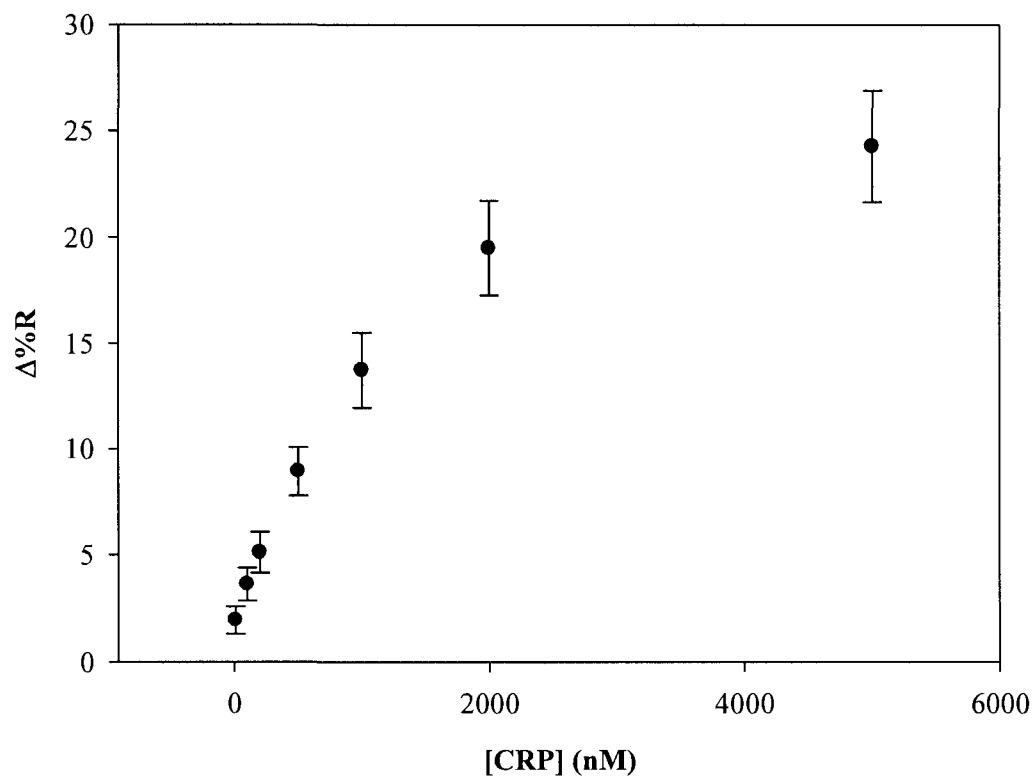


Figure 3.07. Plot of $\Delta\%R$ versus His₆-tagged CRP concentration in solution for protein dimerization on NTA monolayers. The error bars show the average standard deviation of SPR signals over three-spot measurements.

that of a Langmuir isotherm, the higher values of $\Delta\%R$ are greater than 20% and therefore out of the region of linearity with surface coverage. So quantitative parameters (e.g., K_{ads}) resulting from fitting the data in Figure 3.07 will have a large uncertainty. Despite this limitation, we believe that the relationship between $\Delta\%R$ and CRP concentration is following a Langmuir model.

In addition, we found that the amount of CRP dimerization was dependent on cAMP concentration in solution. In this study, His₆-tagged CRP was first immobilized on the gold surface functionalized with an NTA monolayer. Next, a series of 2 μ M His₆-tagged CRP solutions containing various concentrations of cAMP were introduced to the adsorbed protein layer. SPR difference images were recorded after each solution was added for 10 min. A plot of the $\Delta\%R$ value versus cAMP concentration is depicted in Figure 3.08. The result indicates that CRP dimerization was enhanced when more cAMP was present in solution. Hence, the formation of CRP dimer is controlled by CRP and cAMP concentrations in solution.

3.3. CRP–DNA Interaction

DNA binding to the CRP dimer was studied using a dsDNA strand that was formed by the hybridization of lacPI (5'-ATT AAT GTG AGT TAG CTC ACT CAT TA-3') and lacPI2 (5'-TAA TGA GTG AGC TAA CTC ACA TTA AT-3'). A mixture of 2 μ M

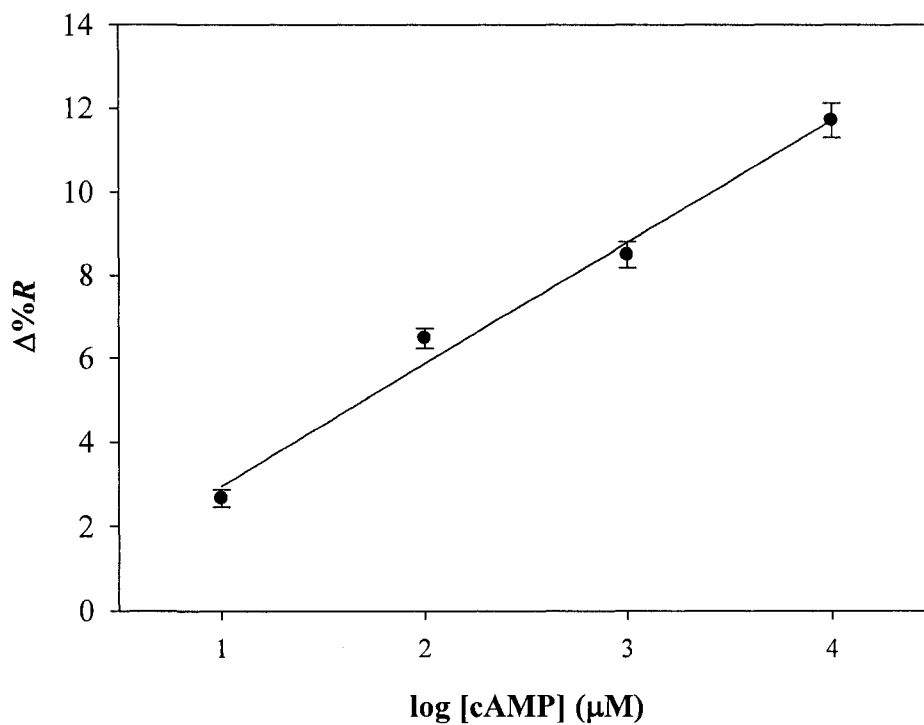


Figure 3.08. Plot for His₆-tagged CRP dimerization on NTA monolayers as a function of cAMP concentration. The error bars indicate the average standard deviation of SPR signals on three-spot measurements.

dsDNA and 1 mM cAMP was introduced to a gold surface containing the CRP dimer and MUO monolayers. Following 10-min incubation, Tris buffer was flowed through the surface to remove nonspecific DNA adsorption. Table 3.04 summarizes the SPR signal ($\Delta\%R$) caused by CRP immobilization, dimerization and binding to DNA on the NTA and MUO monolayers. It is clear from the table that the CRP–DNA interaction was significant compared to little SPR response observed on the MUO monolayer. Also, both CRP immobilization and dimerization were efficiently achieved on the NTA monolayer. So our immobilization method of His₆-tagged protein on NTA–Ni²⁺ monolayers is useful for the study of protein–protein and protein–DNA interactions with SPR imaging.

3.4. MBP–Maltose Interaction

In this work, the binding of maltose to MBP was detected by SPR imaging. Initially, MBP was fused with a His₆-tag and specifically immobilized on an NTA–Ni²⁺ monolayer. Figure 3.09 presents the SPR difference image taken before and after protein adsorption. A larger amount of His₆-tagged MBP was anchored to the NTA monolayer than the MUO and EG3-OMe surfaces. Table 3.05 describes the SPR signal ($\Delta\%R$) obtained for protein immobilization on the various monolayers. The significant $\Delta\%R$ value observed on the NTA monolayer demonstrates that the attachment of His₆-tagged MBP was efficient and specific. In contrast, much less binding of proteins is found on the

| SPR signal ($\Delta\%R$) | | | |
|----------------------------|----------------|--------------|-------------|
| Monolayers | Immobilization | Dimerization | DNA binding |
| NTA | 52.3 (2.8) | 37.6 (1.5) | 11.8 (0.6) |
| MUO | 0.8 (0) | 0.9 (0.1) | 0.6 (0.1) |

Table 3.04. SPR signals for His₆-tagged CRP immobilization, dimerization and binding to DNA on NTA monolayers. MUO monolayers served as a negative control. Numbers in parentheses are standard deviations of the indicated values.

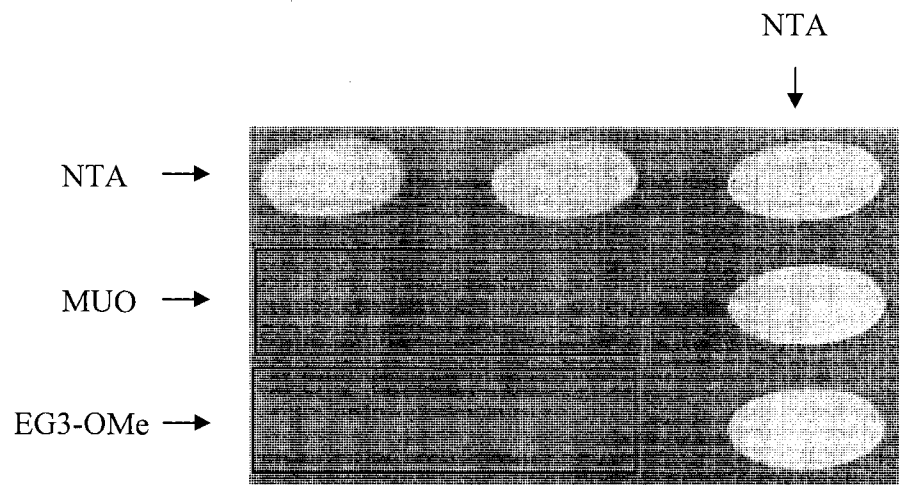


Figure 3.09. SPR difference image of 2 μM His₆-tagged MBP adsorption on NTA monolayers. MUO and EG3-OMe monolayers were used as negative controls.

| Monolayers | SPR signal ($\Delta\%R$) |
|-------------------|--|
| NTA | 30.4 (2.0) |
| MUO | 5.1 (0.9) |
| EG3-OMe | 1.7 (0.6) |

Table 3.05. SPR signals for His₆-tagged MBP immobilization on monolayers of NTA, MUO and EG3-OMe shown in Figure 3.09. Numbers in parentheses are standard deviations of the indicated values.

monolayers of MUO⁵² and EG3-OMe,⁵³ which has been shown to resist nonspecific protein binding.

Maltose is a small molecule with a molecular weight of 342 daltons. It consists of two units of glucose joined with a α (1 \rightarrow 4) linkage, and can bind to MBP with a binding constant of 1.6×10^7 M. In *E. coli*, MBP can transport maltose to a transport complex in the inner membrane of bacterial cells.^{43,46} Here, the strong interaction between maltose and His₆-tagged MBP was monitored with SPR imaging, and the result is shown in Table 3.06. A small SPR response was observed on the NTA monolayer because the binding of the small-molecule maltose to His₆-tagged MBP only caused a slight change in the refractive index of the medium adjacent to the gold surface. Compared to the NTA spots, both MUO and EG3-OMe spots gave less maltose adsorption, probably due to nonspecific adsorption. To date, the smallest molecule detected in SPR imaging has been reported to be 650 daltons.⁵⁴ But our work shows that SPR imaging could be used to detect smaller molecules if protein immobilization method is efficient, and also the protein has a strong affinity for the small molecule.

4. Conclusions

In this chapter, we applied the protein immobilization method developed before to investigate several biomolecular interactions, which included antigen–antibody, CRP

| Monolayers | SPR signal ($\Delta\%R$) |
|-------------------|--|
| NTA | 1.28 (0.7) |
| MUO | 0.7 (0.1) |
| EG3-OMe | 0.7 (0) |

Table 3.06. SPR signals for the MBP–maltose binding on the gold surface bearing NTA, MUO and EG3-OMe monolayers demonstrated in Figure 3.09. Numbers in parentheses are standard deviations of the indicated values.

dimerization, CRP–DNA and MBP–maltose interactions using SPR imaging. Due to an oriented immobilization of His₆-tagged protein achieved on an NTA–Ni²⁺ monolayer, the binding of protein to other biomolecules was observed with high specificity and efficacy. The results were summarized as follows: (1) His₆-tagged CRP was efficiently immobilized on the NTA monolayer compared to thiol-NHS and MUAM monolayers; (2) more anti-CRP antibody was bound to the immobilized CRP on the NTA monolayer than the thiol-NHS and MUAM monolayers; (3) CRP dimer was specifically formed on the Cma layer in the presence of cAMP, and the concentration of both CRP and cAMP in solution affected CRP dimerization on the surface; (4) the specific DNA binding to CRP dimer occurred in the activation of cAMP; (5) the detection of the small-molecule maltose binding to MBP was detected with SPR imaging.

5. References

- (1) MacBeath, G.; Schreiber, S. L. *Science* **2000**, *289*, 1760–1763.
- (2) Jones, R. B.; Gordus, A.; Krall, J. A.; MacBeath, G. *Nature* **2006**, *439*, 168–174.
- (3) Laurell, T.; Marko-Varga, G. *Proteomics* **2002**, *2*, 345–351.
- (4) Zhu, H.; Snyder, M. *Curr. Opin. Chem. Biol.* **2003**, *7*, 55–63.
- (5) Zhu, H.; Bilgin, M.; Bangham, R.; Hall, D.; Casamayor, A.; Bertone, P.; Lan, N.; Jansen, R.; Bidlingmaier, S.; Houfek, T.; Mitchell, T.; Miller, P.; Dean, R. A.;

- Gerstein, M.; Snyder, M. *Science* **2001**, *293*, 2101–2105.
- (6) Seong, S.; Choi, C. *Proteomics* **2003**, *3*, 2176–2189.
- (7) Labaer, L.; Ramachandran, N. *Curr. Opin. Chem. Biol.* **2005**, *9*, 14–19.
- (8) Hu, Y.; Uttamchandani, M.; Yao, S. Q. Y. *Comb. Chem. High Throughput Screening* **2006**, *9*, 203–212.
- (9) Liotta, L.; Espina, V.; Mehta, A. I.; Calvert, V.; Rosenblatt, K.; Geho, D.; Munson, P. J.; Young, L.; Mulfkuhle, J.; Petricoin, E. M. *Cancer Cell* **2003**, *3*, 317–325.
- (10) Lueking, A.; Cahill, D. J.; Müllner, S. *Drug Discovery Today* **2005**, *10*, 789–794.
- (11) Ma, H.; Horiuchi, K. Y. *Drug Discovery Today* **2006**, *16*, 661–668.
- (12) Zhou, H.; Roy, S.; Schulman, H.; Natan, M. J. *Trends Biotechnol.* **2001**, *19*, S34–39.
- (13) Habb, B. B.; Dunham, M. J.; Brown, P. O. *Genome Biol.* **2001**, *2*, 1–13.
- (14) Nedelkov, D.; Nelson, R. W. *Trends Biotechnol.* **2003**, *21*, 301–305.
- (15) Zhu, H.; Klemic, J. F.; Chang, S.; Bertone, P.; Casamayor, A.; Klemic, K. G.; Smith, D.; Gerstein, M. A.; Reed, M. A.; Snyder, M. *Nat. Genet.* **2000**, *26*, 283–289.
- (16) Bichsel, V. E.; Liotta, L. A.; Petricoin, E. F. *Cancer J.* **2001**, *7*, 69–78.
- (17) Burbaum, J.; Tobal, G. M. *Curr. Opin. Chem. Biol.* **2002**, *6*, 427–433.
- (18) Miller, J. C.; Zhou, H.; Kwekel, J.; Cavallo, R.; Burke, J.; Butler, E. B.; The, B. S.; Habb, B. B. *Proteomics* **2003**, *3*, 56–63.

- (19) Moody, M. D.; Van, Arsdell, S. W.; Murphy, K. P.; Orencole, S. F.; Burns, C. *Biotechniques* **2001**, *31*, 186–190.
- (20) Knezevic, V.; Leethanakul, C.; Bichsel, V. E.; Worth, J. M.; Prabhu, V. V.; Gutkind, J. S.; Liotta, L.A.; Munson, P. J.; Petricoin, E. F.; Krizman, D. B. *Proteomics* **2001**, *1*, 1271–1278.
- (21) Kusnezow, W.; Jacob, A.; Walijew, A.; Diehl, F.; Hoheisel, J. D. *Proteomics* **2002**, *2*, 345–351.
- (22) MacBeath, G. *Nat. Genet.* **2002**, *32*, 526–532.
- (23) Yu, X.; Xu, D.; Cheng, Q. *Proteomics* **2006**, *6*, 5493–5503.
- (24) Huang, R.; Lin, Y.; Shi, Q.; Flowers, L.; Ramachandran, S.; Horowitz, I. R.; Parthasarathy, S.; Huang, R. P. *Clin. Cancer Res.* **2004**, *10*, 598–609.
- (25) Sapsford, K. E.; Shubin, Y. S.; Delehanty, J. B.; Gloden, J. P.; Taitt, C. R.; Shriver-lake, L. C.; Ligler, F. S. *J. Appl. Microbiol.* **2004**, *96*, 47–58.
- (26) Kawahashi, Y.; Doi, N.; Takashima, H.; Tsuda, C.; Oishi, Y.; Oyama, R.; Yonezawa, M.; Miyamoto-Sato, E.; Yanagawa, H. *Proteomics* **2003**, *3*, 1236–1243.
- (27) Yi, S. J.; Yuk, J. S.; Jung, S. H.; Zhavnerko, G. K.; Kim, Y. M.; Ha, K. S. *Mol. Cells* **2003**, *15*, 333–340.
- (28) Wegner, G. J.; Lee, H. J.; Corn, R. M. *Anal. Chem.* **2002**, *74*, 5161–5168.
- (29) Wegner, G. J.; Lee, H. J.; Marriott, G.; Corn, R. M. *Anal. Chem.* **2003**, *75*, 4740–4746.

- (30) de Crombrughe, B.; Busby, S.; Buc, H. *Science* **1984**, *224*, 831–838.
- (31) Kolb, A.; Busby, S.; Buc, H.; Garges, S.; Adhya, S. *Annu. Rev. Biochem.* **1993**, *62*, 749–795.
- (32) Busby, A.; Ebright, R. H. *J. Mol. Biol.* **1999**, *293*, 199–213.
- (33) Harman, J. G. *Biophys. Biochim. Acta.* **2001**, *1547*, 1–17.
- (34) Angelo, G.; Ebright, Y. W.; Ebright, R. H. *J. Biol. Chem.* **1992**, *267*, 14713–14720.
- (35) Lin, S.-H.; Kovac, L.; Chin, A. J.; Chin, C. C. Q.; Lee, J. C. *Biochemistry* **2002**, *41*, 2946–2955.
- (36) Weber, I. T.; Gilliland, G. L.; Harman, J. G.; Peterkofsky, A. *J. Biol. Chem.* **1987**, *262*, 5630–5636.
- (37) Vaney, M. C.; Gilliland, G. L.; Harman, J. G.; Peterkofsky, A.; Weber, I. T. *Biochemistry* **1989**, *28*, 4568–4574.
- (38) Schultz, S. C.; Shields, G. C.; Steitz, T. A. *Science* **1991**, *253*, 1001–1007.
- (39) Zhou, Y.; Zhang, Z.; Ebright, R. H. *Proc. Natl. Acad. Sci. U.S.A.* **1993**, *90*, 6081–6085.
- (40) Felder, C. B.; Graul, R. C.; Lee, A. Y.; Merkle, H. P.; Sadee, W. *AAPS Pharm. Sci.* **1999**, *1*, E2.
- (41) Tam, R.; Saier, M. H. Jr. *Microbiol. Mol. Biol. Rev.* **1993**, *57*, 320–346.
- (42) Quioco, F. A.; Ledvina, P. S. *Mol. Microbiol.* **1996**, *20*, 17–25.
- (43) Boos, W.; Shuman, H. *Microbiol. Mol. Biol. Rev.* **1998**, *62*, 204–229.

- (44) Zhou, L. Q.; Cass, A. E. G. *Biosens. Bioelectron.* **1991**, *6*, 445–450.
- (45) Gilardi, G.; Zhou, L. Q.; Hibbert, L.; Cass, A. E. G. *Anal. Chem.* **1994**, *66*, 3840–3847.
- (46) Shuman, H. A.; Panagiotidis, C. H. *J. Bioenerg. Biomembr.* **1993**, *25*, 613–620.
- (47) Spurlino, J. C.; Lu, G.-Y.; Quioco, F. A. *J. Biol. Chem.* **1991**, *266*, 5202–5219.
- (48) Sharff, A. J.; Rodseth, L. E.; Szmelcman, S.; Hofnung, M.; Quioco, F. A. *J. Mol. Biol.* **1995**, *246*, 8–13.
- (49) Shilton, B. H.; Flocco, M. M.; Nilsson, M.; Mowbray, S. L. *J. Mol. Biol.* **1996**, *264*, 350–363.
- (50) Shilton, B. H.; Shuman, H. A.; Mowbray, S. L. *J. Mol. Biol.* **1996**, *264*, 364–376.
- (51) Christofides, N. D. In *The Immunoassay Handbook*, 2nd ed.; Wild, D., Ed.; Nature Publishing Group: New York, 2001; pp 61–77.
- (52) Martins, M. C. L.; Fonseca, C.; Barbosa, M. A.; Ratner, B. D. *Biomaterials* **2003**, *24*, 3697–3706.
- (53) Prime, K. L.; Whitesides, G. M. *J. Am. Chem. Soc.* **1993**, *115*, 10714–10721.
- (54) <http://www.gwctechnologies.com/gwcFAQs.htm>

Chapter IV

Bacterial Pathogen Detection with Surface Plasmon Resonance Imaging

1. Introduction

Detection of bacterial pathogens is of great importance to food health and safety.¹⁻³ It is estimated that foodborne diseases lead to 76 million illnesses, 325,000 hospitalizations and 5,000 deaths in the United States each year.⁴ *Escherichia coli* (*E. coli*) has been identified as one of the most dangerous pathogenic bacteria because it can cause diarrhea, hemorrhagic colitis and hemolytic uremic syndrome in humans.⁵⁻⁷ Human infections with *E. coli* can be attributed to the ingestion of a number of contaminated food, such as ground beef, milk, apple juice, lettuce, bean sprouts, tomatoes, green onions, etc.⁸⁻¹⁰ To detect bacterial pathogens in food, several conventional techniques have been widely used, including the culture and colony counting method,¹¹⁻¹³ polymerase chain reaction (PCR)¹⁴⁻¹⁶ and immunology-based assays.¹⁷⁻²⁰ While these methods can produce highly sensitive and selective results, they are quite time-consuming. In the past few years, various types of biosensors have been developed to rapidly identify bacterial pathogens with good sensitivity and specificity.²¹⁻²⁶ Surface plasmon resonance (SPR) is an optical biosensor that has successfully been applied to bacterial successfully detection²⁷⁻²⁹ because of the ability to provide label-free and real-time monitoring of

biomolecular interactions on metal surfaces.^{30–32}

Previous studies of bacterial pathogen detection based on SPR biosensors have predominantly been conducted by means of the interaction between antibodies and bacteria.^{33–36} Fratamico et al.³⁷ employed protein A and protein G to immobilize antibodies that were used to capture *E. coli* O157:H7 on a gold surface. They amplified the SPR signal for bacterial detection using a secondary antibody. The results showed that the limit of detection (LOD) was $5\text{--}7 \times 10^7$ cells/mL in a sandwich assay. Also, they tested that either *Salmonella typhimurium* or *Yersinia enterocolitica* did not generate a significant SPR response on the sensing surface. In 2006, Subramanian et al.³⁸ reported an SPR detection of *E. coli* O157:H7 based on a mixed self-assembled monolayer (SAM). The mixed SAM was composed of two alkanethiols terminated with tri(ethylene glycol) (EG₃-OH) and hexa(ethylene glycol)-carboxylic acid (EG₆-COOH). Antibodies against *E. coli* O157:H7 were attached to the mixed SAM using the amine–NHS coupling method. Then, both direct and sandwich assays were carried out to detect the bacterium. The SPR results indicated that the sandwich assay enhanced the sensitivity by 1000 times compared to the direct assay. In buffer, the LOD was found to be 10^6 CFU/mL for direct detection and 10^3 CFU/mL using a sandwich assay. In apple juice, the LOD was 10^8 CFU/mL for direct detection and 10^6 CFU/mL in the sandwich assay. While the use of antibodies allowed bacteria to be identified with good sensitivity and specificity, the antibody preparation is complicated and laborious.

In our work, the capture of *E. coli* bacteria on a gold surface was achieved through the protein–protein interaction between colicin M (Cma) and ferric hydroxamate uptake protein component A (FhuA). Cma is a toxin protein that consists of a single polypeptide chain and has a molecular weight of 27,000 daltons. This protein can cause *E. coli* lysis in the presence of Ca^{2+} ions.^{39–41} FhuA is a receptor protein located in the outer membrane of *E. coli*, and responsible for the transport of Fe^{3+} ions as a ferrichrome complex.^{42–44} It is also found that FhuA can bind Cma and carry it across the outer membrane of bacteria.⁴⁵ Therefore, Cma could be utilized as a bacterial ligand to capture *E. coli* if target bacterial cells contain a certain amount of FhuA protein in the outer membrane. Figure 4.01 illustrates a representation of protein immobilization and bacterial capture on a gold surface with NTA monolayers. First, a gold surface was incubated in thiol-functionalized NTA (tNTA) to form an NTA monolayer. Then, His₆-tagged Cma was efficiently immobilized on the NTA monolayer in the presence of Ni^{2+} ions. Finally, *E. coli* bacteria were bound to the surface via the Cma–FhuA interaction. SPR imaging was used to characterize the binding events, and also examined the sensitivity and specificity for bacterial detection.

2. Experimental

2.1. Materials

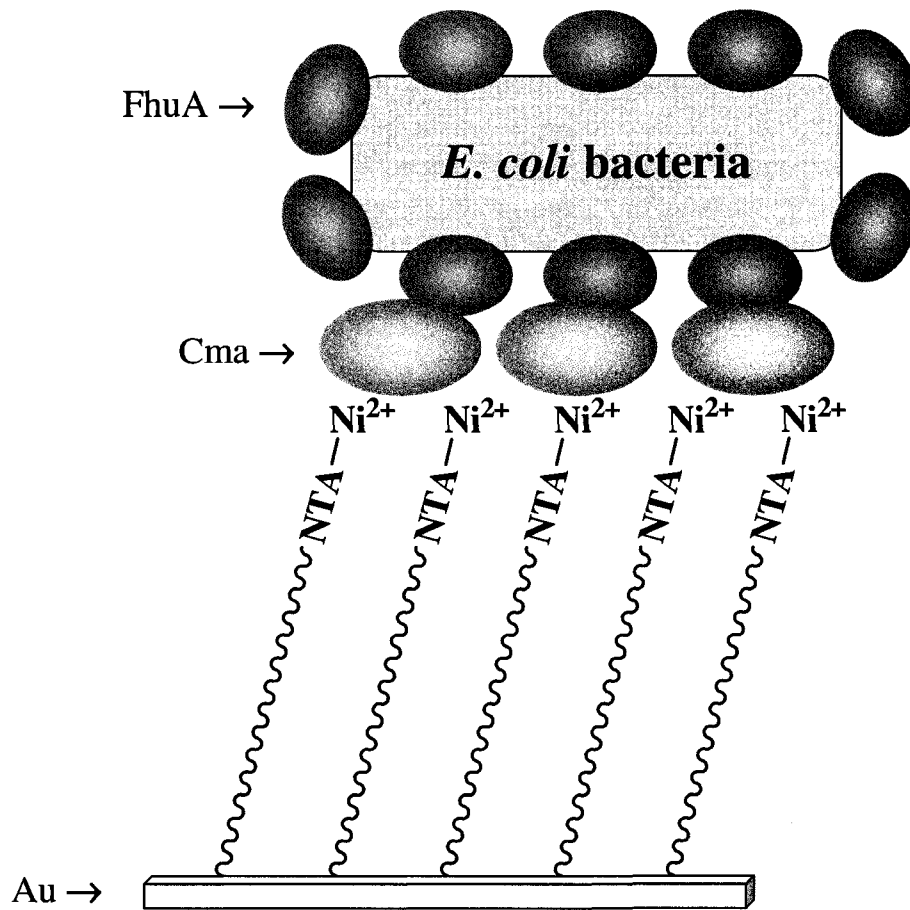


Figure 4.01. Cartoon of His₆-tagged Cma immobilization and *E. coli* bacteria capture on a gold surface modified with NTA-Ni²⁺ monolayers.

11-Mercapto-1-undecanol (MUO), 1,9-nonanedithiol and bovine serum albumin (BSA) were purchased from Sigma–Aldrich (St. Louis, MO). Tridecafluoro-1,1,2,2-tetrahydrooctyl-1-dimethylchlorosilane was obtained from United Chemical Technologies, Inc. (Bristol, PA). *N*-[5-(3'-Maleimidopropylamido)- 1-carboxypentyl]-iminodiacetic acid, disodium salt (maleimido-C₃-NTA) and 11-mercaptoundecylamine (MUAM) were purchased from Dojindo Laboratories (Kumamoto, Japan). All the chemicals were used as received. Thiol-functionalized NTA (tNTA) was synthesized according to the experimental procedure described in Chapter II. His₆-tagged proteins [cyclic AMP receptor protein (CRP; 22.5 kDa), colicin M (Cma; 27.0 kDa)] and bacteria [*E. coli*, *Lactobacillus bulgaricus* (*L. bulgaricus*)] were prepared by Glen Zhang in the laboratory of Professor Joel Weiner (Biochemistry Department, University of Alberta). His₆-tagged CRP was prepared in Tris buffer (50 mM Tris·HCl, 100 mM KCl, pH 7.8). His₆-tagged Cma and bacteria were diluted in Tris buffer (25 mM Tris·HCl, 150 mM NaCl, 0.1% Triton X–100, 10 mM CaCl₂, pH 7.4.). 0.1% BSA was prepared in phosphate-buffered saline (PBS; 8.1 mM Na₂HPO₄, 1.5 mM KH₂PO₄, 137 mM NaCl, 2.7 mM KCl, pH 7.4).

2.2. Surface Modification

SF-10 glass (Schott Glass, Toronto, ON) was soaked into fresh piranha solution (3:1 H₂SO₄–H₂O₂) for 30 min, totally rinsed with 18 MΩ Nanopure water (Barnstead

International, Dubuque, IA) and dried under a stream of argon gas. The glass surface was then fluorinated with tridecafluoro-1,1,2,2-tetrahydrooctyl-1-dimethyl chloro- silane under vacuum to produce a hydrophobic background. 1 nm Cr and 45 nm Au were sequentially coated on the glass by the thermal evaporation (Torr International Inc., New Windsor, NY). Prior to surface modification, the gold chip was cleaned by oxidation in a UV-Ozone cleaner (Jelight Company Inc., Irvine, CA) for 5 min. After washed with 18 M Ω water, the substrate was incubated in an aqueous solution of 0.1 mM tNTA at room temperature for 12 h to form an NTA monolayer. Finally, the NTA monolayer was exposed to 100 mM NaOH for deprotonation followed by coordination with 50 mM NiSO₄ to create an NTA-Ni²⁺ complex on the surface.

2.3. Bacterial Capture

The *E. coli* bacterium was captured by His₆-tagged Cma adsorbed on a gold surface. The procedure of bacterial binding to the surface is described as follows: a solution of 2 μ M His₆-tagged Cma was flowed over a gold surface presenting NTA-Ni²⁺ monolayers for 10 min. The surface was then thoroughly washed with Tris buffer to remove the weakly bound protein. Bioaffinity immobilization of His₆-tagged Cma was achieved through the affinity interaction between His₆-tags and NTA-Ni²⁺ monolayers. A solution of 0.1% BSA was introduced to the chip surface for 10 min to passivate the protein layer

in order for minimizing nonspecific bacterial adsorption. A series of 10-fold diluted *E. coli* solutions were applied to the surface from the lowest to highest concentration. Each bacterial solution was interacted with the bound His₆-tagged Cma for 10 min. SPR images were taken before and after Tris buffer was flushed across the entire chip for 5 min.

2.4. Detection Methods

The capture of *E. coli* on the surface by Cma was detected using a SPR imager (GWC Technologies, Madison, WI). In this apparatus, an incoherent white light source was coupled with a polarizer to generate *p*-polarized light that was directed at the back of gold chip through a SF-10 prism. A flow cell was attached to the chip, which allowed desired solutions to be introduced over the entire surface. The incident angle was controlled by changing the position of a rotation stage where the sample assembly was mounted. The reflected light was directed by a narrow band-pass filter ($\lambda = 800$ nm), and then recorded by a CCD camera. The software Digital Optics V++ 4.0 was utilized to further analyze the images resulting from the experiment. In addition, the presence of *E. coli* on the surface was visualized with an optical microscope. A 5-fold objective was initially used to focus the substrate surface, and then a 50-fold objective was used to detect bacterial cells bound to the surface.

2.5. Sample Preparation

100 g iceberg lettuce was incubated in a 100 mL solution of *E. coli* bacteria at room temperature for 30 min. The lettuce was then removed from the bacterial solution, and totally rinsed with Tris buffer three times. The rinsed solution containing bacterial cells was collected into a beaker through a funnel with glass wool. A Millipore filter (0.22 μm) was used to concentrate the bacterial solution in the beaker. 7 mL Tris buffer was introduced to dissolve the residue *E. coli* remained on the filter. The resulting bacterial solution was centrifuged at 7000 rpm for 10 min using a Beckman J2-21 High Speed Centrifuge (Global Medical Instrumentation, Inc., Ramsey, MN). Pellets of bacterial cells were resuspended in 800 μL Tris buffer. The optical density at 600 nm (i.e., OD_{600}) was measured with a Jenway 6300 spectrophotometer (Barloworld Scientific Ltd, Essex, UK). The concentration of *E. coli* solution was then calculated from the OD_{600} value according to the following relationship: $1.0 \text{ OD}_{600} \approx 1 \times 10^9 \text{ cells/mL}$.

3. Results and Discussion

3.1. *E. coli* Capture by Cma

E. coli GZ25113 was captured to a gold surface through the interaction of immobilized His₆-tagged Cma with FhuA located in the outer membrane of bacterial cells.

In this study, a solution of His₆-tagged Cma was first introduced to a SPR chip containing NTA–Ni²⁺, BSA and MUO monolayers for 10 min. Tris buffer was then flowed across the surface for 5 min to remove nonspecifically adsorbed protein. The resulting SPR difference image is shown in Figure 4.02, and the corresponding SPR signal are listed in Table 4.01. It is clear from the table that His₆-tagged Cma was specifically attached to the NTA monolayer. Both BSA and MUO spots functioned as negative controls with little bound protein. Following His₆-tagged Cma immobilization, a solution of ~10¹¹ cells/mL wild-type *E. coli* was flowed and allowed to sit on the Cma layer for 10 min. Tris buffer was used to wash the surface for 5 min. An SPR difference image was obtained by subtracting the reference image taken before the addition of bacterial solution from the image taken after bacterial capture. Figure 4.03 shows the SPR difference image of *E. coli* binding to immobilized Cma. Table 4.02 presents the SPR signals derived from Figure 4.03. It is demonstrated that a number of bacterial cells were captured on NTA monolayers by the immobilized His₆-tagged Cma. In contrast, little signal was observed on either BSA or MUO monolayer.

To put our method of bacterial detection into practice, *E. coli* was isolated from iceberg lettuce and detected with SPR imaging. First, lettuce was infected with *E. coli* bacteria for 30 min at room temperature. The bacterial cells were then extracted using Tris buffer, filtered and concentrated to ~ 1 × 10⁹ cells/mL for SPR measurements. Table 4.03 summarizes the SPR response obtained after a solution of *E. coli* from lettuce was

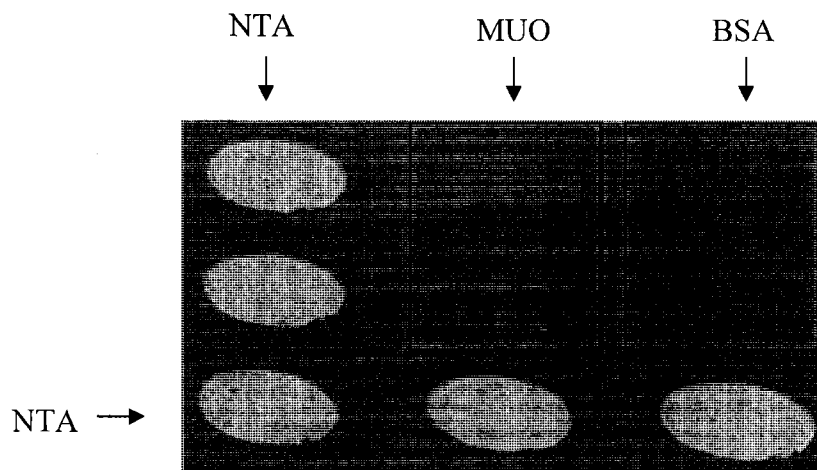


Figure 4.02. SPR difference image of 2 μM His₆-tagged Cma immobilization on the chip containing NTA, MUO and BSA monolayers. The MUO and BSA spots were used as negative controls.

| Monolayer | SPR signal ($\Delta\%R$) |
|------------------|--|
| NTA | 27.0 (1.7) |
| MUO | 2.2 (0.3) |
| BSA | -1.0 (1.1) |

Table 4.01. SPR signals for immobilizing 2 μM His₆-tagged Cma on the various monolayers shown in Figure 4.02. Numbers in parentheses are standard deviations of the indicated values.

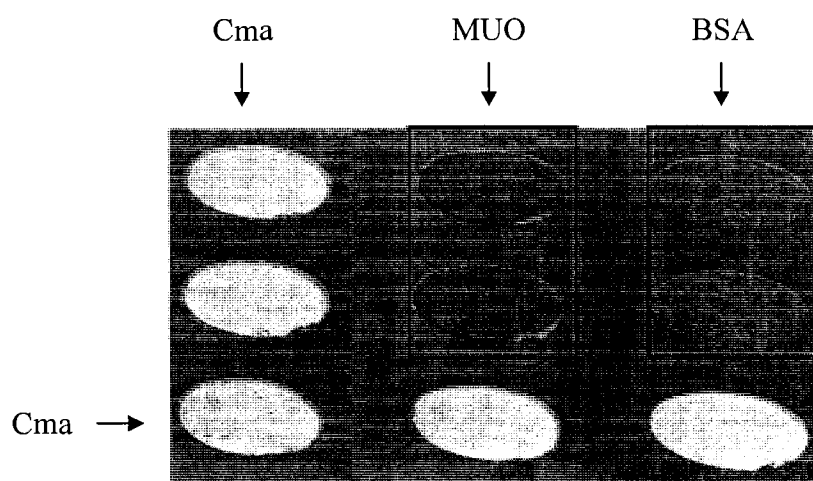


Figure 4.03. SPR difference image of $\sim 5 \times 10^9$ cells/mL *E. coli* capture on the immobilized Cma, MUO and BSA monolayers. The MUO and BSA served as negative controls.

| Monolayer | SPR signal ($\Delta\%R$) |
|------------------|--|
| Cma | 17.6 (1.6) |
| MUO | 0.6 (0.2) |
| BSA | 1.2 (0.5) |

Table 4.02. SPR signals for $\sim 5 \times 10^9$ cells/mL *E. coli* capture on the various monolayers illustrated in Figure 4.03. Numbers in parentheses are standard deviations of the indicated values.

| Monolayer | SPR signal ($\Delta\%R$) |
|-----------|----------------------------|
| Cma | 3.1 (0.4) |
| MUO | 1.2 (0.2) |

Table 4.03. SPR signals for detection of $\sim 5 \times 10^8$ cells/mL *E. coli E. coli* bacteria from iceberg lettuce. The Cma layer was used to bind bacterial cells, and the MUO monolayers as a negative control. Numbers in parentheses are standard deviations of the indicated values.

introduced to the immobilized Cma for 10 min. Although the signal of *E. coli* binding to Cma is relatively low, it is still significantly different from the signal observed on the MUO monolayer. Besides, we employed an optical microscope to confirm the presence of *E. coli* captured on the gold surface. In Figure 4.04 A, immobilized His₆-tagged Cma and MUO monolayers were patterned using a poly(dimethylsiloxane) (PDMS) microfluidic device.⁴⁶ The captured bacterial cells are clearly visible and evenly distributed on the gold surface adsorbing His₆-tagged Cma (Figure 4.04 B). As a negative control, the MUO monolayer prevented the binding of bacteria to the surface, and consequently there was no bacterial cell found in Figure 4.04 C.

3.2. Specificity Testing

The specificity of *E. coli* binding to immobilized His₆-tagged Cma was probed using SPR imaging. First, we tested the binding difference between mutant and wild-type strains of *E. coli* bacteria. In this case, the mutant strain was prepared without FhuA present in the outer membrane, so this bacterium is not expected to bind His₆-tagged Cma on the surface. To probe the binding of the mutant strain, the gold surface was initially modified with an NTA-Ni²⁺ monolayer for His₆-tagged Cma attachment. A solution of the mutant *E. coli* was then flowed over the surface and containing 1 M NaCl was used to regenerate the Cma layer by removing any captured bacteria from the surface. A solution

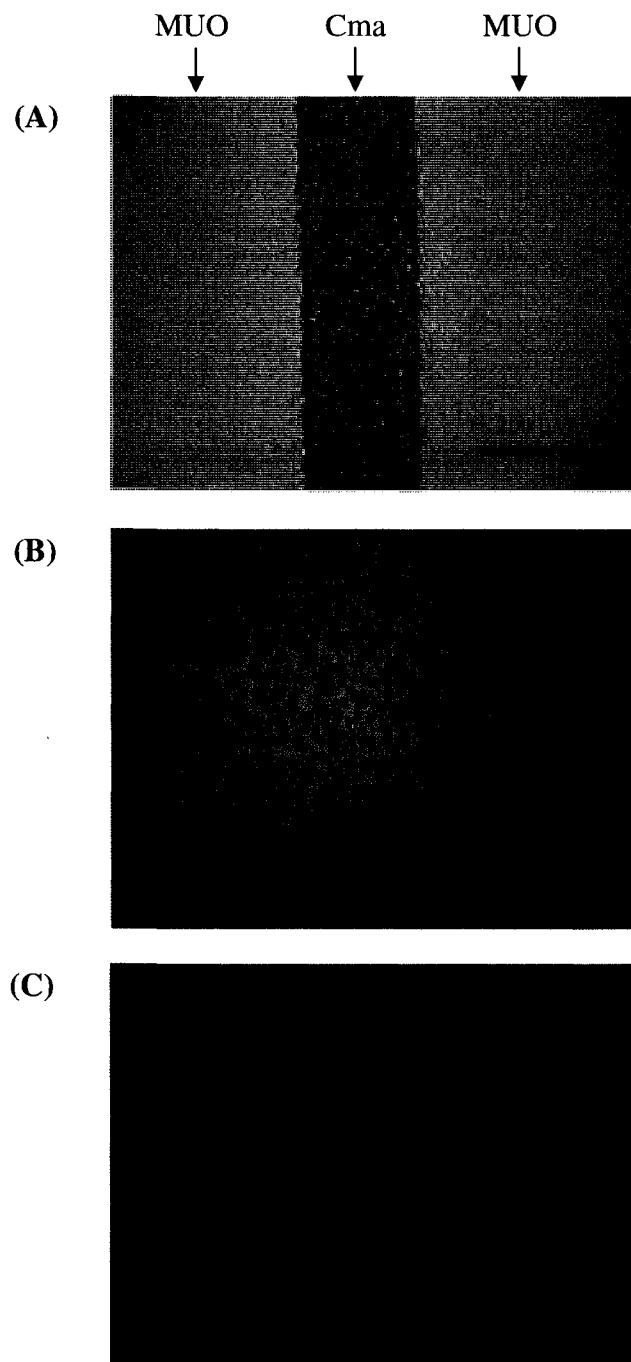


Figure 4.04. Optical images of $\sim 10^{12}$ cells/mL *E. coli* binding on a gold surface containing (A) patterned Cma and MUO; (B) the immobilized Cma; (C) the MUO monolayer.

of the wild-type *E. coli* was delivered to the chip surface for 10 min followed by 5-min washing with Tris buffer. Figure 4.05 compares the two different strains captured on the immobilized. A MUO monolayer was employed as a negative control to avoid protein and bacterial binding. It is clear from the figure that a significant SPR signal resulted from the binding of wild-type *E. coli* to the surface. In contrast, much less SPR response was observed for the mutant strain. This result is quite consistent with our expectation, which indicates that the interaction between Cma and *E. coli* was specific and required the presence of FhuA in bacterial cells.

Also, we evaluated the specificity of *E. coli* detection relative to other bacteria. *L. bulgaricus* is a Gram-positive bacterium that is often utilized for the production of yogurt.⁴⁷ During the fermentation of milk, this bacterium breaks down lactose, and releases lactic acid that reacts with the milk protein to produce yogurt. Since this bacterium does not contain FhuA in the outer membrane, it cannot be captured by Cma. To verify our supposition, a solution of *L. bulgaricus* was introduced to the surface bearing immobilized His₆-tagged Cma for 10 min. Tris buffer containing 1 M NaCl was flushed through the chip surface for 5 min to minimize nonspecific bacterial adsorption. A wild-type *E. coli* solution was then injected over the surface for 10 min. Regular Tris buffer was flushed across the surface before and after the addition of each analyte solution. In Figure 4.06, a bar graph is shown to compare the binding of the two bacteria on Cma. The $\Delta\%R$ value for *E. coli* adsorption is much greater than *L. bulgaricus*, which

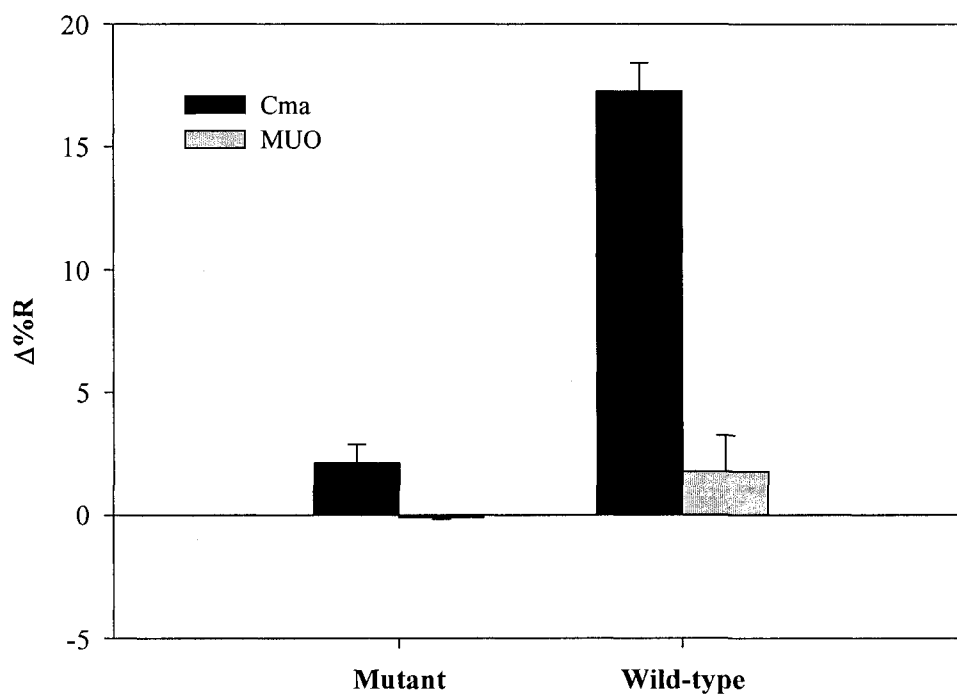


Figure 4.05. SPR signals ($\Delta\%R$) of immobilized His₆-tagged Cma against the mutant and wild-type strains of *E. coli* bacteria. The bacterial concentration is $\sim 5 \times 10^9$ cells/mL. The MUO monolayer is a negative control. The error bars illustrate the standard deviation of three-spots SPR measurements.

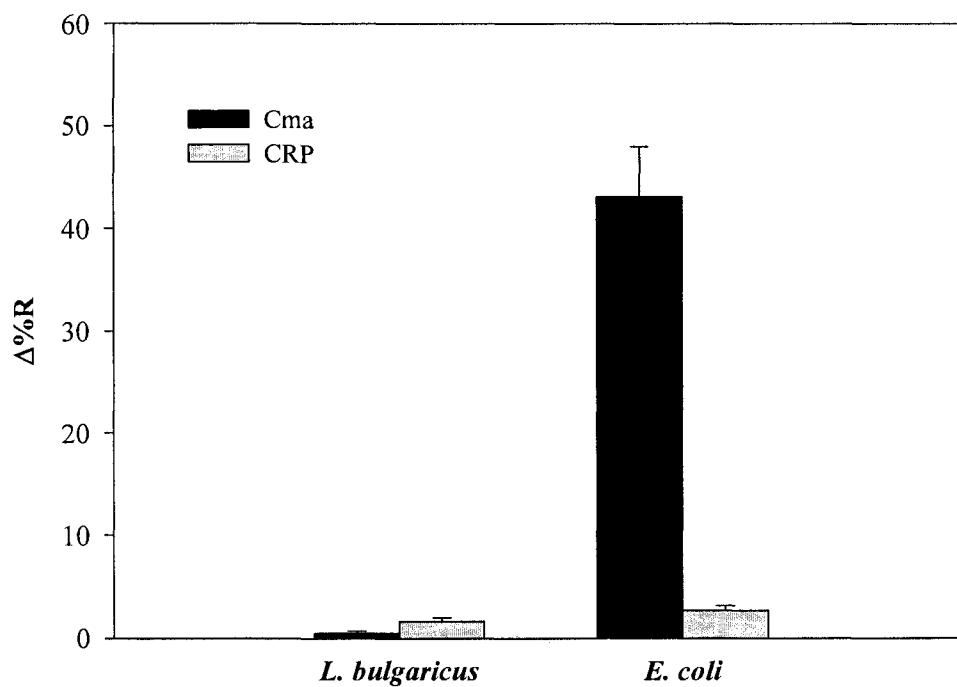


Figure 4.06. SPR signals ($\Delta\%R$) of immobilized His₆-tagged Cma against the *L. bulgaricus* and *E. coli* bacteria. The concentration of bacteria is $\sim 10^{11}$ cells/mL. His₆-tagged CRP adsorbed on NTA monolayers is a negative control. The error bars stand for the standard deviation on three-spot SPR measurements.

indicates that the specificity of *E. coli* detection was relatively high. Here, Immobilized His₆-tagged CRP was used as a negative control because no interaction existed between CRP and *E. coli* or *L. bulgaricus*. Also, since CRP was immobilized through the same His₆-NTA interaction as Cma, this provided a measure of nonspecific bacterial binding to unreacted NTA groups on the chip. A low SPR signal observed on the CRP spots proves that nonspecific adsorption of bacteria was minimal in our assay.

3.3. Binding Curve and Sensitivity

To further quantify the interaction between Cma and *E. coli*, we investigate bacterial capture at various concentration of bacterial solutions. In this study, a series of *E. coli* solutions at various concentrations were sequentially flowed and allowed to react with the His₆-tagged Cma layer for 10 min. The surface was rinsed with Tris buffer before and after the introduction of each bacterial solution. Figure 4.07 shows an overlay of *E. coli* binding to the two bound His₆-tagged proteins Cma and CRP. It is evident from the figure that the amount of captured bacteria on the Cma layer is increased with the amount of bacterial cells in solution. The immobilized His₆-tagged CRP was used as a negative control. The LOD value was estimated to be $\sim 1 \times 10^7$ cells/mL. Previous studies have been reported on the sensitivity of *E. coli* detection using SPR biosensors. Taylor et al.³⁴ determined the LOD to be 10^6 cells/mL for viable *E. coli*. Their SPR

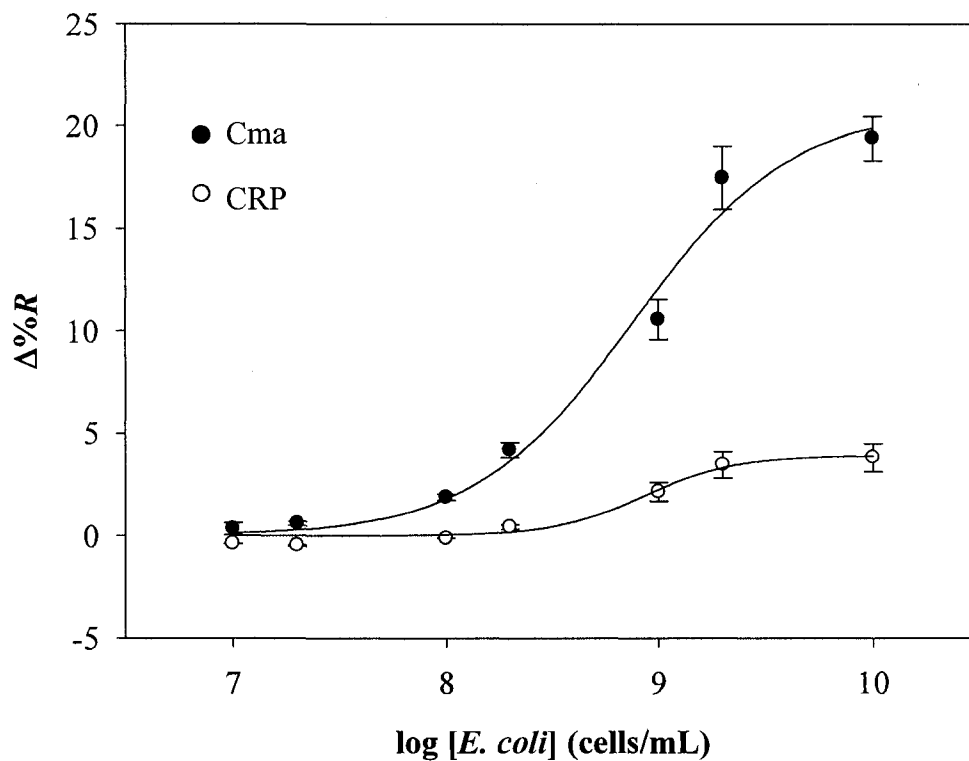


Figure 4.07. Curve of *E. coli* binding to the immobilized His₆-tagged Cma and His₆-tagged CRP on NTA monolayers. The CRP layer served as a negative control. The error bars represent the standard deviation of three-spot SPR measurements.

measurements also involved antibodies for bacterial capture and signal amplification by a sandwich assay. While we used a different surface chemistry, bacterial capture ligand and SPR biosensor, the LOD in our method seems comparable to other methods. However, this sensitivity is quite low for food monitoring, so it requires considerable improvement in order to detect bacterial pathogens in a real sample.

4. Conclusions

In this chapter, a new method was developed for detection of *E. coli* bacteria with SPR imaging. This work was the first attempt to bind *E. coli* using a bacterial protein instead of an antibody. The specificity of bacterial binding to the immobilized Cma on NTA-Ni²⁺ monolayers was evaluated by testing the mutant strain of *E. coli* and the *L. bulgaricus* bacterium. Little bacterial binding was observed when FhuA was absent in the outer membrane of bacterial cells. Moreover, the LOD of *E. coli* detection was determined to be $\sim 1 \times 10^7$ cells/mL in a direct assay. The use of an optical microscope allowed to confirm the presence of *E. coli* captured on the immobilized Cma surface. Thus, our results demonstrated that Cma can be employed as a specific binding ligand to capture *E. coli* bacteria on the surface. SPR imaging also has the potential to monitor the protein-bacterium interaction without the labeling step. However, applications of our method in detection of bacteria in food need further investigation. In future studies, we

will amplify SPR signals of bacterial binding to enhance the sensitivity either using a sandwich assay or by labeling with gold nanoparticles.

5. References

- (1) Patel, P. D. *Trends Anal. Chem.* **2002**, *21*, 96–115.
- (2) Leonard, P.; Hearty, S.; Brennan, J.; Dunne, L.; Quinn, J.; Chakraborty, T.; O’Kennedy, R. *Enzyme Microb. Technol.* **2003**, *32*, 3–13.
- (3) Lazcka, O.; Del Campo, F. J.; Muñoz, F. X. *Biosens. Bioelectron.* **2007**, *22*, 1205–1217.
- (4) Mead, P. S.; Slutsker, L.; Dietz, V. *Emerg. Infect. Dis.* **1999**, *5*, 607–625.
- (5) Griffin, P. M.; Tauxe, R. V. *Epidemiol. Rev.* **1991**, *13*, 60–98.
- (6) Buchanan, R. L.; Doly, M. P. *Food Technol.* **1997**, *51*, 69–76.
- (7) DeCludt, B.; Bouvet, P.; Mariani-Kurkdjian, P.; Grimont, F.; Grimont, P. A. D.; Hubert, B.; Loirat, C. *Epidemiol. Infect.* **2000**, *124*, 215–220.
- (8) Pebody, R. G.; Furtado, C.; Rojas, A.; McCarthy, N.; Nylén, G.; Ruutu, P.; Leino, T.; Chalmers, R.; de Jong, B.; Donnelly, M.; Fisher, I.; Gilham, C.; Graverson, L.; Cheasty, T.; Willshaw, G.; Navarro, M.; Salmon, R.; Leinikki, P.; Wall, P.; Bartlett, C. *Epidemiol. Infect.* **1999**, *123*, 217–223.
- (9) Chapman, P. A.; Siddons, C. A.; Cerdan Malo, A. T.; Harkin, M. A. *Epidemiol.*

- Infect.* **2000**, *124*, 207–213.
- (10) Radke, S. M.; Alocilja, E. C. *Biosens. Bioelectron.* **2005**, *20*, 1662–1667.
- (11) Villari, P. M. E.; Farullo, C.; Torre, I. *Lett. Appl. Microbiol.* **1998**, *27*, 106–110.
- (12) Brooks, B. W.; Devenish, J.; Lutze-Wallace, C. L.; Milnes, D.; Robertson, R. H.; Berlie-Surujballi, G. *Vet. Microbiol.* **2004**, *103*, 77–84.
- (13) Fratamico, P. M. *Mol. Cellular Probes* **2003**, *17*, 215–221.
- (14) Zhou, X.; Jiao, X. *Food Contr.* **2004**, *16*, 125–130.
- (15) Dubosson, C. R.; Conzelmann, C.; Miserez, R.; Boerlin, P.; Frey, J.; Zimmermann, W. *Vet. Microbiol.* **2004**, *102*, 55–65.
- (16) Lazaro, D. R.; Hernandez, M.; Esteve, R.; Hoorfar, J.; Pla, M. *J. Microbiol. Meth.* **2003**, *54*, 381–390.
- (17) Mine, Y. *J. Agric. Food Chem.* **1997**, *45*, 3723–3727.
- (18) Pérez, F. G.; Mascini, M.; Tothill, I. E.; Turner, A. P. F. *Anal. Chem.* **1998**, *70*, 2380–2386.
- (19) Andresen, L. O.; Klausen, J.; Barfod, K.; Sorensen, V. *Vet. Microbiol.* **2002**, *89*, 61–67.
- (20) Gu, H. W.; Xu, K. M.; Xu, C. J.; Xu, B. *Chem. Commun.* **2006**, *9*, 941–949.
- (21) Schneider, B. H.; Edwards, J. G.; Hartman, N. F. *Clin. Chem.* **1997**, *43*, 1757–1763.
- (22) Gehring, A. G.; Patterson, D. L., Tu, S. I.; *Anal. Biochem.* **1998**, *258*, 293–298.

- (23) Abdel-Hamid, I.; Ivnitski, D.; Atanasov, P.; Wilkins, E. *Biosens. Bioelectron.* **1999**, *14*, 309–316.
- (24) Muhammad-Tahir, Z.; Alocilja, E. C. *Biosens. Bioelectron.* **2003**, *18*, 813–819.
- (25) Su, X. L.; Li, Y. *Biosens. Bioelectron.* **2004**, *19*, 563–574.
- (26) Ko, S.; Grant, S. A. *Sens. Actuators B* **2003**, *96*, 372–378.
- (27) Darren, M. D.; David, C. C.; Hong-Xing, Y.; Christopher, R. L. *Biosens. Bioelectron.* **1998**, *13*, 1213–1225.
- (28) Homola, J.; Dostalek, J.; Chen, S. F.; Rasooly, A.; Jing, S. Y.; Yee, S. S. *Int. J. Food Microbiol.* **2002**, *75*, 61–69.
- (29) Yu, Q. M.; Chen, S. F.; Taylor, A. D.; Homola, J.; Hock, B.; Jiang, S. Y. *Sens. Actuators B* **2005**, *107*, 193–201.
- (30) Knoll, W. *Annu. Rev. Phys. Chem.* **1998**, *49*, 569–638.
- (31) Brockman, J. M.; Nelson, B. P.; Corn, R. M. *Annu. Rev. Phys. Chem.* **2000**, *51*, 41–63.
- (32) Smith, E. A.; Corn, R. M. *Appl. Spectrosc.* **2003**, *57*, 320A–332A.
- (33) Sakai, G.; Ogata, K.; Uda, T.; Miura, N.; Yamazoe, N. *Sens. Actuators B* **1998**, *49*, 5–12.
- (34) Taylor, A. D.; Yu, Q.; Chen, S. Homola, J.; Jiang, S. *Sens. Actuators B* **2005**, *107*, 202–208.
- (35) Oh, B.-K.; Lee, W.; Chun, B. S.; Bae, Y. M.; Lee, W. H.; Choi, J.-W. *Colloids*

- Surf. A: Physicochem. Eng. Aspects* **2005**, 257–258, 369–374.
- (36) Oh, B.-K.; Kim, Y.-K.; Lee, W.; Bae, Y. M.; Lee, W. H.; Choi, J.-W. *Biosens. Bioelectron.* **2003**, *18*, 605–611.
- (37) Fratamico, P. M.; Strobaugh, T. P.; Medina, M. B.; Gehring, A. G. *Biotechnol. Tech.* **1998**, *12*, 571–576.
- (38) Subramanian A.; Irudayaraj, J.; Ryan, T. *Biosens. Bioelectron.* **2006**, *21*, 998–1006.
- (39) Braun, V.; Shaller, K.; Wolff, H. *Biochim. Biophys. Acta.* **1973**, *328*, 87–97.
- (40) Braun, V.; Frenz, S.; Hantke, K.; Shaller, K. *J. Bacteriol.* **1980**, *142*, 162–168.
- (41) Schaller, K.; Dreher, R.; Braun, V. *J. Bacteriol.* **1981**, *146*, 54–63.
- (42) Hantke, K.; Braun, V. *J. Bacteriol.* **1978**, *135*, 190–197.
- (43) Killmann, H.; Benz, R.; Braun, V. *J. Bacteriol.* **1996**, *178*, 6913–6920.
- (44) Bonhivers, M.; Ghazi, A.; Boulanger, P.; Letellier, L. *EMBO* **1996**, *15*, 1850–1856.
- (45) Kadner, R. J.; Heller, K.; Coulton, J. W.; Braun, V. *J. Bacteriol.* **1980**, *143*, 256–264.
- (46) Xia, Y.; Whitesides, G. M. *Angew. Chem. Int. Ed.* **1998**, *37*, 550–575.
- (47) Balows, A.; Truper, H. G.; Dworkin, M.; Harder, W.; Sheleifer, K. H. In *The Prokaryotes, 2nd Ed., A Handbook on the Biology of Bacteria*, 1991, pp 1547.

Chapter V

Protein Identification from Bacteria Captured and Lysed on a Single Chip

1. Introduction

E. coli is a bacterium that usually lives in the intestine of warm-blooded animals. Some strains of *E. coli* are pathogenic, such as O157:H7 and O111:B4, can cause serious illness or death in humans.¹⁻³ To reduce foodborne diseases caused by *E. coli*, a variety of methods have recently been reported for bacterial detection in food and water.⁴⁻⁹ In 2003, Muhammad-Tahir et al.⁶ developed a conductometric biosensor to identify foodborne pathogens, including *E. coli* O157:H7, using polyclonal antibodies. The results showed that 7.9×10^1 colony forming units per milliliter (CFU/mL) of *E. coli* could be detected within 2–10 min. In 2008, Liu et al.⁹ used reverse transcription-PCR and electronic microarray to detect viable *E. coli* O157:H7 in drinking water and river water. The limit of detection (LOD) was found to be 1 CFU/L in diluted cultures, 3–4 CFU/L in tap water, 7 CFU/L in river water.

In the previous chapter, it was shown that colicin M (Cma) functioned as a bacterial receptor to bind *E. coli*. However, all *E. coli* strains can be captured and detected because the protein FhuA resides in both pathogenic and non-pathogenic strains.^{10,11} Various components of *E. coli*, such as lipopolysaccharides or RNA,¹²⁻¹⁴ have

been used as a marker for pathogenic bacteria. Building upon the knowledge that immobilized Cma can efficiently capture whole *E. coli*, we envision that these captured bacteria can be lysed, and then cellular components detected on a single SPR chip. Detection of markers specific to pathogenic *E. coli* can potentially provide a route for pathogen determination. To test this idea, an array chip was designed to bind *E. coli* using immobilized Cma at specific array addresses. Addition of an appropriate lysis solution will release all cellular components to the remaining array elements with immobilized antibodies we have chosen to detect the bacterial protein CRP at other addresses on the same chip. We believe that a single chip capable of capturing and typing pathogenic bacteria without rigorous sample preparation will be valuable for pathogen detection.

2. Experimental

2.1. Materials

Thiol-functionalized NTA (tNTA) was synthesized according to the procedure described in Chapter II. 11-Mercaptoundecylamine (MUAM) and *N*-hydroxy-succinimidyl ester of 11-mercaptoundecanoic acid (thiol-NHS) were obtained from Dojindo Laboratories (Kumamoto, Japan) and ProChimia (Gdansk, Poland), respectively. Tridecafluoro-1,1,2,2-tetrahydrooctyl-1-dimethylchlorosilane and Bovine serum albumin (BSA) were purchased from United Chemical Technologies (Bristol, PA) and

Sigma–Aldrich (St. Louis, MO), respectively. Bacterial protein extraction reagent (B-PER) was purchased from Pierce Biotechnology, Inc. (Rockford, IL) and used for bacterial cell lysis. His₆-tagged Cma, anti-CRP antibody and *E. coli* bacteria were provided by Glen Zhang in the laboratory of Professor Joel Weiner (Biochemistry Department, University of Alberta). Tris buffer was used to prepare His₆-tagged Cma, which contained 25 mM Tris·HCl (pH 7.4), 150 mM NaCl and 0.1% Triton X–100. 0.1% BSA solution was prepared in phosphate-buffered saline (PBS, pH 7.4) composed of 8.1 mM Na₂HPO₄, 1.5 mM KH₂PO₄, 137 mM NaCl and 2.7 mM KCl.

2.2. Surface Functionalization

A SPR chip was prepared by coating a thin gold film (45 nm) on SF-10 glass (Schott Glass, Toronto, ON) with the thermal evaporation (Torr International, Inc., New Windsor, NY). Self-assembled monolayers (SAMs) of alkanethiols were used to modify the gold surface to immobilize target proteins and fabricate a protein array. Different gold spots on one chip were separately exposed to solutions of thiol-NHS, MUAM and tNTA for 12 h to form three monolayers terminated with NHS ester, amine and NTA groups, respectively. A solution of anti-CRP antibody was delivered on the NHS monolayer for 3–4 h. An amide bond linkage was formed between the NHS group and the amine group of antibodies. 0.1% BSA was introduced to the monolayer of MUAM for 3–4 h. Physical

adsorption allowed the immobilization of BSA on the gold surface. The NTA-modified spots were treated with 100 mM NaOH for 5 min followed by 50 mM NiSO₄ for 15 min to create an NTA–Ni²⁺ complex that can be used to immobilize 2 μM His₆-tagged Cma by a specific affinity interaction. Thus, the SPR chip consisted of three components, that is, anti-CRP antibody, BSA and NTA–Ni²⁺ group.

2.3. Bacterial Lysis and Protein Detection

Figure 5.01 depicts a representative scheme for bacterial capture and protein identification after cell lysis. First, a solution of 2 μM His₆-tagged Cma was flowed over an SPR chip modified with anti-CRP antibody, BSA and NTA–Ni²⁺ for 10 min. This process resulted in an efficient immobilization of His₆-tagged Cma on the NTA spots. The sensor surface was then washed with Tris buffer for 5 min to remove nonspecifically bound protein. Secondly, a solution of ~ 10¹¹ cells/mL wild-type *E. coli* was introduced to the sensor surface for 10 min followed by 5-min washing with Tris buffer. Bacterial cells were bound to the surface through the specific interaction between Cma and FhuA residing in the outer membrane of *E. coli*. Thirdly, bacterial protein extraction reagent (B-PER II) was flowed across the chip surface and allowed to sit there for 15 min to lyse the captured bacteria. Products of bacterial lysis contained the bacterial protein CRP, which was then recognized by anti-CRP antibody immobilized on the same chip.

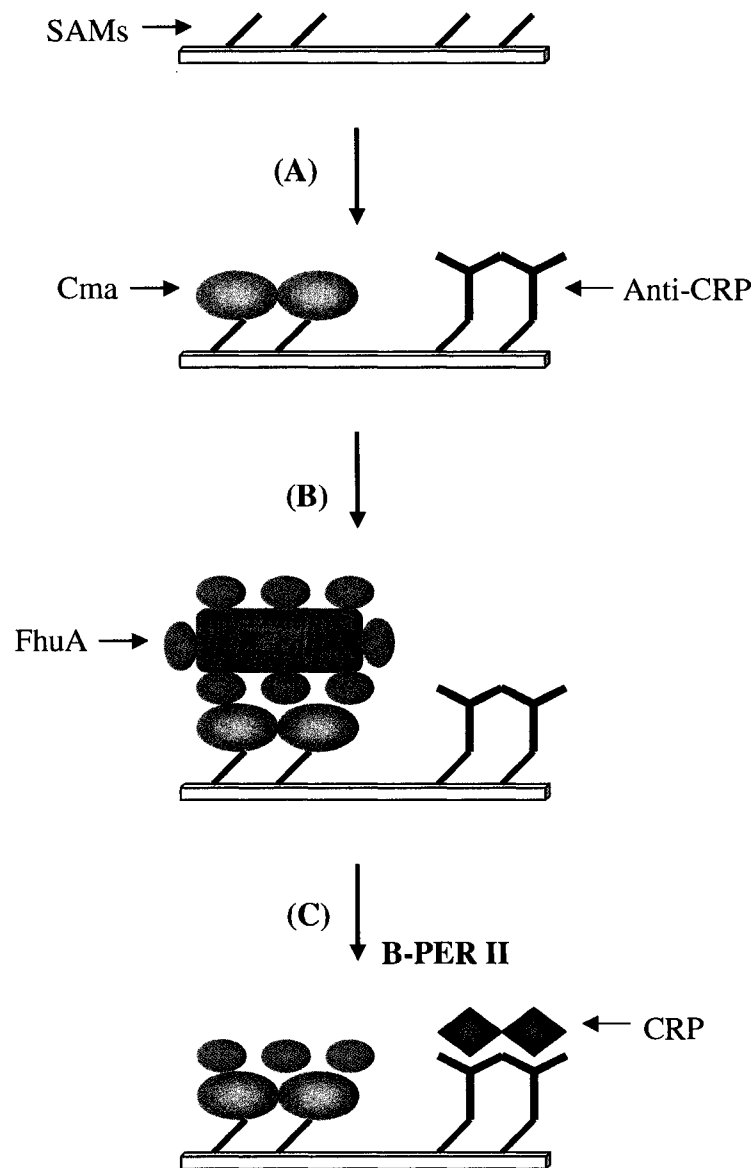


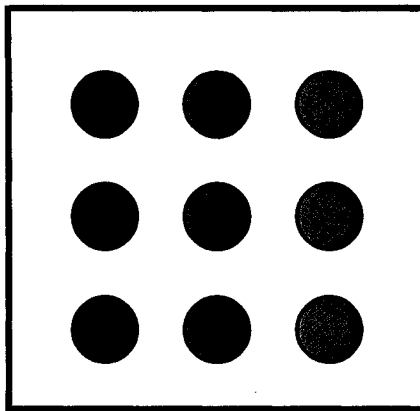
Figure 5.01. Scheme of Cma immobilization, *E. coli* capture and CRP identification after cell lysis. (A) Cma and anti-CRP were anchored on NTA-Ni²⁺ and MUAM monolayers, respectively. (B) *E. coli* bacteria were bound to the Cma layer. (C) Captured cells were lysed and the released CRP was captured by anti-CRP antibody.

2.4. SPR imaging

SPR imaging was utilized to monitor bacterial cell lysis and to detect the binding of bacterial proteins released from lysed captured cells. In a SPR imager (GWC Technologies, Madison, WI), a polarizer is installed to create *p*-polarized light from a white light source. A SF-10 prism is coupled with a SF-10 glass slide deposited with 1 nm Cr and 45 nm Au. The angle of incident light is adjusted by the rotation stage where a sample assembly (i.e., prism/thin gold film) is located. Desired solutions are delivered to the entire sensor surface through a flow cell that is attached to the gold film. The reflected light from the backside of the glass slide passes through a narrow band-pass filter ($\lambda = 830$ nm), and immediately detected by a CCD camera. All SPR images are the average of 100 frames and further analyzed with the software package Digital Optics V++ 4.0.

3. Results and Discussion

In an effort to provide the identification of captured bacteria on a single chip, we designed an experiment to detect specific bacterial proteins released from lysed captured cells. A chip was fabricated with spots to capture *E. coli* bacteria and spots to detect the bacterial protein CRP following lysis of captured cells. The chip layout is shown in Figure 5.02. Spots containing a layer of immobilized BSA were used as a negative



- MUAM + BSA
- Thiol-NHS + anti-CRP
- NTA-Ni²⁺ + His₆-tagged Cma

Figure 5.02. Layout of the SPR chip used for bacterial capture and bacterial protein detection after cell lysis. 0.1% BSA was physically adsorbed on an MUAM monolayer. Anti-CRP antibody was covalently attached to an NHS monolayer. His₆-tagged Cma was specifically immobilized via the affinity interaction between the His₆ tag and NTA-Ni²⁺ group.

control. Different strategies were employed to immobilize anti-CRP antibody, BSA and His₆-tagged Cma. Covalent attachment of anti-CRP to gold surfaces was achieved by the formation of an amide bond linkage on the NHS monolayer. BSA was anchored on the chip by physical adsorption. His₆-tagged Cma was adsorbed via an affinity interaction, and this method can provide an efficient and oriented protein immobilization.

The preceding chapters have demonstrated that His₆-tagged Cma can be specifically immobilized on an NTA-modified gold surface in the presence of Ni²⁺ ions. Figure 5.03 presents a SPR difference image obtained after the addition of 2 μM His₆-tagged Cma to the sensor surface for 10 min. A significant signal was observed on the spots with NTA–Ni²⁺ species, compared to the spots containing anti-CRP and BSA. To better quantify the immobilization of His₆-tagged Cma, Table 5.01 lists SPR signals on the various monolayers based the image shown in Figure 5.03. A much greater Δ%R was found on the NTA spots, which was caused by the efficient adsorption of His₆-tagged Cma. In contrast, the spots of either anti-CRP antibody or BSA showed much less SPR signals, indicating that the immobilization of His₆-tagged Cma was quite specific for the surface bearing NTA–Ni²⁺ moieties. The low SPR response arose from nonspecific protein binding. Now the resulting protein array was ready to capture bacterial cells in solution.

To bind bacteria on the gold surface, a solution of ~ 10¹¹ cells/mL wild-type *E. coli* was flowed over the protein array containing anti-CRP antibody, BSA and Cma for 10

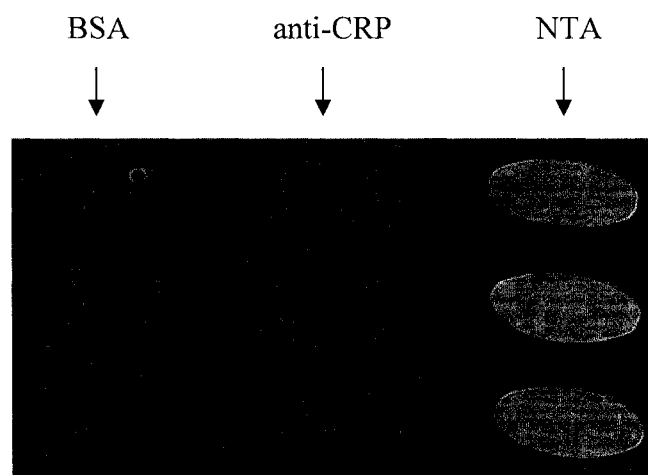


Figure 5.03. SPR difference image of 2 μM His₆-tagged Cma immobilization on the gold chip with BSA, anti-CRP antibody and NTA monolayers.

| Monolayer | SPR signal ($\Delta\%R$) |
|------------------|--|
| BSA | 1.7 (0.6) |
| Anti-CRP | 1.8 (0.4) |
| NTA | 18.5 (0.8) |

Table 5.01. SPR signals for 2 μM His₆-tagged Cma adsorption on the various monolayers shown in Figure 5.03. Numbers in parentheses are standard deviations of the indicated values.

min. Figure 5.04 displays a SPR difference image recorded following the introduction of bacterial solution. It is evident from the figure that the bacteria were only captured on the Cma spots. It is also found that little bacteria were bound on the BSA or anti-CRP spots. This result indicates that nonspecifically adsorbed Cma in the previous step was not active for capturing *E. coli*. Similarly, Table 5.02 gives the SPR signal of bacterial capture on the various monolayers. It is clear from the table that the binding of *E. coli* to Cma was very specific.

Once *E. coli* bacteria were captured on the surface, B-PER II was used to lyse the bacterial cells bound on the surface. This reagent allowed bacterial cells to be broken under gentle conditions, so proteins released from the lysed cells were not denatured.⁸ Then, the released bacterial protein CRP was anchored to the immobilized anti-CRP antibody, and the antigen–antibody interaction was detected with SPR imaging. Table 5.03 summarizes the SPR signals obtained after bacterial cell lysis. A negative $\Delta\%R$ value was observed on the Cma layer, which was consistent with the destruction of the bound cells. The small SPR signal obtained on the anti-CRP spots indicates that we probably captured the target protein CRP released from bacterial lysis. At this point, our detected signal is very low. However, the result is still promising and suggests that bacterial capture and identification may be performed on a single chip. Moreover, this method has the potential to distinguish pathogenic bacteria from non-pathogenic bacteria if specific bacterial proteins in pathogenic bacteria are recognized by suitable ligands that

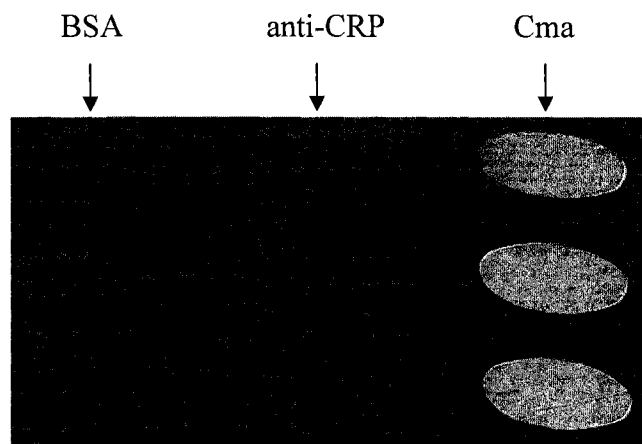


Figure 5.04. SPR difference image of $\sim 10^{11}$ cells/mL *E. coli* binding to the immobilized Cma. BSA spots were employed for a negative control.

| Monolayer | SPR signal ($\Delta\%R$) |
|-----------|----------------------------|
| BSA | 0.3 (0.9) |
| Anti-CRP | 0.2 (0.3) |
| Cma | 25.3 (4.4) |

Table 5.02. SPR signals for the capture of $\sim 10^{11}$ cells/mL *E. coli* on the various monolayers displayed in Figure 5.04. Numbers in parentheses represents standard deviations of the indicated values.

| Monolayer | SPR signal ($\Delta\%R$) |
|------------------|--|
| BSA | 0.3 (0.2) |
| Anti-CRP | 1.5 (0.3) |
| <i>E. coli</i> | -30.9 (9.3) |

Table 5.03. SPR signals for identification of CRP released after lysis of the captured bacterial cells using anti-CRP antibody. Numbers in parentheses stand for standard deviations of the indicated values.

include antibodies, DNA and peptides.

4. Conclusions

In this chapter, we demonstrate the identification of a specific bacterial protein after bacterial lysis using SPR imaging. This study is a further application of the method we previously developed for protein immobilization and bacterial detection. Protein arrays are also involved due to its high-throughput ability. The B-PER II reagent was utilized to lyse captured bacterial cells under non-denaturation conditions. Specific antibodies were employed to bind bacterial proteins released from the lysed cells. While the SPR signal on the antigen–antibody binding is quite low, there is still a promise that the pathogenic property of captured bacteria could be determined through the detection of representative bacterial proteins using appropriate protein ligands. In addition, multiple analysis on a single SPR chip offers a simple and rapid way to confirm the identity of captured bacteria.

5. References

- (1) Vogt, R. L.; Dippold, L. *Public Health Reports* **2005**, *2*, 174–178.
- (2) Hudault, S.; Guignot, J.; Servin, A. L. *Gut* **2001**, *49*, 47–45.
- (3) Karch, H.; Tarr, P.; Bielaszewska, M. *Int. J. Med. Microbiol.* **2005**, *295*, 405–418.

- (4) Fratamico, P. M.; Strobaugh, T. P.; Medina, M. B.; Gehring, A. G. *Biotechnol. Tech.* **1998**, *12*, 571–576.
- (5) Tims, T. B.; Lim, D. V. *J. Microbiol. Methods* **2003**, *55*, 141–147.
- (6) Muhammad-Tahir, Z.; Alocilja, E. *Biosens. Bioelectron.* **2003**, *18*, 813–819.
- (7) Brooks, B. W.; Devenish, J.; Lutze-wallace, C. L.; Milnes, D.; Robertson, R. H.; Berlie-Surujballi, G. *Vet. Microbiol.* **2004**, *103*, 77–84.
- (8) Taylor, A. D.; Yu, Q. M.; Chen, S. F.; Homola, J.; Jiang S. *Sens. Actuators B* **2005**, *107*, 202–208.
- (9) Liu, Y.; Gilchrist, A.; Zhang, J.; Li, X.-F. *Appl. Environ. Microbiol.* **2008**, *74*, 1502–1507.
- (10) Killmann, H.; Benz, R. Braun, V. *J. Bacteriol.* **1996**, *178*, 6913–6920.
- (11) Killmann, H.; Herrmann, C.; Torun, A.; Jung, G.; Braun, V. *Microbiology* **2002**, *148*, 3497–3509.
- (12) Liu, Y.; Gong, Z.; Morin, N.; Pui, O.; Cheung, M.; Zhang, H.; Li, X. F. *Anal. Chim. Acta* **2006**, *578*, 75–81.
- (13) Bekal, S.; Brousseau, Masson, L.; Profontaine, G.; Fairbrother, J.; Harel, J. *J. Clin. Microbiol.* **2003**, *41*, 2113–2115.
- (14) Wu, C. F.; Valdes, J. J.; Bentley, W. E.; Sekowski, J. W. *Biosens. Bioelectron.* **2003**, *19*, 1–8.

Chapter VI

Conclusions and Future Work

1. Conclusions

In this thesis, we have developed a simple and efficient method to immobilize bacterial proteins on gold surfaces for the study of protein adsorption and interaction with other molecules. Protein arrays were fabricated via surface modification with self-assembled monolayers (SAMs) and various methods of protein immobilization, which were also used for probing protein interaction. Whole bacteria were captured on the chip by the specific interaction between bacterial proteins. Surface plasmon resonance (SPR) imaging was employed as a useful tool to monitor biomolecular interactions and bacterial binding on the surface. The pathogenicity of captured bacteria was examined by the identification of released proteins from lysed bacteria using specific antibodies.

To explore the interaction of bacterial proteins with other molecules, a protein immobilization method was developed based on a chemically modified gold surface. A surface capture agent containing a nitrilotriacetic acid (NTA) group was synthesized and reacted with gold to form a SAM. Bacterial proteins fused with His₆ tags were specifically anchored to the SAM via an affinity interaction of His₆-tags with NTA groups in the presence of Ni²⁺ ions. Infrared reflection absorption spectroscopy (IRRAS)

was utilized to characterize the structure of NTA monolayers, and SPR imaging measurements were performed to investigate protein adsorption and desorption. The results indicated that the immobilization of His₆-tagged proteins on the NTA monolayer was very efficient and specific. In addition, the NTA-modified chip can be readily regenerated, and therefore reused for multiple analysis by treatment with imidazole, EDTA or NiSO₄.

The use of the immobilization method we developed allowed us to study biomolecular interactions with SPR imaging, including antigen–antibody recognition, protein dimerization, protein–DNA and protein–sugar interactions. Bioaffinity immobilization of proteins was shown to provide a greater binding between the antibody and antigen compared to physical adsorption and covalent attachment. Protein dimerization and binding to specific DNA sequences were also observed in the activation of the cyclic nucleotides cAMP. The formation of protein dimers was dependent on the concentration of both the protein and cAMP. The results demonstrated that our method of protein immobilization was useful for monitoring protein interactions with other biomolecules on the surface. In addition, the binding of the small molecule maltose to maltose-binding protein (MBP) was successfully detected using SPR imaging.

Further applications of our methodology in bacterial capture and lysed cell analysis were demonstrated. Instead of using antibodies, *E. coli* bacteria were captured to colicin M (Cma) that served as a bacterial receptor. Also, a semi- quantitative analysis of

captured bacteria was also made by the construction of a binding curve, and the limit of detection (LOD) was estimated to be $\sim 1 \times 10^7$ cell/mL. While a high level of specificity were achieved by testing different strains and types of bacteria, the sensitivity needs to be greatly enhanced in order to render our method practical for detection of bacterial pathogens in food. Lysis of bacterial cells and identification of representative bacterial proteins released from lysed bacteria can be performed on the same sensor chip, which may offer a potential route to determine whether captured bacteria are pathogenic or not.

2. Future Work

The amount of CRP contained in each *E. coli* cell may be estimated by the detection of CRP binding to immobilized anti-CRP after captured bacterial cells are lysed. First, we covalently immobilize anti-CRP antibody on a NHS-terminated monolayer via the formation of an amide bond linkage. Then, a set of CRP solutions at various concentrations will be introduced to the antibody layer. A SPR signal ($\Delta\%R$) is calculated for CRP adsorption at each concentration. A binding curve is then fitted by a Langmuir isotherm model, which is later used to quantitate the released CRP from lysed bacterial cells. In the meanwhile, the number of captured bacteria on the surface can be counted using an optical microscope. Thus, the $\Delta\%R$ value resulting from the CRP–anti-CRP curve constructed before.

Compared to conventional methods, such as culturing method and polymerase reaction chain (PCR), the sensitivity of *E. coli* detection in our assay requires considerable improvement in order to identify bacteria in food or water. One approach to enhance the sensitivity is using a sandwich assay, which are widely used in enzyme-linked immunosorbent assays (ELISAs) due to its sensitivity and robustness.³ In the sandwich assay, the sensitivity is increased because each primary antibody contains several epitopes that can be bound by the labeled secondary antibody, allowing for signal amplification. In our method, another Cma can be introduced to the surface after bacteria are captured. SPR signal may be amplified due to an increase in mass of the medium next to the surface. Another possible way is to label bacterial cells with gold nanoparticles. This method also takes advantage of large mass of nanoparticles to improve SPR signals.⁴

In addition, our protein immobilization method could be used to detect various other proteins, bacteria or toxins if an appropriate protein or ligand is found for specific binding. Also, we will try to use other fusion tags, such as glutathione *S*-transferase (GST)⁵ and FLAG peptide,⁶ for the development new methods to immobilize target proteins in a well-defined orientation. Hopefully, the performance of SPR imaging for monitoring biomolecular interactions can be enhanced due to better retained biological activity of proteins.

3. References

- (1) Daly, P.; Collier, T.; Doyle, S. *Lett. Appl. Microbiol.* **2002**, *34*, 222–226.
- (2) Fu, Z.; Rogelj, S.; Kieft, T. L. *Int. J. Food Microbiol.* **2005**, *99*, 47–57.
- (3) Wink, S.; van Zuiken, S. J.; Bult, A.; van Bennekom, W. P. *Anal. Chem.* **1998**, *70*, 827–832.
- (4) Nikitin, P. I.; Beloglazov, A. A.; Kochergin, V. E.; Valeiko, M. V.; Ksenevich, T. I. *Sens. Actuators B* **1999**, *54*, 43–50.
- (5) Simons, P. C.; Vander Jagt, D. L. *Methods Enzymol.* **1981**, *77*, 235–237.
- (6) Hopp, T. H.; Prickett, K. S.; Price, V. L.; Libby, R. T.; March, C. J.; Cerretti, D. P.; Urdal, D. L.; Conlon, P. J. *Bio/Technology* **1988**, *6*, 1204–1210.